Experimental and Numerical Study on Performance Optimization and Scalability of Salt Hydrate-Based Phase Change Materials for Thermal Energy Storage in Buildings

Thesis submitted in partial fulfilment

for the award of the degree

Doctor of Philosophy

by

AMARENDRA UTTAM

RAJIV GANDHI INSTITUTE OF PETROLEUM TECHNOLOGY

JAIS, 229304

Roll No.: 21CE0011

2026

CERTIFICATE

It is certified that the work contained in the thesis titled **"*Experimental and Numerical Study on Performance Optimization and Scalability of Salt Hydrate-Based Phase Change Materials for Thermal Energy Storage in Buildings*"** has been carried out under my supervision and that this work has not been submitted elsewhere for a degree.

It is further certified that the student has fulfilled all the requirements of Comprehensive, Candidacy, and SOTA.

Dr. Venkata Subbarayudu Sistla

(Supervisor)

DECLARATION BY THE CANDIDATE

I, ***Amarendra Uttam***, certify that the work embodied in this thesis is my own bonafide work and was carried out by me under the supervision of ***Dr. Venkata Subbarayudu Sistla*** from August 2021 to January 2026*,* at the *Department of Chemical and Biochemical Engineering,* Rajiv Gandhi Institute of Petroleum Technology, Jais. The matter embodied in this thesis has not been submitted for the award of any other degree. I declare that I have faithfully acknowledged and given credits to the research workers wherever their works have been cited in my work in this thesis. I further declare that I have not wilfully copied any other's work, paragraphs, text, data, results, etc., reported in journals, books, magazines, reports, dissertations, theses, etc., or available on websites and have not included them in this thesis and have not cited as my work.

Date:

Place: RGIPT, Jais, Amethi **Amarendra Uttam**

CERTIFICATE BY THE SUPERVISOR

It is certified that the above statement made by the student is correct to the best of my knowledge.

Dr. Venkata Subbarayudu Sistla

(Supervisor) Signature & Seal of Head of Department

CERTIFICATE

CERTIFIED that the work contained in the thesis titled **"*Experimental and Numerical Study on Performance Optimization and Scalability of Salt Hydrate-Based Phase Change Materials for Thermal Energy Storage in Buildings"*** by **Mr. Amarendra Uttam** has been carried out under my supervision. It is also certified that he fulfilled the mandatory requirement of TWO quality publications that arose out of his thesis work.

It is further certified that the two publications (copies enclosed) of the aforesaid **Mr. Amarendra Uttam** have been published in the Journals indexed by -

(a) SCI

(b) SCI Extended

(c) SCOPUS

Dr. Venkata Subbarayudu Sistla **Dr. Vivek Kumar**

(Supervisor) (Convener, DPGC)

COPYRIGHT TRANSFER CERTIFICATE

Title of the Thesis: Experimental and Numerical Study on Performance Optimization and Scalability of Salt Hydrate-Based Phase Change Materials for Thermal Energy Storage in Buildings

Name of the Student: Amarendra Uttam

Copyright Transfer

The undersigned hereby assigns to the Rajiv Gandhi Institute of Petroleum Technology Jais all rights under copyright that may exist in and for the above thesis submitted for the award of the **"DOCTOR OF PHILOSOPHY".**

Date:

Place: RGIPT, Jais, Amethi **Amarendra Uttam**

Note: However, the author may reproduce or authorize others to reproduce material extracted verbatim from the thesis or derivative of the thesis for the author's personal use provided that the source and the Institute's copyright notice are indicated

Acknowledgements

The successful completion and undertaking of the Ph.D. would not have been possible without the blessing of God, my thesis advisor and my parents. I want to thank all for their blessings and valuable suggestions during the whole tenure of my Ph.D. work.

I express my deep sense of gratitude to my institution, Rajiv Gandhi Institute of Petroleum Technology (RGIPT), Jais, for providing the opportunity and necessary facilities to pursue and complete this thesis work. I also sincerely acknowledge the support from Chemical and Biochemical Engineering Department for offering an excellent academic and research environment throughout the duration of this work.

I am deeply grateful to my esteemed thesis advisor, Dr. V. S. Sistla from Department of Chemical and Biochemical Engineering for his excellent guidance and continuous support. His most appreciated quality is being easily accessible for discussion on academic or personal matters. Dr. V. S. Sistla not only supervised me in the thesis but also gave valuable suggestions regarding my career. I would also like to acknowledge all the faculty members and staff of Chemical and Biochemical Engineering Department for their kind support and cooperation.

Besides my advisor, I am also grateful to my RPEC committee members, Prof. Atul Sharma from the Department of Energy and Human Sciences, Dr. Karan Malik, and Dr. Supriya Pulipaka both from Department of Chemical and Biochemical Engineering, for their constructive feedback, valuable suggestions, and constant support, which have significantly improved the quality of this work.

I would like to express my sincere gratitude to Dr. Bijoy Kumar Purohit, a former research scholar in my lab, for his support in my thesis work through the provision of valuable references from his research. I also extend my special thanks to Dr. Pawan Kumar (Ph.D. from IIT Roorkee) and Dr. Rohit Kumar Singh for their continuous discussion and guidance, which greatly helped in completing this thesis.

I extend my heartfelt thanks to my lab mates, Bhupendra Kumar, Anki Singh, Shalu Yadav, Puja Pandey and Sachin Kumar and my other fellow Ph.D. colleagues for their continuous assistance, cooperation, and encouragement during experiments and day-to-day research activities. Their support has greatly contributed to the successful completion of this thesis.

I also acknowledge Saurabh Kumar Mishra my friend and roommate during the Ph.D. journey, for his constant support and companionship.

Finally, I express my heartfelt gratitude to my parents, wife, sons, brothers, and friends for their unconditional love, patience, and encouragement, which have been a constant source of strength throughout my doctoral journey.

Amarendra Uttam

Dedicated

to

My Beloved Family

Mr. Ramdhani Uttam and Mrs. Sushma Uttam (Parents)

Anju (Wife), Reyansh (Son)

Amit and Ayush (Brothers)

for their unconditional support throughout my **Ph.D.**

TABLE OF CONTENTS

LIST OF FIGURES

LIST OF TABLES

LIST OF ABBREVIATIONS

PCM:	Phase change material
PU-PCM:	Polyurethane-phase change material
CMC:	Carboxyl methylcellulose
DSC:	Differential Scanning calorimetry
LHS:	Latent heat storage
PU:	Polyurethane
SHS:	Sensible heat storage
SSD:	Sodium sulphate decahydrate ($Na_2SO_4.10H_2O$)
TES:	Thermal energy storage
TGA:	Thermogravimetry Analysis

LIST OF NOMENCLATURE

English Symbols

C_P:	Specific heat capacity at constant pressure	(J kg^{-1} K^{-1})
$C_{P,FM}$:	Specific heat capacity of fluid medium (porous media)	(J kg^{-1} K^{-1})
$C_{P,L}$:	Specific heat capacity of PCM in liquid phase	(J kg^{-1} K^{-1})
$C_{P,P}$:	Specific heat capacity of solid medium (porous media)	(J kg^{-1} K^{-1})
$C_{P,S}$:	Specific heat capacity of PCM in solid phase	(J kg^{-1} K^{-1})
H:	Specific enthalpy	(J kg^{-1})
H_L:	Enthalpy of PCM in liquid phase	(J kg^{-1})
H_S:	Enthalpy of PCM in Solid phase	(J kg^{-1})
k:	Thermal conductivity	(W m^{-1} K^{-1})
k_{eff}:	Effective thermal conductivity	(W m^{-1} K^{-1})
k_{FM}:	Thermal conductivity of fluid medium (porous media)	(W m^{-1} K^{-1})
k_L:	Thermal conductivity of PCM in liquid phase	(W m^{-1} K^{-1})
k_S:	Thermal conductivity of PCM in solid phase	(W m^{-1} K^{-1})
k_P:	Thermal conductivity of solid media (porous media)	(W m^{-1} K^{-1})
L:	Latent heat of melting	(kJ kg^{-1})
Q:	Heat sources other than viscous dissipation and pressure work	(W m^{-3})
Q_P:	Heat sources due to pressure work	(W m^{-3})
Q_{vd}:	Heat sources due to viscous dissipation	(W m^{-3})
T_1:	Reactor inner space temperature	(°C)
T_2:	Reactor jacketed space temperature	(°C)
(T_2-T_1):	Temperature difference between reactor jacketed space temperature and inner space temperature	(°C)

Greek Symbols

α_m:	Effective thermal diffusivity	(m^2 s^{-1})
ΔT:	Phase change temperature range	
θ:	Phase change fraction	
θ_P:	Volume fraction of Solid medium (porous media)	
ρ:	Density	(kg m^{-3})
ρ_F:	Density of fluid medium (porous media)	(kg m^{-3})
ρ_L:	Density of PCM in liquid phase	(kg m^{-3})
ρ_P:	Density of solid medium (porous media)	(kg m^{-3})
ρ_S:	Density of PCM in solid phase	(kg m^{-3})
$(\rho C_P)_{eff}$:	Effective volumetric heat capacity (porous media)	(J m^{-3} K^{-1})

PREFACE

The growing global energy demand and the increasing need for sustainable building solutions have triggered research on efficient thermal energy storage (TES) systems. Phase change materials (PCMs) are a promising alternative for the passive cooling of buildings and load shifting through the utilization of the latent heat during phase change transition. Among the various PCMs, sodium sulphate decahydrate (Na2SO4·10H2O), has attracted considerable attention because of its high latent heat capacity, low cost, and abundant availability. However, its practical application is hindered by persistent challenges such as supercooling, phase separation and thermal cycling instability, which restrict the long-term performance and large-scale implementation.

In this thesis, these challenges are addressed through the development, stabilization and scale-up a polyurethane-based PCM (PU-PCM) composite incorporating an aqueous Na2SO4·10H2O solution, Laponite® Gel as thickening agent and borax as a nucleating agent. Differential Scanning Calorimetry (DSC) measurements were used to determine thermal properties such as latent heat and melting point of PU-PCM composite. COMSOL Multiphysics simulations were performed at different scales (600 mL to 5 L) to systematically assess the thermal performance, stability, and scalability of the composite. Additionally, the computational models were validation and extended to larger scales. Numerical simulations accurately captured transient heat transfer and phase change kinetics. Furthermore, parametric analyses were conducted to determine the optimal composite thickness and to quantify the effect of phase change temperature range (ΔT) and latent heat (L) on system performance.

Furthermore, a three-dimensional building wall model incorporating the PU-PCM composite was developed to investigate its passive cooling performance under hot-climate conditions. The simulation results demonstrated reductions in peak indoor temperature, delayed heat transfer, and improved thermal comfort, confirming the suitability of $Na_2SO_4 \cdot 10H_2O$-based composite for building-integrated TES applications. Overall, this work establishes a validated multi-scale experimental-numerical framework for the development, scale-up, and building integration of $Na_2SO_4 \cdot 10H_2O$-PU composite, providing a pathway toward sustainable and energy-efficient thermal management systems.

Organisation of the Thesis

Chapter 1 introduces the growing need for efficient thermal energy storage (TES) systems in response to increasing energy demand and sustainability requirements. It highlights the role of PCMs in building cooling and load shifting and identifies $Na_2SO_4 \cdot 10H_2O$ as a promising salt hydrate PCM due to its high latent heat, low cost, and availability. The chapter also discuss the key challenges associated with its application such as supercooling, phase separation, and cycling instability.

Chapter 2 presents a comprehensive literature review on salt hydrates as PCMs, focusing on strategies to overcome limitations including phase segregation, supercooling, low thermal conductivity, and encapsulation challenges. Emphasis is placed on building energy system applications and the need for scalable and practically deployable TES solutions.

Chapter 3 details the experimental and numerical investigation of $Na_2SO_4 \cdot 10H_2O$-based PU-PCM composite. A 600 mL physical model was fabricated to evaluate heating and cooling cycles, and experimental data were used to develop and validate a computational model in COMSOL Multiphysics. DSC was conducted to determine phase transition temperature, latent heat storage capacity, and thermal stability. The results confirm the feasibility of integrating the PU-PCM composite into building wall assemblies with promising thermal performance.

Chapter 4 focuses on the scalability analysis of $Na_2SO_4 \cdot 10H_2O$-based TES systems using PU-PCM composite. Physical models ranging from 600 mL to 5 L were developed to study thermal charging and discharging behaviour. Experimental results were validated using numerical simulations capturing transient heat transfer and phase change kinetics. DSC confirmed thermal stability over repeated cycles. Numerical studies identified optimum composite thickness for 2 L and 5 L systems and examined the influence of phase change temperature range (ΔT) and latent heat (L) on temperature difference profiles. The findings demonstrate effective thermal management across scales and strong potential for building and industrial applications.

Chapter 5 presents a numerical investigation of the thermal performance of a brick wall integrated with a PU-PCM composite for passive cooling. A three-dimensional room model

was developed in COMSOL Multiphysics to assess reductions in peak indoor temperature, heat transfer delay, and thermal comfort improvement under realistic climatic conditions. A parametric study examined the effects of wall thickness and ambient conditions, confirming the applicability of salt hydrate-based PCMs for large-scale building cooling.

Chapter 6 summarizes the major conclusions and outlines future research directions. The study confirms the high latent heat potential of $Na_2SO_4 \cdot 10H_2O$-based PCMs while emphasising the need for improved stabilization and heat transfer enhancement during scale-up. Future work will focus on microencapsulated and hybrid PCM systems, long-term field evaluation, and improved thermal and mechanical stability to advance practical TES technologies.

***Note on Published Work**

Parts of this thesis are based on the author's published and accepted research papers.

- Chapter 3 is based on "*$Na_2SO_4.10H_2O$ Salt hydrates-based Phase Change Materials for Thermal energy storage: A scale-up approach*" published in ChemistrySelect, 2025 Nov;10(43). DOI: https://doi.org/10.1002/slct.202504616.

- Chapter 4 is based on: "*Performance analysis of a multi-scale thermal energy storage system with varying volumes using polyurethane-encapsulated sodium sulphate decahydrate for building applications*" published in Energy and Building, 2025 Sep 5;347:116390-0. DOI: https://doi.org/10.1016/j.enbuild.2025.116390.

These above papers were authored by Mr. Amarendra Uttam (first author) under the supervision of Dr. V. S. Sistla. The results have been reproduced in this thesis with permission from the respective publishers, and all necessary acknowledgements have been provided.

CHAPTER - 1

Introduction

1.1 Background and Motivation

Energy is central to the functioning of modern society, and the manner in which it is generated, stored, and utilized has direct consequences for economic growth, environmental sustainability, and quality of life [1]. In the contemporary era, global energy demand is rising rapidly, driven by urbanization, population growth, and increasing living standards. Simultaneously, mounting concerns over climate change, greenhouse gas emissions, and the finite nature of fossil fuel reserves are compelling governments, industries, and researchers to pursue a fundamental transformation in energy systems [2–4].

Within this context, the building sector has emerged as one of the most significant contributors to global energy consumption, accounting for a substantial share of final energy use and associated carbon emissions [2]. Buildings consume energy primarily for maintaining indoor thermal comfort through heating, ventilation, and air-conditioning (HVAC) systems. In regions with hot and composite climates, such as large parts of India, cooling demand dominates the annual energy budget[3]. The rapid proliferation of air-conditioning systems has led to a steep rise in peak electricity demand, straining power grids and increasing dependence on fossil-fuel-based electricity generation [5].

While conventional approaches such as enhanced thermal insulation, high-efficiency HVAC systems, and renewable energy integration have demonstrated measurable reductions in building energy use, these measures alone do not resolve a fundamental challenge: the temporal mismatch between energy availability and energy demand [9,10]. Solar energy, for instance, is most abundant during daytime hours, whereas cooling demand

in hot climates often extends into the evening and night. Bridging this temporal gap requires reliable and efficient thermal energy storage (TES) solutions capable of decoupling energy supply from consumption [12,13]. This thesis is motivated by the critical need for scalable, practical, and cost-effective TES technologies suitable for building integration under Indian and similar climatic conditions.

1.2 Origin and Importance of the Problem

The problem addressed in this thesis originates from two intersecting challenges: (i) the growing cooling energy burden on buildings in hot climates, and (ii) the absence of thermally efficient, stable, scalable, and cost-effective PCM-based TES systems suitable for integration into building envelopes.

Modern buildings are no longer passive enclosures; rather, they function as dynamic thermal systems that continuously exchange heat with the surrounding environment. A significant portion of building energy consumption is associated with maintaining indoor thermal comfort through heating, ventilation, and air-conditioning (HVAC) systems[6]. In hot and composite climates, buildings experience substantial solar heat gain through walls and roofs during daytime, causing indoor temperature to frequently exceed the human thermal comfort range of 18-26 °C. The resulting over-reliance on air-conditioning leads to higher electricity consumption, peak electricity load problems, increased carbon emissions, and urban heat island effects [5,6]. In this context, passive cooling technologies that can absorb excess heat during daytime and release it during cooler nights offer a compelling alternative or complement to active HVAC systems.

Thermal energy storage through phase change materials (PCMs) has been recognized as one of the most promising passive cooling strategies. PCMs absorb heat isothermally during melting and release it during solidification, providing high energy storage density within a narrow temperature range matched to indoor comfort requirements [13,17,20].

However, despite decades of PCM research, the widespread adoption of PCM-based TES in buildings remains limited due to several unresolved material and system-level challenges.

For inorganic PCMs particularly salt hydrates such as sodium sulfate decahydrate ($Na_2SO_4 \cdot 10H_2O$) the primary challenges are supercooling, phase segregation, and long-term instability under repeated thermal cycling [28,32]. These issues compromise the reliability and durability of salt hydrate systems. In addition, most existing research is confined to small-scale material characterization, with insufficient attention to scale-up, building-level integration, and performance optimization across different PCM configurations [65-67]. This gap between laboratory research and practical implementation constitutes the central problem motivating this thesis.

$Na_2SO_4 \cdot 10H_2O$ is specifically selected in this work due to its phase change temperature of approximately 32 °C well within the range relevant for passive cooling in Indian buildings—combined with high latent heat (~254 kJ/kg), non-flammability, environmental safety, and low material cost [43,44]. By incorporating this salt hydrate into an open-cell polyurethane (PU) foam matrix, the thesis develops a shape-stabilized PU-PCM composite that addresses phase segregation and leakage while enabling practical fabrication and building integration.

In regions characterized by hot or composite climates and pronounced diurnal temperature variations—such as many parts of India—cooling demand dominates annual building energy use. The rapid proliferation of air-conditioning systems has resulted in a steep rise in electricity consumption, particularly during peak daytime and evening hours. This growing cooling demand often coincides with peak electricity loads, placing considerable stress on power grids and increasing dependence on fossil-fuel-based power generation[7].

Conventional strategies to reduce building energy consumption—such as enhanced thermal insulation, deployment of high-efficiency HVAC systems, and integration of renewable energy sources—have demonstrated measurable reductions in operational energy use and carbon emissions in buildings [3,8,9]. However, these approaches alone do not fully address a fundamental limitation of building energy systems: the temporal mismatch between energy availability and energy demand [10,11]. For instance, solar energy availability peaks during daytime hours, whereas cooling demand in hot and composite climates often extends into the evening and night [12]. Bridging this gap necessitates the implementation of effective and reliable thermal energy storage (TES) solutions, which can decouple energy generation from consumption and enable time-shifted utilization of stored thermal energy[13,14]

1.3 Thermal Energy Storage: Principles and Classification

Thermal Energy Storage Systems (TESS) is a medium that temporarily holds thermal energy (available/excess), which can be utilized later. The fundamental working principle of a thermal energy storage (TES) system can be understood by the Figure 1.1. Thermal energy storage (TES) acts as an effective buffer between energy supply and demand by enabling excess thermal energy to be stored during periods of availability and released when required[15]. By decoupling energy generation from consumption, TES systems enhance overall energy efficiency, reduce peak electricity demand, and contribute to improved grid stability and reliability [10,11].

TES technologies can be broadly classified into three main categories based on their storage mechanism[16,17]:

1. **Sensible Heat Storage (SHS)**
2. **Latent Heat Storage (LHS)**
3. **Thermochemical Energy Storage (TCES)**

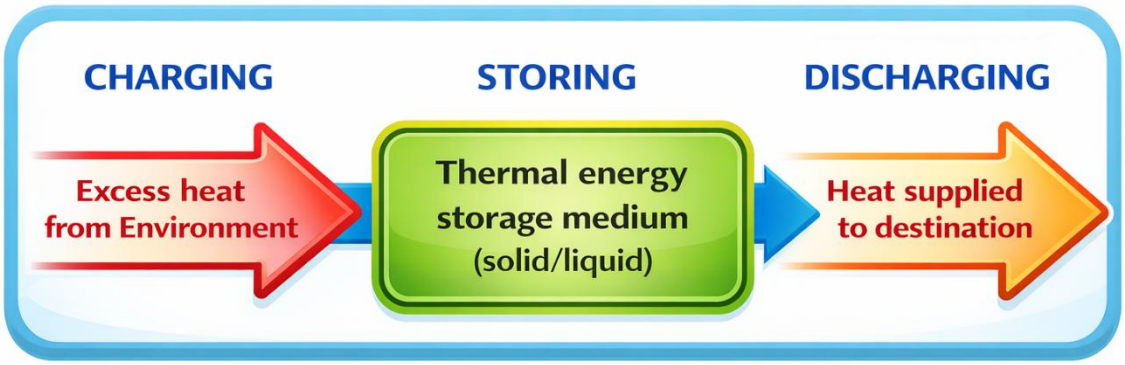

Figure 1.1: Working principle of thermal energy storage

Among these, latent heat storage has attracted significant attention for building applications due to its high energy storage density and its ability to store and release large amounts of thermal energy within a narrow and nearly constant temperature range, which closely matches indoor thermal comfort requirements[14,18,19].

1.3.1 Sensible Heat Storage (SHS)

Sensible heat storage (SHS) relies on raising or lowering the temperature of a storage medium—such as water, concrete, rocks, or molten salts—without undergoing any phase change[18,20]. The amount of thermal energy stored in an SHS system is governed by the specific heat capacity of the medium, its mass, and the temperature difference between the charging and discharging states. Due to their simple design, material availability, and relatively low cost, SHS systems are widely used in building heating and cooling applications [14]. However, the relatively low energy storage density of SHS necessitates large storage volumes to store substantial amounts of energy, which limits their compactness and integration potential in buildings [16].

1.3.2 Latent Heat Storage (LHS)

Latent heat storage (LHS) systems utilize phase change materials (PCMs) to store and release thermal energy during a phase transition, most commonly between solid and liquid states [16,21]. During the phase change process, a large amount of energy—known as latent heat of fusion—is absorbed or released at a nearly constant temperature, resulting

in significantly higher energy storage density compared to SHS [22]. This characteristic makes LHS particularly attractive for building applications, where thermal comfort must be maintained within a narrow temperature range[19].

1.3.3 Thermochemical Energy Storage (TCES)

Thermochemical energy storage (TCES) systems store and release thermal energy through reversible chemical reactions, typically involving endothermic and exothermic processes [23]. TCES offers the highest theoretical energy storage density among TES technologies and enables long-term, loss-free energy storage when the reactants are kept separate[24]. Despite these advantages, TCES systems remain largely at the research and development stage due to challenges associated with material stability, reaction kinetics, reactor design, and system integration [25,26]. Consequently, their widespread application in buildings is currently limited compared to SHS and LHS technologies.

1.4 Phase Change Materials for Latent Heat Thermal Energy Storage

Latent heat storage systems utilize phase change materials (PCMs) to store and release thermal energy during phase transitions, most commonly between solid and liquid states[16,21]. During this process, large amounts of energy are absorbed or released at nearly constant temperature, making PCMs particularly attractive for maintaining indoor thermal comfort in buildings[19,27].

The working principle of the phase change material (PCM) is governed by its ability to absorb and release thermal energy through phase transitions. During the daytime, when the outdoor temperature (T_o) exceeds the PCM melting temperature (T_m), the PCM absorbs heat from the surroundings and undergoes a solid-to-liquid phase change, as depicted in Figure 1.2. The absorbed thermal energy is stored in the form of latent heat, which helps limit the rise in indoor temperature. During nighttime, as the outdoor temperature drops below the PCM melting temperature ($T_m < T_i$), the PCM begins to solidify and releases the

stored latent heat. This released heat is transferred either toward the cooler outdoor environment or gradually toward the indoor space, depending on the prevailing thermal gradient. As a result, sudden temperature drops are mitigated, and a more stable and comfortable indoor thermal environment is maintained[14,16].

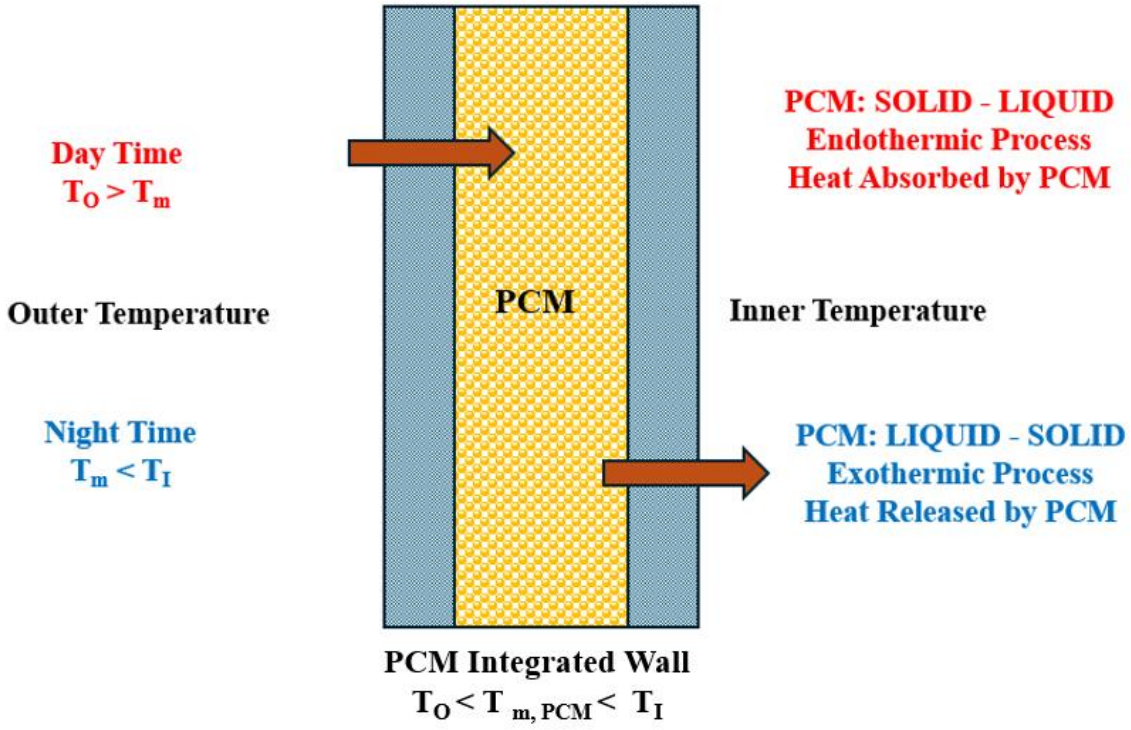

Figure 1.2: Working principle of Phase change material

The PCM operates effectively only when its melting temperature lies between the outdoor and indoor temperature $T_O < T_{m,PCM} < T_I$

Compared to sensible heat storage materials such as water or concrete, PCMs provide significantly higher energy storage density per unit volume and enhanced thermal regulation capability within a narrow operating temperature range[16]. Owing to these advantages, extensive research over the past decades has focused on the development and characterization of PCMs for building-integrated thermal energy storage applications [18]. Based on their chemical composition and phase change behavior, PCMs are broadly classified into organic, inorganic, and eutectic materials [14].

Organic PCMs, including paraffins and fatty acids, are widely studied due to their chemical stability, negligible supercooling, and excellent long-term cycling reliability [28]. However, their practical application in buildings is often limited by low thermal conductivity, flammability concerns, and relatively high material cost[29]. In contrast, inorganic PCMs, particularly salt hydrates, offer high latent heat of fusion, higher thermal conductivity, and low raw material cost, making them promising candidates for building-integrated TES systems[30–32]. These characteristics are especially advantageous for passive and active thermal regulation in buildings operating within comfort-relevant temperature ranges.

1.4.1 Properties of phase change materials

The selection of an appropriate phase change material (PCM) is a critical step in the design of efficient latent heat thermal energy storage systems. An ideal PCM should possess a suitable combination of thermophysical, physical, kinetic, chemical, and economic properties to ensure effective, reliable, and safe operation over long-term cycling[14,22,31].

Thermal properties: From a thermal perspective, a PCM should exhibit a suitable phase transition temperature, high latent heat of transition, and good heat transfer characteristics[30,33]. The phase transition temperature of the PCM must closely match the operating temperature range of the intended heating or cooling application to ensure effective thermal regulation. A high latent heat of transition particularly on a volumetric basis is desirable to maximize energy storage capacity while minimizing the physical size of the storage system. Furthermore, higher thermal conductivity facilitates faster charging and discharging rates, improving the overall thermal response of the storage system [16].

Physical properties: The physical properties of PCMs strongly influence system stability and containment requirements. Desirable characteristics include favourable phase equilibrium, high density, minimal volume change during phase transition, and low vapor pressure at operating temperature [16]. Phase stability during freezing melting would help towards setting heat storage and high density is desirable to allow a smaller size of storage container. Small volume changes during phase transformation and low vapor pressure at operating temperature to reduce the containment problem[29].

Kinetic properties: Kinetic behavior plays a crucial role in the practical applicability of PCMs. An ideal PCM should exhibit negligible supercooling and a sufficient crystallization rate during solidification[21]. Supercooling has been a troublesome aspect of PCM development, particularly for salt hydrates. Supercooling of more than a few degrees will interfere with proper heat extraction from the store. Supercooling, particularly prevalent in inorganic PCMs such as salt hydrates, delays the onset of solidification and can significantly hinder heat extraction from the storage system. Supercooling exceeding a few degrees Celsius can compromise system reliability and must therefore be minimized through material modification or nucleation enhancement strategies[31].

Chemical properties: PCMs must demonstrate long-term chemical stability over repeated thermal cycles and be compatible with materials of construction, such as metals, polymers, or encapsulation shells [32]. Degradation mechanisms may include dehydration (especially in salt hydrates), chemical decomposition, or corrosive interactions with containment materials. In addition, PCMs should be non-toxic, non-flammable, and non-explosive to ensure safe handling and integration within building environments [13].

Economics: Finally, economic feasibility is a decisive factor for large-scale implementation. PCMs should be abundant, readily available, and cost-effective, particularly for building-integrated thermal energy storage systems [19]. Low material cost

combined with scalable availability is essential to enable widespread adoption of PCM-based TES technologies in residential and commercial buildings.

1.4.2 Classification of PCMs

Phase change materials (PCMs) are commonly classified based on their chemical composition and type of phase transition involved during energy storage and release. From a chemical perspective, PCMs can be broadly categorized into organic, inorganic, and eutectic mixtures, while from a phase-transition standpoint, most PCMs operate through solid-liquid transitions, with solid-solid PCMs forming a distinct sub-class as shown in Figure 1.3 [14,16,32].

1.4.2.1 Organic Phase Change Materials

Organic phase change materials are generally classified into paraffinic and non-paraffinic compounds. A key advantage of organic PCMs is their ability to undergo repeated melting and freezing cycles without phase segregation or significant degradation of latent heat, making them attractive for long-term thermal energy storage applications [14,30]. Table 1.1 shows the thermophysical properties (melting point/range Tm, average thermal conductivity k, and latent heat H) of some organic PCMs used in buildings.

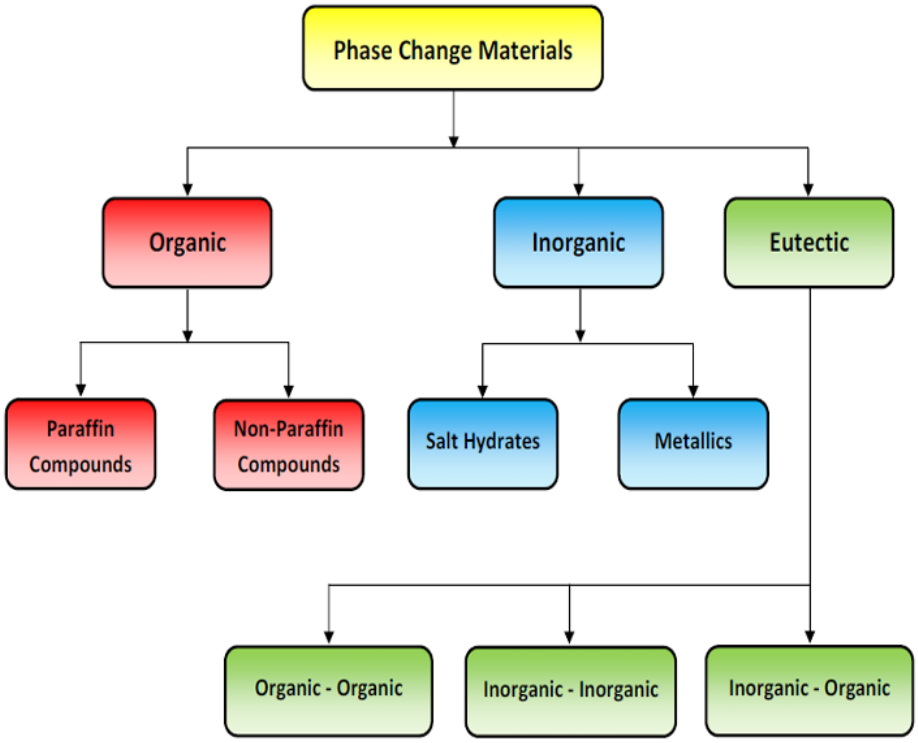

Figure 1.3: Classification of PCMs[14,16]

1.4.2.1.1 Paraffin's

Paraffins, with the general chemical formula C_nH_{2n+2}, are a group of saturated hydrocarbons that exhibit relatively uniform thermophysical properties. Paraffins with carbon numbers between C_5 and C_{15} are liquids at room temperature, while higher carbon-number paraffins exist as waxy solids. Paraffin wax is one of the most widely used organic PCMs for commercial thermal energy storage applications and consists of straight-chain hydrocarbons with melting temperature typically ranging from 23 °C to 67 °C, depending on molecular weight[21].

Advantages of paraffins

- Available over a wide range of phase transition temperature
- Exhibit negligible supercooling
- Chemically stable over repeated thermal cycling
- Possess relatively high latent heat of fusion
- Do not undergo phase segregation

- Non-corrosive and generally safe to handle

Disadvantages of paraffins

- Low thermal conductivity, leading to slower heat transfer rates
- Significant volume change between solid and liquid phases
- Commercial paraffins often exhibit broad melting ranges rather than sharp melting points
- Flammability, posing fire safety concerns
- Relatively high cost for high-purity grades
- Limited compatibility with certain plastic containers

1.4.2.1.2 Non-Paraffin's

Non-paraffinic organic PCMs encompass a wide variety of compounds, each possessing distinct thermophysical and chemical characteristics. These materials include fatty acids, esters, alcohols, and glycols. An extensive survey conducted by Abhat [30] identified several such materials as potential candidates for thermal energy storage. Based on their chemical nature, non-paraffinic organic PCMs are commonly subdivided into fatty acids and other organic compounds [14].

Advantages of non-paraffinic organics

- High latent heat of fusion, particularly for fatty acids
- Relatively sharp phase transition temperature

Disadvantages of non-paraffinic organics

- Low thermal conductivity
- Low flash points, leading to safety concerns
- Thermal instability at elevated temperature for some compounds

1.4.2.1.3 Fatty acids

Fatty acids constitute an important class of non-paraffinic organic phase change materials. The general chemical formula of fatty acids can be expressed as $CH_3(CH_2)_{2n}COOH$. Fatty acids exhibit thermophysical characteristics similar to those of paraffinic PCMs but generally possess higher latent heat of fusion, making them attractive for latent heat thermal energy storage applications [30].

Table 1.1: Thermophysical properties of some organic PCM for building application

S.No.	PCM	Tm (°C)	H (kJ/kg)	k (W/(m·K))
1	n-Octadecane [35]	24.9	204.91	0.192
2	Tetradecane [36]	5.8	227	-
3	Pentadecane [36]	9.9	206	-
4	Hexadecane [36]	18.1	236	-
5	n-Eicosane [37]	36.58	248.5	0.25
6	Paraffin [36]	21.7-22.7	161.6	0.21
7	Paraffin [38]	27-29	245	-
8	Lauric acid [39]	43.93	178.11	-
9	Myristic acid [39]	54.28	191.27	-
10	Palmitic acid [39]	62.73	206.16	-
11	Stearic acid [39]	69.62	217.62	-
12	Lauryl alcohol [40]	24	217	0.221

A key advantage of fatty acids is their ability to undergo repeated melting and solidification cycles with negligible supercooling, coupled with sharper and more well-defined phase transition temperature compared to technical-grade paraffins [30,34]. These features contribute to reliable and predictable thermal performance over long-term cycling.

Despite these advantages, the widespread application of fatty acids as PCMs is limited by certain drawbacks. The material cost of fatty acids is typically 2-2.5 times higher than that of technical-grade paraffins, which significantly affects their economic feasibility for large-scale building applications. In addition, fatty acids exhibit mild corrosive behaviour toward some metallic containment materials, necessitating careful material selection and encapsulation strategies[14].

1.4.2.2 Inorganic Phase Change Materials

Inorganic phase change materials are primarily classified into salt hydrates and metallic phase change materials. Among these, salt hydrates are the most extensively investigated inorganic PCMs for low- and medium-temperature latent heat thermal energy storage applications, particularly in buildings[31,41]. Table 1.2 shows the thermophysical properties (melting point/range Tm, average thermal conductivity k, and latent heat H) of some inorganic PCMs used in buildings.

1.4.2.2.1 Salt hydrates

Salt hydrates consist of a salt and water that combine in a crystalline matrix when the material solidifies[31]. There are many different salt hydrates having melting temperature ranges between 15°C - 117°C, Salt hydrates are considered as the most important group of PCMs that have been studied for application in latent thermal energy storage systems [16]. Glauber salt ($Na_2SO_4 \cdot 10H_2O$) consists of 44% Na_2SO_4 and 56% H_2O by weight. It has a melting temperature around 32.4°C, a latent heat of fusion of 254 kJ/kg (377), and is one of the cheapest materials that can be used for latent thermal energy storage; Its main drawback is the problems of phase segregation and subcooling[42,43]. Following are the advantages and disadvantages of salt hydrates [6,14]:

Table 1.2: Thermophysical properties of some inorganic PCM for building application

S.No.	PCM	Classification	Tm (°C)	H (kJ/kg)	K (W/(m·K))
1	$Na_2SO_4 \cdot 10H_2O$ [44]	Salt hydrate	32.24	239.9	0.34
2	$CaCl_2.6H_2O$ [45]	Salt hydrate	29.6	212	0.82
3	$Na_2HPO_4.12H_2O$ [46]	Salt hydrate	35.1	209.5	1.25
4	$CH_3COONa.3H_2O$ [47]	Salt hydrate	58.3	286.3	-
5	$Na_2CO_3.10H_2O$[48]	Salt hydrate	33	247	0.6
6	$FeCl_3.6H_2O$ [49]	Salt hydrate	37	223	-
7	$Mg(NO_3)_2.6H_2O$ [50]	Salt hydrate	91.5	146	0.4
8	$Zn(NO3)_2.6H_2O$ [51][73]	Salt hydrate	34.6	140	-
9	Gallium [52]	Metal	29.78	80.16	32
10	Bi-Sn-In [52]	Alloy	60.9	29.18	16.4

Advantages of Salt Hydrates

- High latent heat of fusion per unit mass and volume, typically higher than that of paraffinic PCMs
- Higher thermal conductivity compared to organic PCMs, enabling improved heat transfer
- Sharp and well-defined phase change temperature
- Relatively small volume change during melting and solidification
- High availability of raw materials
- Low material cost, making them economically attractive

Disadvantages of Salt Hydrates

- Phase segregation, resulting from the formation of lower hydrates or anhydrous salts that settle during repeated melting-freezing cycles, thereby reducing effective thermal storage capacity.

- Supercooling, due to the inability of the melt to initiate crystallization at the equilibrium freezing temperature; this issue can be mitigated by the incorporation of suitable nucleating agents.
- Corrosion of metallic containers, which poses challenges for system durability and necessitates the use of protective coatings, compatible container materials, or encapsulation strategies.

1.4.2.2.2 Metallic's

Metallic phase change materials include low-melting-point metals and metal eutectic alloys. These materials have received comparatively limited attention for latent heat thermal energy storage applications, primarily due to their high density and heavy weight, which make them less suitable for weight-sensitive systems such as building envelopes [14,16]. However, in applications where volume constraints are more critical than mass, metallic PCMs can be attractive because of their high latent heat of fusion per unit volume and excellent thermal conductivity [16].

Metallic PCMs are also characterized by high heat transfer rates, owing to their inherently high thermal conductivity, and low vapor pressure at operating temperature, which reduces containment and safety concerns[31]. Nevertheless, their low latent heat per unit mass, low specific heat, and high material cost have limited their widespread adoption compared to organic and salt hydrate PCMs [32].

Some features of these materials are:

- Low heat of fusion per unit weight.
- High heat of fusion per unit volume.
- High thermal conductivity.
- Low specific heat.
- Relatively low vapour pressure

1.4.2.3 Eutectics

Eutectic phase change materials consist of two or more components that melt and solidify congruently at a fixed composition and temperature, behaving effectively as a single homogeneous material during the phase transition process [14,16]. During solidification, the eutectic mixture crystallizes simultaneously into its constituent phases, maintaining uniform composition throughout the material [14].

In contrast to many inorganic PCMs, eutectic materials generally melt and freeze without phase segregation, as both components liquefy and solidify at the same temperature, eliminating the possibility of component separation during the phase change process[16,30]. This congruent melting and solidification behavior makes eutectic PCMs attractive for thermal energy storage applications requiring stable and repeatable thermal performance [53].

1.5 Salt Hydrates Phase Change Materials for Thermal Energy Storage: Advantages and Applications

Salt hydrates are a class of inorganic phase change materials composed of an anhydrous salt chemically bound with a specific number of water molecules within a crystalline lattice. During melting and solidification, salt hydrates undergo hydration-dehydration reactions, absorbing or releasing a substantial amount of latent heat at nearly constant temperature, which makes them highly efficient for thermal energy storage (TES) applications[13,16,31].

Owing to their favourable thermophysical properties, salt hydrates have been extensively investigated for low- and medium-temperature TES systems, particularly in the context of building energy management and solar thermal applications [27].

1.5.1 Advantages of Salt Hydrates

High energy density: Salt hydrates exhibit high latent heat of fusion, resulting in significantly higher volumetric energy storage density compared to most organic PCMs, which enables compact TES system design [30,31].

Cost-effectiveness: In comparison to organic PCMs such as paraffins and fatty acids, salt hydrates are generally abundant and inexpensive, making them economically attractive for large-scale and building-integrated thermal energy storage systems [14].

Wide availability: Several salt hydrates, including sodium acetate trihydrate ($CH_3COONa \cdot 3H_2O$), calcium chloride hexahydrate ($CaCl_2 \cdot 6H_2O$), and sodium sulphate decahydrate ($Na_2SO_4 \cdot 10H_2O$), are readily available and have melting temperature suitable for building thermal comfort applications [21,31].

Environmental friendliness and safety: Many salt hydrates are non-toxic and non-flammable, which enhances their safety and suitability for practical applications in residential and commercial buildings [13,29].

1.5.2 Applications of Salt Hydrates

Solar thermal energy storage: Salt hydrates are widely used to store excess solar thermal energy for domestic hot water systems and space heating applications, enabling better utilization of intermittent solar resources[32].

Building energy efficiency enhancement: The integration of salt hydrates into building envelopes, such as wallboards, ceilings, and composite panels, improves indoor thermal regulation, reduces peak cooling and heating loads, and lowers overall HVAC energy consumption[19,27].

Industrial waste heat recovery : Salt hydrate-based TES systems have also been explored for capturing and reusing low- to medium-grade industrial waste heat, contributing to improved energy efficiency and reduced thermal losses in industrial processes[16,23].

1.5.3 Challenges in Using Salt Hydrates

Despite their attractive thermophysical properties and cost advantages, salt hydrate-based phase change materials (PCMs) face several inherent challenges that hinder their widespread and long-term application in thermal energy storage systems[13,16,31].

Supercooling: Supercooling occurs when the liquid phase of a salt hydrate fails to crystallize at its equilibrium freezing temperature, resulting in delayed solidification and postponed release of stored thermal energy [27,31]. Excessive supercooling can significantly reduce system efficiency and reliability, particularly in building applications requiring predictable thermal response[30].

Phase segregation: During repeated melting and solidification cycles, salt hydrates may undergo phase segregation, in which the salt and water components separate due to differences in density or incongruent melting behavior. This leads to inhomogeneous composition, loss of effective latent heat capacity, and deterioration of long-term thermal performance[14,21,31].

Low thermal conductivity: Many salt hydrates exhibit relatively low thermal conductivity, which restricts heat transfer rates during the charging and discharging processes and limits the overall power density of the TES system[29,31].

Long-term instability: Repeated melting and solidification cycles can induce material degradation, such as dehydration, structural breakdown, or chemical incompatibility with containment materials[19,32].These effects can result in a gradual reduction of storage capacity and cycling stability over time.

1.6 Heat Storage and Release Mechanisms in Salt Hydrate Phase Change Materials

Salt hydrates store and release thermal energy primarily through latent heat associated with phase change, which makes them highly attractive materials for thermal energy storage (TES) in building and energy systems[31,54]. Unlike organic phase change materials, where energy storage is governed mainly by physical melting and freezing, the heat transition mechanism in salt hydrates is fundamentally controlled by hydration and dehydration reactions within the crystalline structure[55,56].

During heat charging (heating), a salt hydrate absorbs thermal energy and undergoes dehydration, involving the breaking of ionic and hydrogen bonds between the salt and its crystallization water[51]. The absorbed heat is stored as latent heat corresponding to the energy required to overcome these bonding forces within the hydrate lattice. Depending on the specific salt hydrate system, dehydration may occur as a complete or partial process[54].

During heat discharging (cooling), the reverse reaction takes place. The anhydrous or partially dehydrated salt reacts with available water molecules to reform the hydrated crystalline structure through hydration, releasing the previously stored latent heat to the surroundings [16,32]. This reversible hydration-dehydration mechanism enables effective thermal regulation in TES applications.

Melting behaviour of salt hydrates

The nature of heat storage and release in salt hydrates strongly depends on their melting behaviour[54,57]:

Congruent melting: The salt hydrate melts uniformly, forming an anhydrous salt and liquid water that remain in thermodynamic equilibrium. Upon cooling, the original hydrate reforms completely, enabling highly reversible heat storage and release.

Incongruent melting: The hydrate decomposes into a lower hydrate or anhydrous salt that does not fully dissolve in the released water, limiting rehydration and reducing latent heat recovery.

Semi-congruent melting: Only a fraction of the salt converts back to the original hydrate, resulting in intermediate and partially reversible heat storage behaviour.

Hydration-dehydration reaction mechanisms

Let AB represent an inorganic salt. For salt hydrates exhibiting congruent melting behaviour, heat charging causes the salt hydrate ($AB{\cdot}nH_2O$) to absorb the heat of fusion (Q_3) and decompose into solid anhydrous salt and liquid water, as expressed by Equation 1.1[51,54]. During cooling, the reverse reaction occurs, releasing the stored latent heat (Q_3) and reforming the salt hydrate, as shown in Equation 1.2[54].

Dehydration:

$$AB \cdot nH_2O \overset{Q_3}{\rightarrow} AB + nH_2O \quad \textbf{(1.1)}$$

Hydration:

$$AB + nH_2O \overset{Q_3}{\rightarrow} AB \cdot nH_2O \quad \textbf{(1.2)}$$

In salt hydrates exhibiting incongruent or semi-congruent melting, heating may result in partial dehydration, forming lower hydrates instead of the anhydrous salt (Equation 1.3). During cooling, insufficient water availability may prevent complete rehydration, leading to the formation of a lower hydrate rather than the original compound (Equation 1.4)[58,59].

Partial dehydration:

$$AB.nH_2O \overset{Q_4}{\rightarrow} AB \cdot lH_2O + (n-l)H_2O (l < n) \quad \textbf{(1.3)}$$

Partial hydration:

$$AB.nH_2O \overset{Q_4}{\rightarrow} AB \cdot pH_2O + (n-p)H_2O(p < n) \quad \textbf{(1.4)}$$

Such incomplete reversibility adversely affects long-term thermal performance and is a major limitation of many salt hydrate PCMs[60].

1.7 Polyurethane Foam as a PCM Support Matrix

One effective strategy to overcome the limitations of salt hydrate PCMs involves incorporating them into porous supporting matrices. Open-cell polyurethane (PU) foam has emerged as a particularly promising host material due to its interconnected pore structure and mechanical flexibility[61-64].

The capillary confinement provided by PU foam suppresses phase segregation and leakage while promoting more uniform nucleation and crystallization during thermal cycling. By immobilizing the PCM within the foam matrix, PU-PCM composite transform salt hydrates into shape-stabilized thermal energy storage media with improved mechanical integrity and cycling stability[42].

Moreover, PU-PCM composite can be readily integrated into building components such as wall panels, sandwich structures, and modular thermal storage units. However, embedding PCMs within a porous matrix alters the effective thermophysical properties of the system. Parameters such as effective thermal conductivity, latent heat storage capacity, phase change kinetics, and solid-liquid interface evolution become strongly dependent on PCM loading, composite morphology, and thickness[65].

1.8 Role of Numerical Modelling in PCM System Design

Numerical modelling plays a crucial role in the analysis, design, and optimization of thermal energy storage (TES) systems, particularly those based on phase change materials. Advanced numerical simulation tools enable detailed visualization of transient temperature fields, phase fraction evolution, and coupled heat transfer mechanisms, which are often

difficult or impractical to capture experimentally, especially within opaque or embedded PCM system.

When rigorously validated against experimental data, numerical models evolve into powerful predictive tools for parametric optimization, allowing systematic investigation of key design and operating parameters such as PCM thickness, storage module or reactor size, boundary conditions, and operating temperature ranges. Such modelling approaches significantly reduce experimental trial-and-error and support scale-up from laboratory specimens to building-integrated TES systems.

Numerical modelling is particularly valuable for polyurethane-based PCM (PU-PCM) composite, where coupled heat conduction, latent heat effects, and phase change dynamics occur within a heterogeneous porous medium. In these systems, numerical methods such as the enthalpy-based formulation are essential for accurately capturing the complex interactions between the PCM, polymer matrix, and external thermal boundary conditions, thereby enabling informed performance optimization and scalability assessment.

1.9 Need for Performance Optimization and Scalability Studies

Most PCM studies reported in the literature are limited to small-scale samples and idealized boundary conditions. While these studies provide valuable insights into intrinsic material behaviour, they often fail to capture the complexities associated with scaling up TES systems for real building applications[66–68].

As PCM volume, composite thickness, or reactor size increases, heat transfer pathways, phase change dynamics, and thermal response times can change significantly. A PCM configuration that performs well at laboratory scale may exhibit delayed charging and discharging, incomplete phase change, or non-uniform temperature distribution at larger scales[64].

Therefore, performance optimization cannot be decoupled from scalability. Systematic investigation of scale-dependent thermal behaviour is essential for translating PCM concepts into practical, building-integrated solutions.

1.10 Summary

This chapter establishes the motivation for the research by highlighting the growing global energy demand and the disproportionate contribution of the building sector to energy consumption, particularly through cooling loads in hot and composite climates like India. It introduces thermal energy storage (TES) as a solution to the temporal mismatch between energy availability and demand, and classifies TES technologies into sensible heat storage, latent heat storage, and thermochemical energy storage, emphasising the superior energy density of latent heat storage using phase change materials (PCMs). The chapter then classifies PCMs into organic, inorganic, and eutectic categories, detailing their thermophysical, kinetic, chemical, and economic properties, and identifies salt hydrates specifically sodium sulphate decahydrate ($Na_2SO_4 \cdot 10H_4O$) as a promising candidate owing to its high latent heat (~254 kJ/kg), low cost, and phase transition temperature of ~32 °C suited to passive building cooling. It further discusses the challenges associated with salt hydrates (supercooling, phase segregation, low thermal conductivity) and introduces the polyurethane foam composite (PU-PCM) approach and numerical modelling as strategies to overcome these limitations.

CHAPTER - 2

Literature Review

2.1 Introduction

This chapter presents a systematic and critical review of the literature on salt hydrate-based phase change materials (PCMs) for latent heat thermal energy storage (TES), with particular emphasis on applications relevant to building thermal management. The review traces the problem from its origins through the state of the art, identifies specific research gaps, and derives the research objectives and scope of the present thesis.

Salt hydrates have emerged as promising Phase Change Materials (PCMs) for thermal energy storage (TES) due to their high energy density, affordability, and wide availability [13,69]. These materials utilize the latent heat of fusion during phase transitions to store and release thermal energy, making them ideal for applications in renewable energy systems, building heating and cooling, and industrial waste heat recovery [51,70]. Despite their advantages, the practical implementation of salt hydrates is limited by challenges such as supercooling, phase segregation, low thermal conductivity, and long-term thermal instability [71,72].

Recent advancements have addressed these issues through innovative strategies. Supercooling mitigation has been achieved by incorporating nucleating agents such as borax, graphene oxide, and metal nanoparticles to enhance crystallization [73,74]. To counter phase segregation, researchers have utilized thickening agents like carboxymethyl cellulose (CMC) and silica gels, as well as polymer-salt composite for improved structural stability [75,76]. Furthermore, the thermal conductivity of salt hydrates has been significantly enhanced using thermally conductive additives such as carbon nanotubes (CNTs), graphene, and metal foams, enabling faster heat transfer. Encapsulation

technologies, including microencapsulation and microencapsulation, have played a crucial role in preventing leakage, reducing supercooling, and enhancing PCM durability [77,78].

Despite these advancements, challenges remain in achieving long-term performance, scalability for industrial applications, and economic feasibility. Future research directions include the development of hybrid PCM systems, intelligent PCMs with adaptive thermal properties, and computational modelling for performance optimization [69,78,79].

This chapter provides a comprehensive review of recent advancements, challenges, and future opportunities for salt hydrates as PCMs. By critically analysing state-of-the-art research, this review highlights the potential of salt hydrates to contribute to sustainable energy solutions and identifies key pathways for overcoming existing limitations, ensuring their effective deployment in thermal energy storage systems.

2.2 Supercooling: Mechanisms, Effects, and Mitigation Strategies

2.2.1 Definition, Mechanism and Practical Implications

Supercooling in salt hydrate PCMs is the depression of the effective crystallization (freezing) temperature below the thermodynamic equilibrium melting point, which delays or suppresses heat release and can cause incomplete solidification, phase separation and loss of latent heat capacity over repeated cycles [51,72].

Supercooling in hydrated salts arises because the liquid phase persists metastably in the absence of sufficient crystal nuclei, so crystallization starts only when a critical undercooling, $\Delta T = T_{\mathrm{m}} - T_{\mathrm{c}}$ is reached [51,80]. Excessive supercooling (often 10-30 °C or more for systems such as sodium acetate trihydrate and sodium sulfate decahydrate) leads to delayed thermal discharge, non-predictable operating temperature and “thermal hysteresis” in storage units, which is detrimental for building and cold-chain applications that require tight temperature control [72,76,81].Moreover, repeated cycling under severe

supercooling conditions can exacerbate phase segregation (formation of anhydrous salt sediments and water-rich layers), thereby reducing effective latent heat, and accelerating material degradation, as widely reported for $Na_2SO_4 \cdot 10H_2O$ and $Na_2HPO_4 \cdot 12H_2O$ eutectics and other hydrated salts [81–83].

2.2.2 Nucleating agents for mitigation of Supercooling

The primary mitigation strategy is to introduce nucleating agents (often used in combination with thickeners or supporting matrices) that provide heterogeneous nucleation sites, reduce the critical free-energy barrier for crystal formation and thus increase the crystallization temperature closer to the melting point [49,51,84]. Recent studies on $Ba(OH)_2 \cdot 8H_2O$, sodium acetate trihydrate, $Na_2SO_4 \cdot 10H_2O$ based mixtures and other hydrated salts demonstrate that well- optimized combinations of inorganic salts (e.g., borax, $BaCl_2 \cdot 2H_2O$, $Na_2SiO_3 \cdot 9H_2O$), nanoparticles (metal oxides, carbon materials) and polymeric thickeners can reduce supercooling from greater than 10-20 °C to as low 1-5 °C while simultaneously enhancing thermal conductivity and cycling stability [76,85].

2.2.2.1 Borax

Borax ($Na_2B_4O_7 \cdot 10H_2O$) is among the earliest and most effective nucleators for Glauber's salt ($Na_2SO_4 \cdot 10H_2O$), where it promotes the formation of $Na_2SO_4 \cdot 10H_2O$ crystals and can reduce the degree of supercooling from approximately 20 °C to below 5 °C in $Na_2SO_4 \cdot 10H_2O$ and $Na_2SO_4 \cdot 10H_2O$-$Na_2HPO_4 \cdot 12H_2O$ eutectics [76,81]. Experimental investigations on $Na_2SO_4 \cdot 10H_2O$ / $Na_2HPO_4 \cdot 12H_2O$ mixtures for cold storage report that borax additions not only decrease supercooling and stabilize the crystallization temperature over more than 150 cycles, but also help maintain nearly constant energy storage capacity, indicating good nucleation reproducibility and minimal degradation[81,82]. Furthermore, polymer-salt systems, borax can also participate in dynamic covalent networks (such as PVA-borax salogels), where it facilitates to gel

formation and, indirectly, promotes better distribution and stabilization of the hydrate phase, although these salogels focus more on leakage and reversibility than on direct supercooling reduction[82].

2.2.2.2 Metal Oxide Nanoparticles (Al_2O_3, TiO_2)

Dispersing metal oxide nanoparticles, such as $Al_2O_3$and TiO_2, into salt hydrate based PCMs serve a dual functional role role. These nanoparticle act as high-surface-area heterogeneous nucleation sites, which promote earlier crystallization and effectively reduce supercooling, while simultaneously enhancing thermal conductivity, thereby accelerating heat transfer during both charging and discharging processes [20,86].Comprehensive reviews of nanoparticle-enhanced PCMs reports that alumina nanoparticles, at loadings of up to approximately 10 wt%, can increase effective thermal conductivity of PCMs by about 25% and reduce melting and solidification times by 10-20%, with several studies also reporting partial mitigation of supercooling due to improved nucleation and heat removal[20,87].

In the context of latent heat storage for solar and PV systems, Al_2O_3 and TiO_2 nanoparticles added to salt hydrates or paraffin-salt-hydrate composite system have been shown to decrease the degree of supercooling while simultaneously enhancing overall heat transfer performance of heat exchangers and PV/T modules[88,89]. Nevertheless, excessive nanoparticle loading may lead to increase viscosity, promote agglomeration and reduction in latent heat per unit mass, so recent studies emphasize optimized low concentrations (typically below 2-3 wt% for hydrated salts), along with surface modification strategies to balance nucleation benefits with stability and storage capacity[86].

2.2.2.3 Graphene oxide

Graphene oxide (GO), as a two dimensional carbon based material enriched with oxygen-containing functional groups, offers a large specific surface area and abundant sites for hydrogen bonding with crystallization water in hydrated salts[73].Comprehensive review on carbon-enhanced hydrated salt PCMs summarizes that GO and related carbon fillers, including graphene, carbon nanotubes (CNTs), expanded graphite, biochar, can significantly improve thermal conductivity while simultaneously suppressing supercooling and phase separation by offering effective hetrogeneous nucleation surfaces and physical confinement of the salt hydrate phase[73].For instance, Tang et al. incorporated a small fraction of GO (~0.2 wt%) into dihydrogen phosphate dodecahydrate (DHPD) encapsulated in expanded vermiculite; the GO-modified composite showed increased latent heat (from 167 J/g to 229 J/g) and reduced crystallization hysteresis, attributed to strong interactions between GO functional groups and water molecules that helped maintain hydrate structure and promote more uniform nucleation. Furthermore, GO can also be combined with other fillers such as surface-modified AlN and carbon fibers to form multifunctional networks where GO improves dispersion and interfacial bonding, indirectly contributing to more consistent nucleation and lower supercooling in hydrated salts [73].

Recent research increasingly emphasizes hybrid additive systems that combine nucleating salts, polymeric thickeners and high-thermal conductivity fillers (carbon- based or ceramic) to simultaneously key limitation of salt hydrates PCMs, including supercooling, phase separation, leakage and low conductivity simultaneously [73,82,84,90]. For example He et al. reported a $Ba(OH)_2 \cdot 8H_2O$-based composite PCM in which the addition of 2 wt% $BaCl_2 \cdot 2H_2O$ (as nucleator) and 1 wt% carboxymethyl cellulose (CMC), as thickener reduced supercooling from approximately 14 °C to 1 °C, while expanded graphite addition significantly enhanced thermal conductivity and provided

structural stability over 1000 thermal cycles [84]. These results highlight how carefully designed hybrid formulation can overcome multiple performance bottlenecks within a single composite system.

Similarly, Tang et al. developed optimized DHPD-based composite using a multicomponent hybrid formulation consisting $Na_2SiO_3 \cdot 9H_2O$ as a nucleator), CMC as a thickener, surface-modified AlN (high-k filler and co-nucleator) and short carbon fibers, achieving simultaneous suppression of supercooling, mitigation of phase separation and significant thermal conductivity improvement [91]. Polymer-salt "salogels" and polyelectrolyte-salt mixtures represent another hybrid approach, where hydrogen-bonded or covalent polymer networks immobilize nitrate or chloride salt hydrates at exceeding 90 wt% loading; these systems primarily target shape stabilization and segregation, but also reduce effective supercooling by maintaining intimate contact between the hydrate and nucleating domains within a continuous gel network[90].More recently, emerging 3D-printed salt-hydrate composite, produced by direct-ink-writing with integrated nucleators and rheology modifiers, illustrate how hybrid formulations can be tailored for application-specific geometry and cycling conditions while embedding nucleation sites throughout the printed structure to avoid localized supercooling[49].

2.2.3 Encapsulation Techniques to Reduce Supercooling

Encapsulation of salt hydrate PCMs physically confines the phase change material and its water of crystallization, which can moderate supercooling by providing abundant nucleation interfaces, stabilizing composition, and improving heat transfer during crystallization[92].

Encapsulation at micro- or macro-scale effectively limits phase separation, minimizes water loss, and introduces solid-liquid interfaces that promote heterogeneous nucleation, thereby shifting the crystallization temperature closer to the equilibrium

melting point and significantly reducing supercooling [51,92,93]. Recent investigations on salt hydrates such as $CaCl_2 \cdot 6H_2O$, $Na_2SO_4 \cdot 10H_2O$, $Mg(NO_3)_2 \cdot 6H_2O$ and eutectic hydrated salt systems, demonstrate that well-designed core-shell capsules or encapsulated composite structures can reduce supercooling to only a few degrees Celsius while maintaining high latent heat storage capacity and long-term cycling stability [1,49,94].

Microencapsulation involves the formation of core-shell particles or fibers typically ranging from 1-500 μm in size (and in some cases extending to the submicron scale), in which salt hydrate are confined with in polymeric or inorganic shell. This strategy increases the effective heat transfer area, prevents leakage of the liquid phase, and stabilizes the local micro-environment of the hydrate, thereby mitigating phase separation and suppressing supercooling [92,95]. By introducing abundant solid-liquid interfaces, microencapsulation facilitates heterogeneous nucleation and promotes crystallization at temperature closer to equilibrium, making it particularly attractive for long-term thermal energy storage applications.

Several recent experimental studies have demonstrated the effectiveness of microencapsulation in reducing supercooling and improving cycling stability. A study fabricated microcapsules with eutectic hydrated salt (EHS) cores via complex coacervation at room temperature, reporting that both the degree of supercooling and the loss of melting enthalpy after 100 thermal cycles were significantly lower than those observed in bulk salt hydrates, owing to the stable core-shell interface and restricted component segregation[95]. Similarly, Mahakul et al. microencapsulated $CaCl_2 \cdot 6H_2O$ within a rigid silica shell using electrohydrodynamic atomization, producing nearly spherical microcapsules with a narrow size distribution and stable latent heat over repeated cycling; the inorganic silica shell effectively suppressed leakage and alleviated the severe supercooling commonly encountered in bulk $CaCl_2 \cdot 6H_2O$ [96,97].

More advanced encapsulation architectures further highlight the role of confinement and interfacial effects in controlling supercooling behavior. A 2025 study employing coaxial electrospinning produced core-shell fibers with $CaCl_2 \cdot 6H_2O$ as the core and PVP/PMMA as the shell, where DSC measurements revealed that bulk $CaCl_2 \cdot 6H_2O$ crystallized near −10 °C despite a melting point of ~30 °C, while the encapsulated fibers exhibited a substantially higher crystallization temperature, indicating pronounced supercooling reduction due to nanoscale confinement and the presence of continuous interfaces along the fiber walls [94].

For magnesium nitrate hexahydrate ($Mg(NO_3)_2 \cdot 6H_2O$), microcapsules prepared using nonaqueous Pickering emulsions stabilized by alkylated graphene oxide, followed by polymer shell formation, showed suppressed undercooling, with GO nanosheets acting as internal nonspecific nucleating agents while also reinforcing the capsule structure[49]. Earlier nano- and micro-scale encapsulation studies of $Mg(NO_3)_2 \cdot 6H_2O$ and $Na_2SO_4 \cdot 10H_2O$ using polymer shells formed via miniemulsion techniques similarly demonstrated that nanoscale confinement and robust shell integrity can markedly reduce supercooling and preserve hydration levels over at least 100 thermal cycles, laying the foundation for recent microencapsulation designs aimed at building-integrated TES systems[92,93].

Macroencapsulation involves embedding salt hydrate phase change materials (PCMs) within relatively large containers, such as metal or plastic tubes, pouches, panels, hollow bricks, or concrete blocks. Although the characteristic dimensions are on the centimeter scale, the container walls provide solid interfaces that act as preferential heterogeneous nucleation sites and, when combined with suitable additives, can significantly suppress supercooling[51,98]. In addition to nucleation control, macroencapsulation limits leakage, improves handling safety, and facilitates direct

integration of PCMs into building components, making it particularly suitable for building-scale thermal energy storage applications.

Several recent studies demonstrate the effectiveness of macroencapsulation for stabilizing the thermal behavior of salt hydrate PCMs in buildings. Rehman et al. (2023) evaluated a macroencapsulated salt hydrate PCM with a melting point of approximately 21 °C, integrated into standard concrete blocks, and reported that the encapsulated configuration enhanced wall thermal inertia while maintaining stable and repeatable melting/freezing temperature over repeated thermal cycles; importantly, supercooling was confined within a narrow temperature band, rendering the system suitable for passive building operation[99]. Similarly, macroencapsulation within hollow bricks or concrete blocks for shelter walls has been shown to provide effective thermal management in cold climates, where the phase change temperature remained consistent and the degree of undercooling was sufficiently low to ensure reliable nighttime solidification and daytime melting under both simulated and real operating conditions[100].

At larger composite scales, recent studies (2023-2025) have demonstrated that macroencapsulation combined with highly conductive porous matrices can nearly eliminate supercooling. In particular, $CaCl_2 \cdot 6H_2O$ -based composite incorporated into compressed expanded graphite (EG) matrices, which function as rigid macroencapsulated porous monoliths, achieved thermal conductivities of approximately 4 W m^{-1} K^{-1}, supercooling below 1 °C, and latent heat values as high as ~183 J g^{-1}, with no measurable degradation in latent heat over 200 thermal cycles [1]. These results highlight that rigid, high-conductivity matrices can synergistically combine encapsulation, confinement, and nucleation effects to enable near-supercooling-free operation. In a similar vein, a recently developed prefabricated composite panel consisting of $CaCl_2 \cdot 6H_2O$-KCl salt hydrate embedded within a porous support material exhibited reduced supercooling and enhanced

cycling stability, which was attributed to the combined influence of nucleating agents, pore-level confinement, and improved thermal conductivity of the composite structure[57].

Encapsulation studies on specific salt hydrates further underline the importance of design parameters. Experimental investigations on encapsulated sodium acetate trihydrate (SAT) have shown that capsule size, initial PCM temperature, and filling ratio significantly affect the degree of supercooling, with smaller capsule volumes and carefully controlled preconditioning temperature resulting in lower undercooling, thereby providing practical design guidelines for real-world SAT-based TES systems [34]. Comprehensive reviews of core-shell encapsulated salt hydrates and nano-additive-enhanced PCM systems consistently emphasize that encapsulation is most effective when combined with nucleating agents and suitable support matrices, enabling simultaneous control of supercooling, phase separation, leakage, and low thermal conductivity, which is critical for applications in building envelopes, cold storage, and solar thermal energy storage [92,101].

2.3 Phase Segregation: Mechanisms, Consequences, and Prevention Strategies

Phase segregation in salt hydrate PCMs is the irreversible separation of salt-rich and water-rich phases during melting/solidification, which reduces the fraction of material that actually crystallizes as hydrate and therefore causes progressive loss of latent heat and unstable operating temperature.

2.3.1 Phase segregation and inefficiency

In hydrated salt phase change materials, phase segregation commonly occurs when dense anhydrous or low-hydrate crystals settle under gravity while lighter, water-rich liquid phases rise, particularly during repeated thermal cycling; this phenomenon prevents complete rehydration and causes a gradual deviation of the PCM composition from its intended stoichiometry[51,102,103]. As a consequence, the material experiences a rapid deterioration of effective latent heat storage capacity, accompanied by broadening and

progressive shifting of the phase change temperature range, and in severe cases, complete functional failure after only tens to hundreds of cycles. Such degradation behavior has been widely reported for salt hydrate systems including $Na_2SO_4 \cdot 10H_2O$, $CaCl_2 \cdot 6H_2O$, and sodium acetate trihydrate (SAT)[51,104]. Accordingly, recent review studies consistently identify phase segregation—alongside supercooling and inherently low thermal conductivity—as one of the principal obstacles to the large-scale commercialization of salt hydrate PCMs for building-integrated and industrial thermal energy storage applications [103].

2.3.2 Thickening agents for mitigation of phase segregation

2.3.2.1 Carboxymethyl Cellulose (CMC)

One of the most widely adopted strategies to mitigate phase segregation is the incorporation of thickening or gelation agents, which significantly increase the viscosity of the molten salt hydrate or form three-dimensional gel networks, thereby suppressing sedimentation and convective separation while maintaining a homogeneous distribution of salt and water [75,103,105].

Gel-forming additives, such as carboxymethyl cellulose (CMC), xanthan gum (XG), starch, gelatin, and silica-based gels, have been demonstrated to reduce or even eliminate visible phase separation in $Na_2SO_4 \cdot 10H_2O$ based systems as well as sodium acetate trihydrate (SAT); however, this stabilization is often accompanied by a modest reduction in latent heat on a mass basis, attributable to the presence of the inert gel fraction[105,106].

Carboxymethyl cellulose (CMC) is an anionic cellulose derivative that forms hydrogen-bonded and ionically interacting gel networks with water and dissolved salts, enabling the entrapment of hydrated salt domains and the mechanical suppression of segregation of anhydrous crystals and free water[75,107].

Recent systematic investigations have shown that the effectiveness of CMC strongly depends on its molecular weight and formulation parameters. In a 2024 study, CMC with a moderate molecular weight (~90 kg mol^{-1}) was found to form robust and continuous gel networks that maintained compositional homogeneity and effectively reduced phase separation, whereas very high molecular weight CMC (~700 kg mol^{-1}) failed to stabilize certain Na_2SO_4 based systems, resulting in gel rupture and sedimentation of anhydrous salt crystals [75].

The same study further demonstrated that the gel point and stabilization performance of CMC-based systems are governed by multiple interacting factors, including CMC concentration, degree of substitution, ionic strength, and pH. Increased Na^+ content originating from sodium carboxymethyl cellulose can strengthen ionic crosslinking and enhance gel rigidity, but simultaneously raises the fraction of inert material, thereby necessitating a careful optimization between effective segregation control and achievable energy storage density[75]. Beyond conventional thickening, CMC-based hydrogels chemically crosslinked with small organic acids, such as citric acid, are emerging as superabsorbent polymer networks capable of immobilizing large quantities of hydrated salts while resisting syneresis, pointing toward more robust and durable frameworks for next-generation salt hydrate PCM systems[107].

2.3.2.2 Xanthan gum

Xanthan gum (XG) is a high-molecular-weight anionic polysaccharide that is widely employed as a rheology modifier, owing to its coil-network molecular structure and pronounced sensitivity to ionic strength, which enable it to dramatically increase the zero-shear viscosity of aqueous salt solution[108]. An experimental study on the solidification behavior of supercooled sodium acetate trihydrate (SAT) reported that, among several investigated thickening agents—including gelatin, CMC, starch, xanthan gum, urea,

poly(vinyl alcohol) (PVA), and polyacrylamide (PAM)—xanthan gum and CMC were the most effective in suppressing phase segregation while preserving acceptable phase change kinetics[105].

Complementary rheological investigations further reveal that dissolved salts screen electrostatic repulsion along the XG backbone, leading to chain compaction at moderate ionic strengths, whereas at elevated temperature, chain expansion and enhanced intermolecular interactions re-establish a strong viscoelastic network. This salt- and temperature-dependent rheological behavior provides a mechanistic explanation for the effectiveness of xanthan gum in stabilizing hydrated salt PCMs under repeated thermal cycling conditions [108].

2.3.2.3 Silica Gel and Porous Inorganic Matrices

Silica gel offers a rigid and highly porous inorganic framework capable of immobilizing salt hydrate solutions within its pore network, thereby restricting macroscopic liquid water movement and suppressing sedimentation of salt crystals [92,93,103]. In encapsulated salt hydrate PCM systems, silica has been employed both as an external shell material (e.g., silica microcapsules) and as an internal porous scaffold; in either configuration, it provides excellent chemical stability and mechanical robustness, while effectively mitigating leakage and phase segregation during repeated thermal cycling[96,97]. Furthermore, silica-based aerogels and xerogels are able to accommodate very high salt loadings (often exceeding 80-90 wt%) with minimal phase separation, and recent studies on $CaCl_2 \cdot 6H_2O$- and $Na_2SO_4 \cdot 10H_2O$ based composite demonstrate markedly improved cycling stability when salt hydrates are confined within silica networks compared with their bulk counterparts[83,103].

2.3.2.4 Polymer and Nanomaterial Composite

Composite phase change materials (PCMs) integrate salt hydrates with polymeric matrices and/or nanostructured additives to simultaneously mitigate key limitations, including phase segregation, supercooling, and inherently low thermal conductivity[49,51,103]. The underlying design principle involves employing polymer networks or porous support matrices to provide physical confinement and viscosity enhancement, while nanomaterials introduce abundant heterogeneous nucleation sites and continuous heat-transfer pathways, thereby promoting more uniform crystallization behavior and ensuring stable long-term thermal performance under repeated cycling[49,103,109].

Poly(ethylene glycol) (PEG) is a linear, hydrophilic polymer that interacts strongly with water and dissolved salts, enabling the formation of either polymer-salt aqueous biphasic systems or homogeneous gel-like mixtures, depending on composition, chain length, and concentration[110,111]. The phase behavior and miscibility of PEG with the salt hydrate phase are therefore highly tunable, making PEG an attractive component for composite PCM design. Early studies on sodium acetate trihydrate (SAT)-ethylene glycol (EG)/PEG systems demonstrated that the addition of EG or PEG suppresses phase separation by restructuring the hydrogen-bond network of water and increasing solution viscosity, while simultaneously enabling adjustment of the phase change temperature [111,112].

More recent developments further highlight the multifunctional role of PEG in salt hydrate PCMs. A 2025 study reported a novel organic-inorganic eutectic PCM based on SAT and PEG, which exhibited high latent heat and improved cycling stability without pronounced macroscopic phase separation, demonstrating that PEG can function both as a co-PCM and as an effective stabilizer that hinders large-scale demixing [113].

Fundamental investigations of PEG-salt aqueous biphasic systems, such as PEG/K_2HPO_4, using NMR, Raman spectroscopy, and calorimetry, reveal that phase separation is primarily governed by size and shape asymmetry and salting-out effects rather than large enthalpy changes. These mechanistic insights provide valuable guidelines for selecting appropriate PEG molecular weight and salt compositions to maintain single-phase regions, thereby informing the rational design of PEG-salt hydrate composite PCMs with enhanced stability [110].

Polyacrylamide (PAM) hydrogels form three-dimensional, crosslinked polymer networks capable of entrapping large quantities of water and dissolved salts, enabling them to function as shape-stable and leak-free phase change materials when loaded with salt hydrates[106,114]. Comparative investigations of thickening agents for sodium acetate trihydrate (SAT) indicate that PAM alone is generally less effective than xanthan gum or carboxymethyl cellulose (CMC) in suppressing phase segregation; nevertheless, PAM-based hydrogels remain attractive due to their tunable mechanical strength and structural integrity, which allow combination with other polymers or functional fillers to enhance overall stability[105,106]. Consequently, hybrid hydrogel systems that integrate PAM with CMC or other polysaccharides are emerging as promising candidates for mechanically robust, highly loaded salt hydrate composite, capable of maintaining compositional homogeneity under repeated melting-freezing cycles. However, comprehensive long-term cycling and segregation studies for these hybrid systems are still scarce, highlighting an active and important area for future research [75,105].

Nanomaterials including graphene oxide (GO), carbon nanotubes, expanded graphite (EG), nanosilica, and metal oxide nanoparticles such as Al_2O_3 and TiO_2—are widely employed to construct thermally conductive, high-surface-area skeletons that immobilize the salt hydrate phase while simultaneously providing abundant heterogeneous

nucleation sites[49,73,86,109]. A study focused on achieving exceptional thermal stability in salt hydrate composite

demonstrated that confinement of the PCM within a nanostructured porous matrix inhibits the formation of large, sharp-cornered crystals during solidification, which significantly reduces mechanical damage, phase segregation, and performance degradation over prolonged thermal cycling [109].

Recent advances in additive manufacturing further illustrate these benefits, as direct ink writing of salt hydrate composite incorporating nucleating nanoparticles and rheology modifiers has enabled the fabrication of printable, non-corrosive PCM structures, in which the polymer-nanofiller network effectively immobilizes the salt phase, eliminates visible segregation over extended cycling, and enhances thermal conductivity[49]. Similarly, hybrid emulsion-gel systems developed for sodium acetate trihydrate (SAT) that combine GO, suitable emulsifiers, and polymer networks have achieved excellent shape stability, negligible phase separation, and high energy storage density, highlighting the strong synergy between polymer gels and two-dimensional carbon nanofillers in advanced salt hydrate PCM design[79].

2.4 Thermal Conductivity Enhancement of Salt Hydrate PCMs

Salt hydrate PCMs typically have low thermal conductivity (≈0.4-0.7 W/m·K), which severely limits charging/discharging rates in thermal energy storage systems and leads to large temperature gradients and incomplete utilization of latent heat in practical modules[48,51,115].

2.4.1 Poor conductivity of salt hydrates

Inorganic hydrated salts, such as $CaCl_2 \cdot 6H_2O$, sodium acetate trihydrate, and various nitrate- and nitrite-based salts, often exhibit thermal conductivities only marginally higher than those of organic PCMs, such that heat transfer, rather than storage capacity,

becomes the dominant performance bottleneck in thermal energy storage (TES) systems[48,51]. As a result, TES units based on these materials frequently suffer from prolonged melting and solidification times, non-uniform temperature distributions, and reduced effective power density, particularly in large-scale modules or compact heat exchanger configurations, thereby motivating extensive research into thermal conductivity enhancement strategies[48,115,116].

2.4.2 Additives for conductivity enhancement

To address this limitation, two broad classes of conductivity-enhancing additives are commonly employed: high-thermal-conductivity nanomaterials, including carbon-based and metal-oxide-based fillers, and metallic structures such as metal foams; in many advanced formulations, these approaches are combined in hybrid PCMs to form percolated heat-transfer networks throughout the salt hydrate matrix, thereby substantially improving overall heat transport performance[48,73,101].

2.4.3 Nanomaterials for conductivity enhancement

Graphene and graphene-derived materials possess exceptionally high intrinsic in-plane thermal conductivity (reported to be as high as ~2000-5000 W m^{-1} K^{-1}), and when incorporated into hydrated salt PCMs, they can form continuous or semi-percolated thermally conductive networks, thereby enhancing the effective thermal conductivity of the composite and reducing internal temperature gradients[73,117].

A comprehensive review on carbon-enhanced hydrated salt PCMs indicates that graphene nanoplatelets and graphene nanosheets typically achieve thermal conductivity enhancements of approximately 50-75% at relatively low filler loadings, while simultaneously providing heterogeneous nucleation sites and mechanical reinforcement to the PCM matrix [73]. For instance, hydrated salt composite filled with graphene nanosheets have exhibited conductivity increases of up to ~72.5%, which are slightly lower than those

obtained with carbon nanotube (CNT) fillers, but are often accompanied by superior cycling stability and more straightforward processing routes[73]. Furthermore, a investigation into PCM-graphene composite, including salt-based PCMs, demonstrated that carefully optimized graphene loadings can significantly improve heat conduction while preserving high latent heat, particularly when graphene is combined with porous support structures to suppress aggregation and prevent leakage of the molten salt phase [117].

2.4.4 Carbon-Based Additives

Carbon nanotubes (CNTs) combine exceptionally high intrinsic thermal conductivity with a large aspect ratio, enabling efficient percolation and network formation at very low volume fractions; consequently, CNT-reinforced hydrated salt PCMs can more than double their effective thermal conductivity[73,101,118].

According to a comprehensive 2024 review on carbon-enhanced hydrated salt PCMs, CNT-based composite achieved an ~82.5% increase in thermal conductivity, outperforming other carbon fillers such as mesoporous carbon (~75%), graphene nanosheets (~72.5%), and nanographite (~65%) at comparable loadings, a result attributed to the superior connectivity of CNT networks[73].

The effectiveness and durability of CNT-salt systems are further demonstrated in high-temperature “solar salt” PCMs (60:40 $NaNO_3/KNO_3$), where the addition of only 0.5 wt% CNTs increased thermal conductivity by approximately 127% before cycling and 125% after 300 thermal cycles; although latent heat decreased by about 15%, chemical stability was preserved, underscoring the robustness of CNT-based conductive networks under prolonged operation[118]. Additional examples reported in the same review describe amorphous CNT networks achieving thermal conductivities as high as 3.23 $W\ m^{-1}\ K^{-1}$ in salt hydrate composite, with conductivity increasing further after PCM melting due to

improved CNT connectivity in the liquid phase, highlighting the dynamic percolation behavior of CNT-filled PCMs [73].

Metal oxide nanoparticles, particularly Al_2O_3, are widely employed as conductivity-enhancing additives due to their moderate intrinsic thermal conductivity, excellent chemical stability, and relatively low cost; in hydrated salt PCMs, they are typically incorporated at loadings of ≤10 wt% to balance thermal conductivity enhancement against increases in viscosity and reductions in effective latent heat[48,86,119].

A critical review of nanoparticle-enhanced PCMs reports that the addition of alumina nanoparticles can increase thermal conductivity by approximately 25% and shorten melting and solidification times by 10-20%, although the magnitude of these improvements is strongly dependent on particle size, surface characteristics, and dispersion quality within the PCM matrix[86].

More recently, $CaCl_2 \cdot 6H_2O$-based nano-enhanced PCMs developed for battery and electronics cooling applications have employed metal nanoparticles (such as Cu) in combination with Al_2O_3 to accelerate heat removal, with coupled numerical simulations and experimental measurements demonstrating substantial reductions—often exceeding 20-30%—in peak device temperature at optimized nanoparticle loadings, highlighting the practical effectiveness of metal oxide nanoparticles for thermal management-oriented TES systems[48,119].

Open-cell metal foams, typically fabricated from aluminium, copper, or nickel, possess very high intrinsic thermal conductivities (approximately 90-400 W m^{-1} K^{-1}) together with an exceptionally large specific surface area, making them highly effective three-dimensional heat-spreading frameworks when infiltrated with phase change materials (PCMs), including salt hydrates[115,116]. A recent comprehensive review of metal

foam/PCM composite reports that PCM-metal foam systems can achieve effective thermal conductivities up to 218 times higher than those of pure PCMs, depending on foam porosity, pore size, and ligament thickness, with heat conduction through the continuous metallic skeleton dominating the overall heat transfer process[115]. Both numerical simulations and experimental investigations consistently confirm that metal foams reduce melting and solidification times far more effectively than conventional fins or nanoparticle additives alone; however, excessive metal volume fractions can lower the effective energy storage density and significantly increase material cost, necessitating careful optimization of foam architecture[115,120]. In a recent study targeting electronics cooling applications, high-porosity metal foam/PCM composite were shown to markedly enhance heat dissipation and reduce internal PCM temperature, by increasing effective thermal conductivity and promoting more uniform heat distribution throughout the composite structure[121].

Hybrid phase change materials (PCMs) that integrate metal foams with nanoparticle additives are designed to exploit multiscale heat-transfer pathways, wherein the metal foam provides a macroscopic three-dimensional conductive skeleton, while nanomaterials bridge microscale gaps and enhance interfacial thermal contact with the salt hydrate phase [48,101,120]. A study on reverse latent heat power generation employing such hybrid PCMs demonstrated that an optimized configuration—a 15 pores-per-inch (PPI) metal foam combined with 1.0 wt% nanoparticles—reduced the internal temperature of the hybrid PCM by 35.92% and 20.93%, respectively, compared with systems containing only metal foam or only nanoparticles, clearly evidencing a strong synergistic effect[122].

Complementary numerical investigations of latent heat TES systems incorporating fins, nanoparticles, and metal foams reported solidification time reductions of approximately 73.7%, with time savings reaching up to 75% depending on foam

architecture and nanoparticle volume fraction, when nanoparticles were dispersed within PCM-metal foam composite [120]. More recently, advances in additive manufacturing have shown that direct ink writing of salt hydrate composite, integrating carbon black as a nanoscale additive within a polymer matrix, can increase thermal conductivity by at least 33% while maintaining high salt hydrate loadings (up to ~70 wt%), suggesting strong potential for future hybridization with metallic structures to achieve even greater thermal conductivity enhancements [49].

2.5 Advancements in Salt Hydrate PCMs

2.5.1 Purpose and Mechanisms Encapsulation

Encapsulation of salt hydrate PCMs has evolved from simple macro-containers to engineered core-shell micro/nanostructures and continuous fibers, which prevent leakage, improve thermal and chemical stability, and enable more controlled heat release in practical TES systems[1,61,93].

Encapsulation refers to surrounding a salt hydrate core with a solid shell or embedding it within a stabilizing matrix, which effectively isolates the corrosive and volume-changing PCM from the surrounding environment and structural components[92,93]. This strategy offers several key advantages, including leakage prevention, as the shell or porous host retains the molten hydrate and prevents exudation during repeated melting and solidification cycles[92,93,123].

Encapsulation also enhances long-term stability by suppressing water loss, corrosion, phase segregation, and supercooling, thereby extending cycle life and preserving the effective latent heat storage capacity[124].Furthermore, well-defined core-shell geometries and controlled capsule sizes enable predictable melting and freezing behaviour, while the high surface-area-to-volume ratio of encapsulated systems promotes faster and

more uniform heat exchange, resulting in controlled and reliable thermal energy release [125].

2.5.2 Recent advancements in encapsulation technologies

Recent studies clearly distinguish between microscale core-shell architectures (microencapsulation) and macroscale container-based or composite configurations (macroencapsulation), which are increasingly integrated with advanced manufacturing and fabrication techniques to enhance scalability, structural integration, and thermal performance.

Hybrid encapsulation systems integrate conventional core-shell encapsulation with additional supporting matrices or functional fillers, such as porous silica, expanded graphite, or polymer networks, in order to simultaneously mitigate leakage, low thermal conductivity, supercooling, and phase segregation [123,126]. For example, Shkatulov et al. reported the encapsulation of LiCl, $CaCl_2$, and $SrBr_2$ salt hydrates within hollow mesoporous SiO_2 shells, forming salt@HS composite structures that exhibited rapid hydration-dehydration kinetics, high mechanical integrity, and excellent cycling stability, attributed to the permeable yet confining nature of the silica shell [123]. In a related approach, so-called “NePCMs” (nanocapsule phase change materials) with inorganic-organic hybrid shells have been developed for building thermal energy storage, in which hydrated salt cores are enclosed by composite shells (e.g., silica combined with organic polymers) to achieve non-flammability, enhanced structural stability, and improved thermal conductivity within a single architecture[126].

At the macro scale, Oak Ridge National Laboratory (ORNL) and the National Renewable Energy Laboratory (NREL) have demonstrated compressed expanded graphite (EG) matrices that function simultaneously as macroencapsulation media and high-conductivity heat-transfer networks; in these systems, salt hydrates are infiltrated into

surfactant-treated, compressed EG blocks, yielding shape-stable, non-leaking composite with high effective thermal conductivity, well suited for modular and scalable TES applications[1].

Metal-organic frameworks (MOFs) provide chemically tunable, high-surface-area porous networks capable of hosting water molecules and dissolved salts, and recent studies in phase change and thermochemical energy storage demonstrate that confining hydrates or salt solutions within MOF pores can moderate volume changes, suppress leakage, and enable well-defined sorption-desorption behaviour [123,124].

Investigations on salt hydrate infiltration into porous inorganic hosts, including SiO_2-based materials, suggest that analogous confinement strategies are applicable to MOFs, as salts immobilized within mesoporous or microporous frameworks exhibit enhanced cycling stability and reduced phase segregation, with the rigid framework effectively acting as a "molecular cage"[123]. Although MOF-specific encapsulation of hydrated salt PCMs is still at an early stage, recent review articles on hydrated salt modification strategies consistently identify MOFs and other porous crystalline frameworks as promising next-generation supports, offering the potential to integrate sensible heat, latent heat, and sorption-based storage within unified hybrid energy storage devices[77,124].

2.6 Sodium sulphate decahydrate ($Na_2SO_4 \cdot 10H_2O$, SSD) and other salt hydrates as PCM

Glauber's salt ($Na_2SO_4.10H_2O$) is a prominent PCM for storing thermal energy. Temperature at which it undergoes a phase transition is approximately 32 °C, and its melting enthalpy is approximately 254 J/g. There are substantial deposits of Glauber's salt in China's Qinghai province, which is known for its higher latent heat capacity, non-toxic in nature, low cost and abundance [127,128]. Additionally, it exhibits superior thermal

conductivity in comparison to organic PCMs. Sodium sulfate decahydrate (SSD) is a low-cost and widely available salt hydrate PCM; however, it is notoriously prone to phase separation and rapid performance decay, making its stabilization a long-standing focus of research [85,102,129].

A systematic study evaluated eight polymeric thickening agents and one polyelectrolyte for SSD stabilization, revealing that conventional thickeners, including sodium polyacrylate, polyphosphates, and cellulose nanofibers, successfully increased viscosity but simultaneously reduced effective energy storage capacity and slowed freezing kinetics. Despite the higher viscosity, these systems still exhibited noticeable enthalpy degradation over 150 thermal cycles, indicating incomplete suppression of SSD degradation mechanisms [85].

Purohit and Sistla also performed computational and experimental thermal assessment of the PU-PCM composite [42]. Additionally, computational assessments for thermal analysis of PU-PCM composite using COMSOL 5.0 Multiphysics software, comparing simulation results with experimental findings. The simulation findings revealed an average absolute inaccuracy of 1.15 °C for the temperature difference profile and 0.077 for the proportion of salt hydrate formation in the pores over time, providing insights into the growth and nucleation of salt hydrate crystals inside the composite material. Experimental and computational results were compared for the solid phase fraction inside the pores of PU foam, showing a negligible formation of crystals.

Tao et. al. examined the thermal performance of $Na_2SO_4 \cdot 10H_2O$ PCMs with GO-SiO_2 as a nucleating agent [74]. Supercooling behaviour and thermal conductivity were calculated and observed that adding 2.45 wt% GO-SiO_2 reduced supercooling to 1.2°C, improving PCM stability and efficiency. Dong et. al. [130] have observed that the best composition was (SSD:$Na_2B_4O_7 \cdot 10H_2O$:CMC = 100:5:3) which reduces supercooling to

1.5°C and increased thermal conductivity 3.9 times, ensuring better stability and efficiency for thermal energy storage. Li et. al. in their study improved Adding expanded graphite in sodium sulfate decahydrate reduces the supercooling by 19°C, increases conductivity by 3.6 times, and accelerated heating/cooling times, making this composite ideal for thermal energy storage applications [77]. Adding 3 wt% Al/C increased thermal conductivity by 26.41% and slightly reduced latent heat enthalpy by 5.13% [131]. Three different salt hydrate mixtures ratios (70:30, 80:20, 90:10) were tested using Differential Scanning Calorimetry (DSC). The 90:10 composition exhibited the highest latent heat (173.96 J/g) and thermal stability, making it suitable for low-temperature solar energy storage applications [59].

In contrast, DSS-modified SSD maintained a stable, homogeneous suspension with minimal change in energy storage capacity after 150 cycles; rheology showed that DSS did not significantly increase viscosity but reduced SSD particle size and provided electrostatic stabilization, thereby preventing macroscopic phase separation without severely affecting freezing kinetics[85,132]. Complementary benefits of confinement-based strategies have also been demonstrated for SSD-containing systems. In a study on SSD-SAT eutectics encapsulated within porous mineral supports—such as attapulgite and expanded perlite—the addition of 1.5 wt% borax reduced supercooling from 10.8 °C to 0.7 °C. After 200 thermal cycles, the latent heat of the unencapsulated eutectic decreased by 24.6%, whereas polyurethane-encapsulated composite exhibited only a 10.4% reduction, clearly illustrating the effectiveness of encapsulation in preserving long-term thermal performance [129]. Overall, the combined use of appropriate stabilizers—such as CMC or xanthan gum for structural viscosity, silica frameworks for confinement, graphene oxide or Al_2O_3 for interfacial control and thermal conductivity, and tailored organic polymers or polyelectrolytes for colloidal stabilization—has enabled $CaCl_2 \cdot 6H_2O$, SAT, and SSD

systems to maintain far more stable thermal behaviour under accelerated cycling than unmodified salts, thereby bringing hydrated salt PCMs significantly closer to practical, long-life thermal energy storage deployment[31,74].

Several application-based advancements using $Na_2SO_4 \cdot 10H_2O$ as PCM have also been reported. Ali Gholami and Mofid Gorji used $Na_2SO_4 \cdot 10H_2O$ with copper blades to cool PV panels, achieving a 19.8 °C temperature reduction and a 6.17% gain in electrical efficiency[134]. Baolian Zhang et al. addressed leakage issues by creating shape-stabilized SSD composite using expanded vermiculite, confirming improved thermal behaviour for solar greenhouses [135]. Hongzhi Cui et al. incorporated binary salt PCM into melamine foam reducing phase separation and save 5376.68 kWh annually in building energy consumption[57].

Moreover, novel structural innovations have enhanced TES system efficiency. Lijie Liu et al. developed a multi-layer NEV-PCM system for buildings that extended thermal holding by over 90 minutes[44]. Yuanji Li et al. optimized radial metal foam structures using RSM for faster heat release in TES tanks[136]. Yuanji Li et al. also demonstrated that an inverted conical tank design (2:1 radius ratio) enhanced melting uniformity (21.48%), reduced melting time (16.01%), and improved heat storage efficiency by 11.68%[137]. Chuang Wang et al. employed the common ion effect and stable seed crystals to reduce supercooling of composite hydrated salts below 0.5 °C after 500 cycles[83]. Guochen Sang et al. developed a form-stable eutectic hydrated salt/polymer hydrogel PCM (HP-FSPCM) with reduced supercooling (3.2°C), high latent heat (165.5 J/g), and enhanced thermal conductivity (68.7% improvement). The composite showed only 2.2% latent heat loss after 300 cycles, and they proposed Lewis-Nielsen model for thermal behaviour prediction [138]. Hongzhi Cui et al. developed a core-shell thermal energy storage aggregate (TESA) with high latent heat and stability, optimizing TESA-based concrete (TESC) for strength

(15-50 MPa) while balancing energy storage and compressive strength. TESA size and dosage were key factors, highlighting the trade-off between structural integrity and thermal performance [139].

2.7 Applications of Salt Hydrate PCMs

Salt hydrate PCMs are now used or actively developed for solar thermal storage, building heating/cooling, industrial waste heat recovery, and cold-chain logistics, driven by their high volumetric energy density, tunable transition temperature, and comparatively low cost[51,73,78,140].

Hydrated salt phase change materials, such as $CaCl_2 \cdot 6H_2O$, sodium acetate trihydrate (SAT), sodium sulphate decahydrate, and various eutectic compositions, span a broad phase change temperature range from sub-zero values to above 100 °C, making them well suited for both cooling and heating applications[51,78,140]. Recent review studies consistently emphasize that, once key challenges—including supercooling, phase segregation, and corrosion—are effectively mitigated through composite design and encapsulation strategies, salt hydrates emerge as highly competitive candidates for building-integrated thermal energy storage (TES), solar water heating, photovoltaic-thermal (PV/T) systems, cold-chain storage, and industrial process heat recovery, owing to their high energy density, tunable transition temperature, and material availability[60,73,78,140].

2.7.1 Solar thermal energy storage

In solar water heating systems, hydrated salt PCM layers or cartridge-based storage units are commonly coupled with flat-plate or evacuated-tube solar collectors to store excess thermal energy during daytime operation and release it during off-sun periods, thereby increasing the solar fraction and reducing reliance on auxiliary energy sources[140–142].

A comprehensive review on the application of PCMs in solar water heating highlights that hydrated salts—such as sodium acetate trihydrate (SAT)-based eutectics and $CaCl_2 \cdot 6H_2O$ blends—are among the most promising inorganic PCMs, owing to their high latent heat and favourable melting temperature range (approximately 40-80 °C). The integration of PCM-enhanced storage was shown to smooth outlet water temperature fluctuations and extend the availability of hot water into evening and nighttime hours, significantly improving system usability and efficiency [141,142].Further performance gains have been achieved through the development of carbon-enhanced hydrated salt composite. Systems such as SAT/expanded graphite and SAT/biochar composite have demonstrated latent heat values exceeding 200 J g^{-1}, effective thermal conductivities as high as approximately 6.4 W m^{-1} K^{-1}, and solar-thermal conversion efficiencies approaching 80%, enabling more compact and responsive solar thermal storage modules. These advances make carbon-enhanced hydrated salt PCMs particularly attractive for domestic hot water supply and low-temperature applications such as floor radiant heating, where high power density and stable thermal output are essential [73].

Salt hydrate PCMs have been incorporated into box and parabolic solar cookers as thermal batteries, storing heat during peak insolation and releasing it for cooking after sunset or under transient cloud conditions[143]. Experimental studies on solar cookers equipped with hydrated salt thermal energy storage units demonstrate that the integration of salt hydrate PCMs can extend the useful cooking duration by several hours and maintain pot temperature close to the PCM melting point, in contrast to the rapid temperature drop observed in cookers without thermal storage[143]. Comprehensive reviews of PCMs in solar thermal applications further identify hydrated salts—including eutectic hydrate systems—as particularly attractive candidates for cooking applications and low-temperature thermal batteries, due to their higher volumetric energy density and lower

material cost compared with many organic PCMs, provided that long-term stability is ensured through the use of suitable additives or encapsulation strategies[140,141,143].

2.7.2 Building heating and cooling systems

Hydrated salt phase change materials (PCMs) are increasingly incorporated into building envelopes through gypsum wallboards, mortars, concretes, and modular panel systems to passively regulate indoor thermal conditions by absorbing and releasing heat near room-temperature or thermal comfort ranges [60,73,78]. By buffering indoor temperature fluctuations, these PCM-integrated building components reduce peak cooling and heating loads and enhance overall occupant comfort, particularly in climates with large diurnal temperature variations.

Early investigations demonstrated that PCM wallboards can significantly stabilize indoor environments[19]. Kuznik et al. demonstrated that a 5 mm PCM layer doubled thermal storage capacity and significantly reduced temperature fluctuations, confirming PCM suitability for lightweight buildings[144]. Castell et al. experimentally demonstrated that macro-encapsulated PCMs in brick cubicles reduced peak indoor temperature by ~1 °C and lowered cooling electricity use by 15%. Other studies using microencapsulated PCMs in concrete and plaster reported enhanced thermal inertia and reduced indoor temperature fluctuations.[13].

Roofs are ideal for PCM integration due to high solar exposure. Huang et al. showed that PCM-integrated roofs reduced indoor temperature by up to 9 °C and delayed heat transfer by 4-6 hours, highlighting the importance of optimized PCM thickness and encapsulation.[145]. Recent studies have coupled PCMs with solar thermal collectors for enhanced passive heating and cooling. Benkaddour et al. demonstrated improved thermal load leveling and night-time comfort in Moroccan buildings, highlighting the versatility of PCM-based hybrid systems in building energy management [146].

Form-stable composite PCMs, comprising hydrated salts such as sodium acetate trihydrate (SAT), $CaCl_2 \cdot 6H_2O$, and nitrate-based hydrates combined with porous or carbonaceous supports—including expanded graphite, biochar, and foamed glass—have been successfully implemented in wall panels and floor layers. Case studies consistently report reduced indoor temperature swings, effective peak-load shifting, and improved thermal comfort, with some residential systems achieving solar-thermal payback periods of only a few years for space heating and domestic hot water applications[60,73,78].

For example, a SAT/biochar composite developed for building roof applications exhibited very low supercooling (≈0.9 °C), a high latent heat exceeding 200 J g^{-1}, and strong solar absorptance. Field tests on PCM-integrated roofs showed significantly smaller temperature fluctuations compared with conventional reference roofs, and economic analysis indicated a payback period of approximately three years for hot water production, highlighting the techno-economic viability of hydrated salt PCM composite for building-integrated thermal energy storage[73].

Hydrated salt phase change materials (PCMs) are increasingly integrated into HVAC systems in the form of thermal energy storage (TES) tanks, packed-bed storage units, and PCM-enhanced air-handling components, with the aim of shifting cooling and heating loads and improving overall system efficiency[78,140,143].

In cold storage and air-conditioning applications, salt hydrate PCM modules, such as those based on $CaCl_2 \cdot 6H_2O$ or sodium acetate trihydrate (SAT) eutectics, are installed within air ducts or chilled-water circulation loops to store cooling energy during off-peak periods and release it during peak demand hours, thereby flattening electricity demand profiles and reducing frequent chiller cycling[78,140,143].

More recently, an industrial-grade composite SAT formulation with strongly suppressed supercooling and excellent cycling durability has been proposed for residential heating TES, demonstrating that properly optimized hydrated salt PCMs can satisfy the reliability and performance requirements of practical HVAC applications.[147].

2.7.3 Industrial waste heat recovery

Many industrial processes, including metallurgy, food processing, and chemical manufacturing, generate substantial amounts of low- to medium-temperature waste heat (typically ≈40-200 °C); hydrated salt phase change materials (PCMs) operating in this temperature range can effectively capture intermittent or off-peak waste heat and subsequently release it for air or fluid preheating, as well as for auxiliary process demands[140,143,148].

A comprehensive 2025 review on industrial waste heat recovery further emphasizes that hydrated salt-based thermal energy storage (TES) systems offer high energy storage density and relatively low material cost, making them well suited for seasonal storage applications and for integration with intermittent renewable heat sources. However, the review also highlights that practical implementation requires careful system design to mitigate corrosion and ensure long-term cycling stability, which remain critical challenges for industrial deployment[148]. Nano-additive-enhanced salt hydrates and encapsulated composite are being explored as modular TES units attached to flue-gas streams or hot liquid lines, returning heat to upstream processes or district heating networks[101,140,143].

Hydrated salt phase change materials (PCMs) with melting temperature in the refrigeration range (approximately −10 to +10 °C) are widely employed in cold packs, refrigerated transport containers, and passive cooling boxes for food, vaccines, and other temperature-sensitive biologics[78,143,149].

A comprehensive review of hydrated salt PCM applications in the cold chain emphasizes that PCM-filled panels and eutectic plates integrated into refrigerated trucks and containers can stabilize cargo temperature, reduce compressor operating time, and maintain safe storage conditions during power outages or frequent door openings, thereby enhancing both energy efficiency and temperature reliability[149]. In life-science and pharmaceutical logistics, salt hydrate-based PCM shipping boxes have demonstrated the ability to maintain strict temperature windows of 2-8 °C for extended durations without active refrigeration, making them increasingly attractive as sustainable alternatives to dry ice, particularly for vaccine distribution and transport of temperature-sensitive biologics[149].

2.8 Research Gaps Identified from the Literature Review

Based on the review presented in Sections 2.2-2.9, the following major research gaps have been identified:

1. **Lack of effective stabilization strategies for $Na_2SO_4 \cdot 10H_2O$-PU composite:** Although several nucleating and thickening agents have been reported for salt hydrate PCMs, the combined use of borax and Laponite® Gel to simultaneously mitigate supercooling, phase segregation, and cyclic degradation of $Na_2SO_4 \cdot 10H_2O$ within a polyurethane (PU) foam matrix has not been systematically investigated.
2. **Limited understanding of PU foam as a shape-stabilizing and macro-encapsulation medium:** Existing studies primarily focus on microencapsulation or polymer-supported PCMs. The ability of open-cell PU foam to retain $Na_2SO_4 \cdot 10H_2O$, prevent leakage, and maintain thermal stability under repeated thermal cycling remains inadequately explored.

3. **Absence of multi-scale experimental validation and scale-up studies:** Most investigations of salt hydrate PCMs are confined to laboratory-scale experiments. A comprehensive framework validating the thermal behavior of $Na_2SO_4 \cdot 10H_2O$-PU composite across multiple reactor scales is currently lacking.
4. **Insufficient thermal-property characterization for numerical modeling:** The thermal conductivity and heat-transfer characteristics of $Na_2SO_4 \cdot 10H_2O$-PU composite have not been systematically quantified and incorporated into validated numerical models capable of predicting performance at different scales.
5. **Limited studies on building-envelope integration:** The effects of PCM layer thickness and placement within building walls on the thermal performance of $Na_2SO_4 \cdot 10H_2O$-PU composite under hot-climate conditions have not been comprehensively evaluated.
6. **Lack of an integrated experimental-numerical framework:** Existing studies generally address material development, scale-up, or building applications independently. A validated framework linking material characterization, reactor-scale performance, numerical simulation, and building-level thermal assessment is still unavailable.

These gaps highlight the need for a comprehensive investigation of $Na_2SO_4 \cdot 10H_2O$-PU foam composite systems, encompassing material stabilization, scale-up, numerical modeling, and building integration for thermal energy storage applications.

2.9 Problem Statement Derived from the Literature

Based on the systematic review and gap analysis presented above, the central problem addressed in this thesis is stated explicitly as follows:

"Despite the attractive thermophysical properties of $Na_2SO_4 \cdot 10H_2O$ as a low-cost, non-flammable, high-latent-heat PCM for passive cooling of buildings in hot climates, its practical deployment is prevented by incongruent melting, supercooling (up to 20 °C), phase segregation, and long-term instability under repeated cycling. Existing composite and encapsulation strategies address these challenges only for other salt hydrate systems. No validated, scale-aware experimental-numerical framework exists for $Na_2SO_4 \cdot 10H_2O$ *- PU foam composite systems. In particular, multi-scale performance characterization (from 600 mL to 5 L reactors) and systematic building wall integration studies for this composite are absent from the literature."*

The present study focuses on thermal energy storage for passive cooling of residential and commercial buildings under hot climatic conditions representative of India. The target indoor thermal comfort range is maintained between 18-26 °C, consistent with ASHRAE Standard 55 and the National Building Code of India guidelines for occupied spaces. Under peak summer conditions in northern India, ambient temperature frequently exceed 40-45 °C, imposing significant cooling loads on building envelopes — typically in the range of 50-150 W/m² depending on wall construction and orientation. To address this, sodium sulphate decahydrate ($Na_2SO_4 \cdot 10H_2O$) was selected as the phase change material, offering a high latent heat capacity of approximately 250 J g^{-1} and a phase transition temperature of ~32 °C, which lies within the diurnal temperature swing experienced under such conditions. The PU-PCM composite wall system is designed to absorb excess thermal energy during peak daytime heating and release it during cooler nighttime periods, thereby reducing indoor temperature fluctuations by up to 3-5 °C and attenuating peak cooling loads. This thermophysical behaviour directly justifies the characterization of the system as a thermal energy storage solution for buildings, as embodied in the thesis title.

2.10 Objectives of the Present Study

In direct response to the research gaps identified in Section 2.8 and the problem statement in Section 2.9, the following five focused objectives are formulated:

1. **Development and characterization of a stabilized PU-PCM composite** by incorporating $Na_2SO_4 \cdot 10H_2O$ solution into open-cell polyurethane foam with Laponite® Gel as a thickening agent and borax as a nucleating agent to mitigate supercooling, phase segregation, and long-term cycling instability identified in the literature review.
2. **Experimental evaluation of thermal performance and cycling stability** of the PU-PCM composite through DSC characterization and repeated heating-cooling cycle tests in a 600 mL jacketed reactor to assess phase transition behavior, latent heat retention, and mechanical integrity of the foam matrix.
3. **Development and validation of numerical models** using COMSOL Multiphysics to simulate transient heat transfer and phase change dynamics, and to conduct parametric analyses of the effect of latent heat (L) and phase change temperature range (ΔT) on system performance.
4. **Scale-up investigation of the TES system** by extending the experimental and computational study from a 600 mL reactor to 2 L and 5 L reactors, evaluating scale-dependent charging-discharging behavior, and determining the optimal PU-PCM composite thickness for each reactor volume.
5. **Building envelope integration and passive cooling assessment** by incorporating the PU-PCM composite into brick wall assemblies and numerically evaluating the effect of PCM layer placement, thickness, and climatic conditions across different Indian cities and seasons on peak indoor temperature reduction and thermal time lag.

2.11 Scope of the Present Study

The scope of this thesis is defined as follows, consistent with the objectives above and the identified gaps:

- Material system: $Na_2SO_4 \cdot 10H_2O$ stabilized with Laponite® Gel and borax, impregnated into open-cell PU foam. Other salt hydrates are reviewed for context but not investigated experimentally.
- Scale: Experimental reactor volumes of 600 mL, 2 L, and 5 L; building wall modules of defined geometry under controlled boundary conditions. Industrial-scale or full-building implementation is outside the scope.
- Numerical modelling: Transient heat conduction with enthalpy-porosity phase change formulation in COMSOL Multiphysics. Natural convection within the molten PCM is neglected. Whole-building energy simulation is not performed.
- Climate context: Hot and composite climate representative of northern India (Delhi region). Humid/coastal climate performance is identified as a future research direction.
- Performance metrics: Temperature profiles, phase change temperature, latent heat, thermal time lag, peak wall temperature, and passive cooling effectiveness. Life-cycle assessment, detailed techno-economic analysis, and mechanical durability testing are identified as future work.

2.12 Summary

This literature review highlights the significant potential of hydrated salt-based phase change materials (PCMs), particularly $CaCl_2 \cdot 6H_2O$, sodium acetate trihydrate (SAT), and sodium sulfate decahydrate (SSD), for thermal energy storage applications due to their high latent heat storage capacity, suitable phase change temperature, and cost-effectiveness.

Despite challenges such as supercooling, phase segregation, low thermal conductivity, leakage, and corrosion, recent advancements in stabilization techniques, including nucleating agents, polymeric thickeners, porous support matrices, conductive additives, and encapsulation technologies, have substantially improved their thermal reliability and cycling stability. The integration of these approaches has enabled the development of multifunctional composite PCMs with enhanced heat transfer performance, durability, and leakage resistance. Furthermore, successful implementation in buildings, solar thermal systems, HVAC applications, industrial waste heat recovery, and cold-chain storage demonstrates their growing practical relevance. Overall, the literature confirms that properly engineered hydrated salt PCMs are promising candidates for sustainable and low-carbon thermal energy storage systems, while further research is needed to address scale-up, long-term field validation, and application-specific optimization for widespread commercialization.

Chapter-3

Experimental evaluation of thermal performance of $Na_2SO_4 \cdot 10H_2O$ salt hydrate-based phase change materials

3.1 Introduction

This study presents the synthesis, experimental evaluation, and numerical modelling of a polyurethane-phase change material (PU-PCM) composite developed for thermal energy storage and building applications. The composite was fabricated using an aqueous sodium sulphate ($Na_2SO_4 \cdot 10H_2O$) solution embedded within open-cell polyurethane foam, with LAPONITE® Gel employed as a stabilizing and binding agent to improve phase stability. The PU-PCM composite was designed to mitigate common limitations of salt hydrate PCMs, including phase segregation, supercooling, and leakage, while ensuring mechanical compatibility with building materials.

A laboratory-scale physical model with a volume of 600 mL was developed to experimentally investigate the heating and cooling behaviour of the PU-PCM composite under repeated thermal cycles. Differential Scanning Calorimetry (DSC) was conducted to characterize the thermal properties of the composite. The results indicated a melting temperature of approximately 34 °C with a melting enthalpy of 233.4 J/g. During solidification, two freezing peaks were observed at 10 °C and −8 °C, corresponding to freezing enthalpies of 52 J/g and 40 J/g, respectively, reflecting the crystallization behaviour of the composite within the porous matrix.

Based on the experimental results, a transient computational model was developed using COMSOL 5.0 Multiphysics to simulate heat transfer and phase change behavior in the PU-PCM system. The model was validated against experimental temperature profiles and was

further extended to assess the performance of the composite when integrated into building wall assemblies. The numerical analysis enables evaluation of thermal response, energy storage potential, and heat transfer delay introduced by the PU-PCM layer.

The combined experimental and numerical approach demonstrates the feasibility of PU-PCM composite as stable and effective latent thermal energy storage materials, providing a scalable framework for evaluating their performance in energy-efficient and sustainable building applications.

3.2 Experimental description

3.2.1 Methodology of $Na_2SO_4.10H_2O$ salt solution preparation

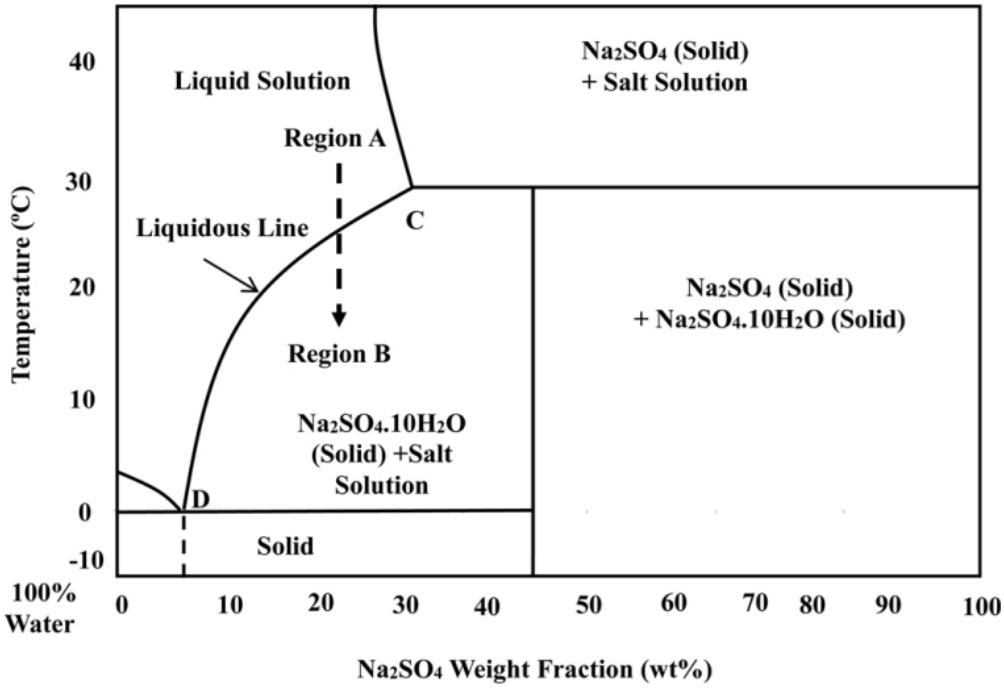

Figure 3.1: Phase diagram for sodium sulphate and water system [42,64]

A saturated sodium sulphate solution was prepared by dissolving 64 grams of Na_2SO_4 (anhydrous sodium sulphate) in 150 mL of distilled water, (30% by weight Na_2SO_4 solution), total volume of 175 mL using solubility phase diagram as shown in Figure 3.1 [42]. While preparing the mixture the salt solution was heated at 35 °C and constantly

stirred to dissolve the salt. A clear solution was obtained using vacuum filtration unit which removes the undissolved particles from the salt solution of which 150 mL solution was utilized for the study.

3.2.2 PU-PCM composite preparation process

The PU-PCM composite was produced by injecting 150 mL (section 3.3.1) of a saturated salt solution (35 °C, 30 wt % Na_2SO_4) into the porous openings of PU foam. To ensure the uniformity of the PU-PCM composite, the PU foam was squeezed and immersed in a salt solution, then released to absorb the maximum salt solution. This process was repeated 4-5 times to obtain a homogeneous and uniform PU-PCM composite. To prevent the solution from evaporation/leakage, the composite was enclosed in a thin cellophane pouch, with a thickness of 0.00006 m.

3.2.3 Experimental configuration and procedure for thermal performance analysis of PU-PCM composite

The experimental setup was designed to evaluate the thermal performance of the PU-PCM composite under controlled heating and cooling conditions. The setup consisted of a 600 mL jacketed glass cylindrical reactor, a heating-cooling circulator (chiller), a hot plate with a magnetic stirrer, a vacuum filtration unit, thermocouples connected to a data acquisition system (data logger), and thermal insulation materials. The reactor had an internal diameter of 0.075 m and a height of 0.125 m. Open-cell polyurethane (PU) foam sheets with a porosity of 97% and a density of 32 kg m^{-3} were used for the preparation of the PU-PCM composite. The prepared composite was enclosed in a zipper pouch and attached to the inner wall of the reactor, while the remaining reactor volume was filled with air. To minimize heat losses, thermal insulation was provided at the top and bottom surfaces of the reactor.

The thermal performance experiments were conducted according to the following procedure:

Step 1: Preparation and Installation of PU–PCM Composite

The synthesized PU-PCM composite, prepared as described in Section 3.2.2, was sealed inside a zipper pouch and fixed uniformly along the inner cylindrical wall of the reactor. The composite dimensions were 0.21 m in length, 0.01 m in width, and 0.075 m in height, ensuring maximum wall coverage and effective heat transfer. Additional insulation layers were applied to the top and bottom surfaces of the reactor. Furthermore, a porous PU foam support was placed beneath the reactor to reduce conductive heat losses through the base. A thermocouple was positioned at the centre of the reactor to monitor temperature variations during the charging and discharging processes.

Step 2: Establishment of Thermal Control System

The inlet and outlet ports of the reactor jacket were connected to a heating–cooling circulator (chiller). Water was used as the heat transfer fluid (HTF) and continuously circulated through the reactor jacket at a controlled flow rate to maintain the desired thermal boundary conditions throughout the experiment.

Step 3: Thermal Charging Process

For the charging cycle, hot water at a predetermined temperature was circulated through the reactor jacket. Heat was transferred from the HTF to the PU–PCM composite, enabling the PCM to absorb thermal energy and undergo a phase transition from solid to liquid state. Temperature data were recorded continuously until thermal equilibrium was achieved.

Step 4: Thermal Discharging Process

Upon completion of the charging cycle, the HTF temperature was reduced by circulating cold water through the reactor jacket. The stored thermal energy within the PU–PCM composite was released during the cooling process, resulting in the phase transition of the

PCM from liquid to solid state. Temperature variations were continuously monitored throughout the discharging cycle.

Step 5: Data Acquisition and Analysis

Temperature data obtained during both charging and discharging cycles were recorded using the data acquisition system. The thermal response, charging time, discharging time, thermal storage behavior, and temperature regulation capability of the PU–PCM composite were subsequently evaluated from the recorded temperature profiles.

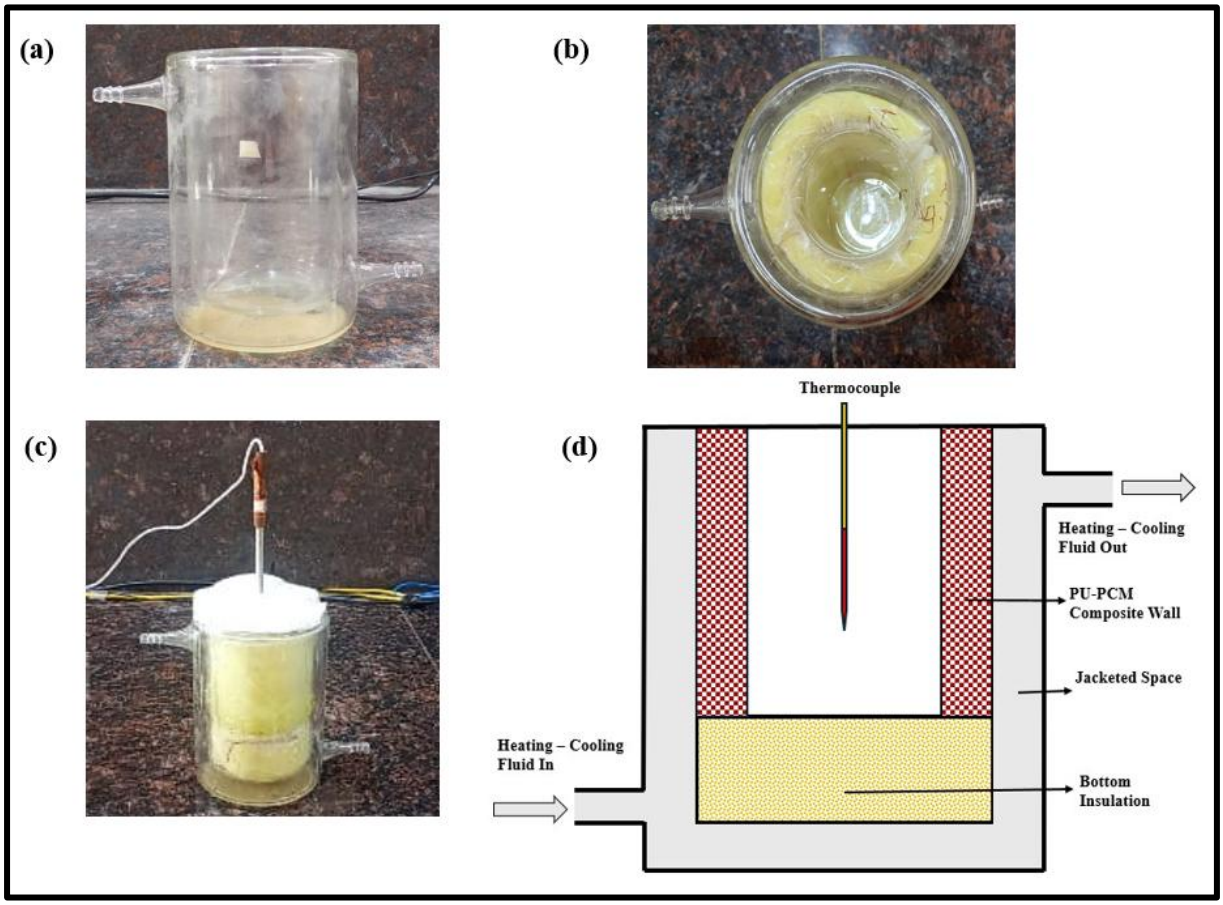

Figure 3.2: (a) 600 mL reactor **(b)** top view of reactor with PU-PCM **(c)** reactor for experimental setup **(d)** cross-sectional view of reactor with PU-PCM composite used for experiment

Figure 3.2 demonstrates the reactor design of 600 mL for the thermal regulation experiments with a PU-PCM composite. Figure 3.2 (a) depicts the glass jacketed cylindrical reactor, having the inlet and outlet ports for the passage of heating-cooling fluids so that

the temperature could be effectively controlled. In Figure 3.2 (b), stainless steel jacketed cylindrical reactor with PU-PCM composite lining the reactor's inner surface, providing insulation and thermal storage to maintain the internal conditions. Furthermore, Figure 3.2 (c) shows the reactor used in the experimental setup, where a thermocouple is inserted in the composite for temperature measurement. Moreover, Figure 3.2 (d) presented cross-sectional view of the reactor, illustrating its layered structure, including PU-PCM composite walls, a jacketing space for circulating heating-cooling fluids, and bottom insulation to minimise heat loss. This setup has been optimized experimentally for controlling temperature within the reactor.

3.2.4 Characterization of PU-PCM composite

Thermogravimetric Analysis (TGA) was used to examine the thermal stability of a PU-PCM composite by measuring weight loss as a function of temperature. The analysis was conducted using TGA PT 1000 instrument procured from LINSEIS at RGIPT, Jais. The sample temperature was gradually increased from room temperature to 900 °C at a heating rate of 10 °C/min within a nitrogen environment with a flow rate of 50 mL/min. Differential Scanning Calorimetry (DSC) was employed to study the thermal properties of pure $Na_2SO_4.10H_2O$ and PU-PCM composite, which has the ability to absorb and release heat energy during a phase transition. The melting and freezing enthalpy value of PU-PCM composite were obtained using differential scanning calorimeter (DSC7020, HITACHI) at RGIPT, Jais. The DSC test was performed in a nitrogen environment with a flow rate of 50 mL/min; the temperature was raised from -20 °C to 80 °C, followed by lowering back to -20 °C at a heating/cooling rate of 5 °C/min. The same PU-PCM composite was further subjected to thermal cyclic test. for Results obtained from the above analysis are discussed in the sections 3.5.1.

3.2.5 Procedure for mechanical properties of PU-Foam

The tensile properties of the PU foam were evaluated using a universal testing machine (UTM, H25KS, Tinius Olsen) at RGIPT, Jais. The PU foam test specimens had dimensions of 10 mm × 10 mm (cross -section) and a 100 mm in length. The applied load was gradually increased during testing, and corresponding elongation was continuously recorded to generate stress-strain curves. This data was used to determine the ultimate tensile strength, elongation at break and breaking strain of the PU foam. The results are discussed in section 3.4.6.

3.2.6 Thermal energy storage capability of PU-PCM composite experiment

Figure 3.3 : Experimental setup for 2 L reactor

Figure 3.3 shows the experimental set-up where the jacketed reactor was connected to chiller to regulate temperature of jacketed space and data loggers used to record the temperature. The reactor's jacket temperature was initially set to 40 °C and sustained at this temperature for 30 minutes. Afterward, the temperature of jacket was gradually reduced to 10 °C at the rate of approximately 0.4 °C/min. It took about 75 minutes for the jacket to

cool down to 10 °C. Subsequently, the jacket temperature was increased back to 40 °C at a rate of approx. 2 °C/min, taking 15 minutes to reach 40 °C. As a result, a complete cooling-heating cycle (40 °C to 10 °C to 40 °C) was achieved in 90 minutes. The formation of hydrates in the pores of PU foam during the cooling phase (40 °C to10 °C) was noticed and it is verified using data of DSC analysis. To assess the heat storage capacity of the PU-PCM composite and insulation properties, the reactor's central temperature was monitored throughout this thermal cooling / heating cycle. The temperature difference between the jacketed space temperature (T_2) and the reactor inner space (T_1), were measured by using PT100 thermocouple attached to the data logger.

3.2.7 Amount of sodium sulphate decahydrate ($Na_2SO_4.10H_2O$) used in 600 mL reactor

The quantity of sodium sulphate decahydrate ($Na_2SO_4.10H_2O$) utilized in 600 mL reactor is determined as indicated in the Table 3.1. The ratio of actual volume to effective volume was calculated using the formula $R = \frac{V_{actual}}{V_{effective}}$

Where V_{actual} = Actual Volume is the physical volume of the reactors inner space without any composite material inside and $V_{effective}$ = Effective Volume refers to the volume of space available for heating or cooling after applying the PU-PCM composite material inside the reactor.

Table 3.1 : Ratio Table

Reactor	Actual volume of Reactor	Effective space volume for heating/Cooling Inside the reactor	Ratio of Actual volume to Effective volume	Quantity Salt Used Na_2SO_4 (anhydrous) (g)	Aqueous Na_2SO_4 solution used (g)
600 mL	552 cm^3	178 cm^3	3.10	64	180

3.3 COMSOL: Model development and computational study

3.3.1 Model reactor development in COMSOL

The present computational analysis used a 2-D, axially symmetric model in COMSOL 5.0 Multiphysics software. The proposed model has 600 mL capacity reactor corresponding to Figure 3.2 as shown in the Figure 3.4. The PU-PCM composite layer, which is made of porous polyurethane (PU) foam, has an inorganic PCMs solution. In our study, sulphate (Na_2SO_4) solution was injected into the pores of the PU foam, as shown in the Figure 3.4. This PU-PCM composite layer is housed within a thin cellophane zipper pouch, having a thickness of 0.00006 m. 600 mL model the layer dimension is 0.075 m height and 0.01 m thickness of PU-PCM.

A highly porous (97%) polyurethane foam insulation is applied beneath the PU-PCM layer to add thermal insulation at the base of the reactor. In the internal space of the reactor, only air was present. In the jacketed model a cooling-heating thermal cyclic temperature profile (T_2) was applied to the jacketed space of the reactor. The temperature (T_1) within the reactor is documented in relation to time with thermocouple, which is represented in the Figure 3.8. Figure 3.5 represents 2-D axis symmetry geometry made in COMSOL 5.0 Multiphysics software for simulation of 600 mL and 2 L reactors.

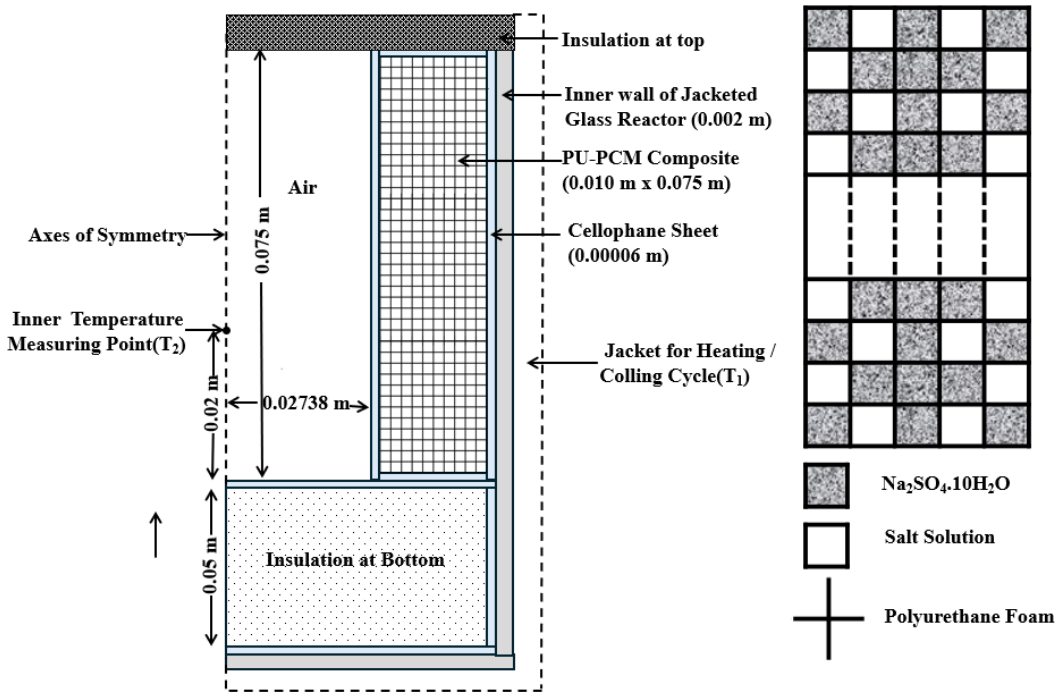

Figure 3.4: Cross-sectional view model for computational study for 600 mL

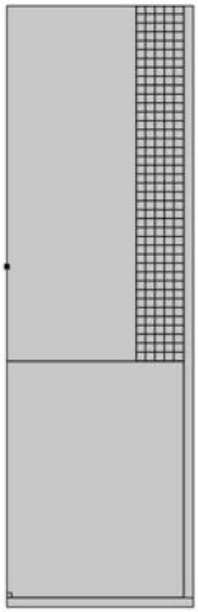

Figure 3.5 : 2-D axis symmetry geometry in COMSOL 5.0 for simulation of 600 mL

3.3.2 Computational technique for experimental investigation

The COMSOL 5.0 Multiphysics software was utilized to conduct the computational study of the physical model. It utilizes finite element approach for modelling and simulating physics-related phenomena. A time-dependent Multiphysics model was used for simulation of crystallization process of sodium sulphate decahydrate from aqueous solution in the PU foam pores over time. This model integrated the heat transfer mechanisms in solids, fluids, and porous media, as well as the heat transfer associated with phase change. The model was exposed to a dynamic outer temperature (which is constant at particular instance of time) throughout the outer boundary as provided in experiments. The corresponding temperature at selected point at the inner volume of the model reactor (given in Figure 3.4) was observed via COMSOL simulation. The results are discussed in sections 3.4.3 and 3.4.4.

In this study, the void space of PU foam was taken experimentally and found to be 97%. While preparing the PU-PCM composite, it was considered that PU foam occupies 3% of total volume and the 97% remaining volume was filled by Na_2SO_4 aqueous salt solution along with additives such as Laponite® Gel and seed of nucleating agent Borax (additives were considered to be negligible in the total solution). To model the PU-PCM composite with 97% void space, the line arrangements, representing the PU foam, were made in such a way that they occupy only the 3% of the total area. The thickness of each line was 0.0325 mm. The remaining 97% of the total volume corresponding to empty spaces remained between the solid lines (arranged in a 5×40 grid), was assigned as salt solution occupation.

Purohit and Sistla [42], have conducted a computational and experimental study on 600mL reactor with 10mm PU-PCM thickness having a saturated solution consisting of 30 wt% salt weighing 185 g (having volume of 150 mL) was poured into the pores of a PU foam, as shown in Figure 3.4 (a), with 97% void space, where the crystallization process takes place. The data derived from the phase diagram (Figure 3.1) and DSC findings

validated the production of $Na_2SO_4.10H_2O$ crystals. Furthermore, the uncrystallised salt solution (mother liquor) remained in the PU-PCM composite has a 11 wt% aqueous Na_2SO_4 solution which has a weight of approx. 78 g. And they assumed that remaining salt and water were crystallized as $Na_2SO_4.10H_2O$ having a weight of approx. 105g. In the present study, similar Na_2SO_4 concentrations in water were considered in both situations before and after crystallization. In order to examine the phase transition of the salt solution contained within the porous medium, a model was developed in COMSOL 5.0 Multiphysics software. This model integrates a mixture comprising 11 wt% Na_2SO_4 salt solution (for instance, 78 g for a 600 mL reactor) alongside liquid and solids of $Na_2SO_4.10H_2O$ (for instance, 105 g for a 600 mL reactor) situated within the open pores of PU foam. The salt solution and liquid $Na_2SO_4.10H_2O$ PCM were added in a ratio of approximately 2:3 (78:105 for 600 mL). The composite's 200 pores were filled at this ratio, with the properties of 11 wt% Na_2SO_4 and liquid $Na_2SO_4.10H_2O$ shown in Figure 3.4. The phase change occurred exclusively in $Na_2SO_4.10H_2O$. Figure 3.4 details the structure and arrangement of the 11 wt% Na_2SO_4 solution and liquid $Na_2SO_4.10H_2O$ within the PU-PCM composite layer used for this computational analysis. The thermal properties of saturated salt solution, $Na_2SO_4.10H_2O$, glass, stainless steel, cellophane sheet and polyurethane foam are provided in Tables 3.2 and 3.3. To determine the thermophysical characteristics of the 11 wt% Na_2SO_4 salt solution, an interpolation technique was used between the properties of pure water (density 1000 kg/m^2, heat capacity 4186 J/kg K, thermal conductivity 0.6 W/m K) and liquid $Na_2SO_4.10H_2O$ (44 wt% Na_2SO_4).

3.3.3 Assumptions and thermal properties

The assumptions for the computational analysis include

(i). The PU foam exhibits the same level of porosity.

(ii). The model's starting temperature is set at ambient temperature (28°C).

(iii). There is negligible or very little expansion of volume during phase change.

(iv). There is little or insignificant leakage of PCM, salt solution or water beyond the pores of PU foam.

(v). In a single phase, the characteristics of PCMs remain constant with temperature.

(vi). The top portion of the reactor was insulated.

(vii). The material itself has no surface impact of the mixed uneven crystallization of the PCM.

(viii). Both residual mother liquor and PCM are contained inside the pores, showing no segregation of phase during the cooling -heating cycle.

Table 3.2: Thermal properties of $Na_2SO_4 \cdot 10H_2O$ PCM [42]

Thermal properties	Solid $Na_2SO_4 \cdot 10H_2O$	Liquid $Na_2SO_4 \cdot 10H_2O$	Salt solution (11 wt%) $Na_2SO_4 \cdot 10H_2O$
Density, ρ ($kg\ m^{-3}$)	1460	1330	1082.5
Heat capacity, C_P ($J\ kg^{-1}\ K^{-1}$)	1920	3260	3491.5
Thermal conductivity, K ($Wm^{-1}\ K^{-1}$)	0.544	0.544	0.597

Table 3.3 : Thermal properties of glass, stainless steel, cellophane sheet and polyurethane foam [42]

Thermal properties	Glass	Stainless Steel	Cellophane Sheet	Polyurethane Foam
Density, ρ ($kg\ m^{-3}$)	2203	7850	1460	32
Heat capacity, C_P ($J\ kg^{-1}\ K^{-1}$)	703	475	1440	2700
Thermal conductivity, K ($Wm^{-1}\ K^{-1}$)	1.38	44.5	0.0035	0.048

3.3.4 The governing equations, Initial and Boundary Conditions

Heat Transfer Equation

The transient heat transfer within the reactor domains was governed by the energy conservation equation, as shown in Equation (3.1):

$$\rho C_P \frac{\partial T}{\partial t} + \rho C_P \upsilon . \nabla T = \nabla . (k \nabla T) + Q + Q_{vd} + Q_P \quad (\mathbf{3.1})$$

Since no fluid flow occurs within the PU-PCM composite, velocity is assumed to be zero (v = 0). Furthermore, viscous dissipation (Q_{vd}) and pressure work (Q_P) are neglected. Under these assumptions, heat transfer is governing by Equation (3.2):

$$\rho C_P \frac{\partial T}{\partial t} + \nabla . (-k \nabla T) = Q \quad (\mathbf{3.2})$$

Apparent Heat Capacity Method

The phase change process was modelled using the apparent heat capacity method available in COMSOL Multiphysics. The effective specific heat capacity is expressed as in Equation (3.3):

$$C_P = \frac{1}{\rho}\left(\theta \rho_L C_{P,L} + (1-\theta)\rho_S C_{P,S}\right) + L \frac{\partial \alpha_m}{\partial T} \quad (\mathbf{3.3})$$

Effective Density

The effective density during phase change is given by Equation (3.4):

$$\rho = \theta \rho_L + (1-\theta)\rho_S \quad (\mathbf{3.4})$$

Phase Fraction Function

The liquid fraction varies with temperature according to Equation (3.5):

$$\theta = [0 \; 1] \begin{cases} 0 & T < \left(T_m - \frac{\Delta T}{2}\right) \\ -1 & \left(T_m + \frac{\Delta T}{2}\right) \leq T \leq \left(T_m - \frac{\Delta T}{2}\right) \\ 1 & T > \left(T_m + \frac{\Delta T}{2}\right) \end{cases} \quad (\mathbf{3.5})$$

Effective Thermal Conductivity

The effective thermal conductivity during phase transition is given by Equation (3.6):

$$k = \theta k_L + (1-\theta)k_S \quad (\mathbf{3.6})$$

Initial Condition

The initial temperature of the reactor was set equal to ambient temperature:

$$\mathrm{T(r, z, 0) = 28^{\circ}C}$$

Boundary Condition

The jacket wall was subjected to the experimentally measured cooling-heating temperature profile:

$$\mathrm{T = T_2(t)}$$

where T_2represents the chiller-controlled jacket temperature.

The remaining insulated boundaries satisfy

$$-\mathbf{n} \cdot (k\nabla T) = 0$$

indicating negligible heat flux through insulated surfaces.

3.4 Results and discussion

3.4.1 TGA analysis PU-PCM composite

TGA curve for a sample labeled "PU-PCM composite" is shown in the Figure 3.6. In the graph X-axis shows the temperature rises from 30°C (room temperature) to 900°C, indicating the temperature at which weight loss occurs and Y-axis shows the weight change (in milligrams).

TGA data revealed several distinct stages of weight loss occurring below 350°C, indicating a complex decomposition process. As shown in the Figure 3.6, the Derivative-TGA (DTG) curve highlights two sharp and well-defined weight-loss events. The first significant reduction of 40.76% in weight is attributed to the release of free and unbounded molecules of water, which are weakly associated with the material, whereas in the second reduction of 9.24% in weight shows more gradual decline, which corresponds to the loss in molecules of water that are bound in the crystal lattice.

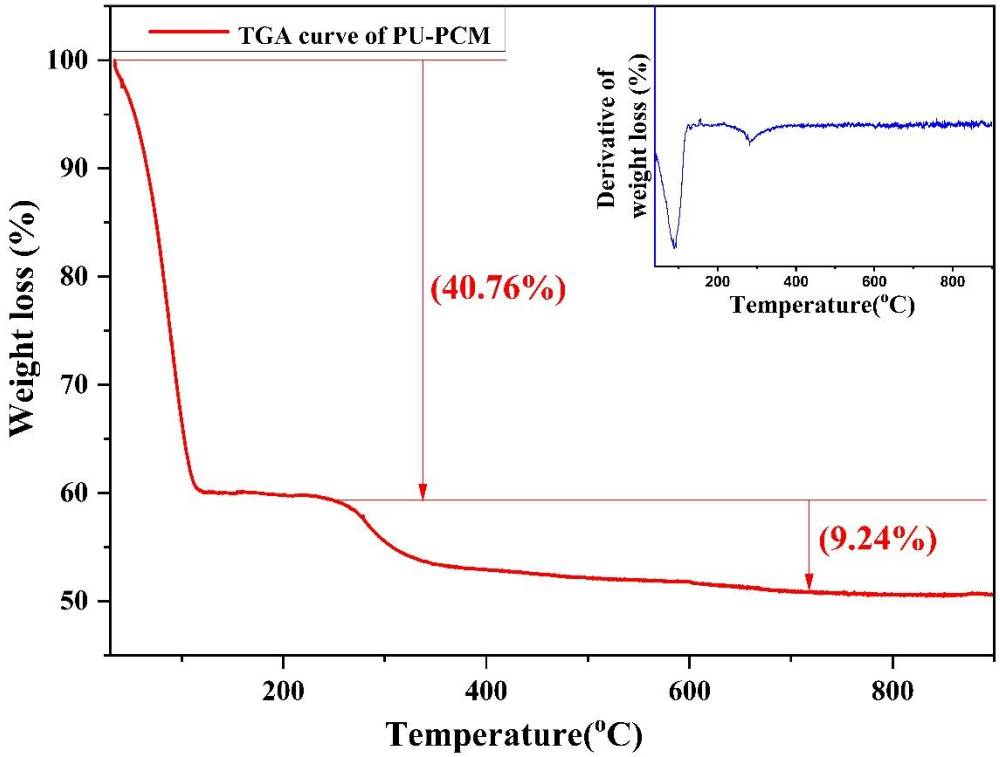

Figure 3.6 : TGA analysis PU-PCM composite

This sequential pattern of weight loss clearly points to different phases in the decomposition process. The initial weight-loss phase, related to the evaporation of unbound water (which may be considered as water, that is present as a salt solution in the PU-PCM composite), is a precursor to the more substantial weight-loss stage, which likely signifies the onset of the salt hydrate's decomposition to lower salt hydrates ($Na_2SO_4.10H_2O$ to $Na_2SO_4.xH_2O$). The second, more prominent weight-loss stage signals the degradation of the material itself, as the bound water is released, and the material undergoes structural breakdown. Therefore, this progression highlights the key stages of decomposition, where the first event initiates the process, and the second reflects the primary degradation event.

3.4.2 DSC analysis of PU-PCM composite

DSC analysis of PU-PCM composite and comparison with pure $Na_2SO_4.10H_2O$ and PU-PCM Composite after 100 thermal cycles

The DSC results of the PU-PCM composite and its comparison with pure $Na_2SO_4.10H_2O$ and PU-PCM Composite after 100 thermal cycles are presented in Figure 3.7(a) and Figure 3.7(b). During heating phase, the temperature increases steadily from -20°C to 80°C, the DSC curve of PU-PCM Composite an endothermic peak is observed around 34°C, having melting enthalpy of 233.4 J/g. as shown in Figure 3.7(a) and Figure 3.7(b). The peak indicates the melting of sodium sulphate decahydrate within the composite. During cooling phase, temperature drops from 80°C to -20°C and two significant exothermic peaks were observed which corresponds to the crystallization of $Na_2SO_4.10H_2O$ during the cooling phase. The first crystallization peak was observed at 15°C with an of enthalpy 52 J/g, at which point the sample crystallizes and releases heat. While the second peak observed around -0.5°C with an enthalpy of 40 J/g, making the solution crystallized completely.

In contrast, the pure $Na_2SO_4.10H_2O$ exhibited a sharp endothermic peak centered at 34.5 °C during the heating process, the corresponding latent heat of fusion was 245.8 J/g. However, the large temperature difference between melting and freezing peaks demonstrates significant supercooling, a common limitation of salt hydrates due to incongruent melting and phase segregation. However, the PU-PCM composite shows a significant reduction in supercooling. The homogeneous encapsulation of $Na_2SO_4 \cdot 10H_2O$ within the PU network and the presence of Laponite® Gel as a nucleating agent effectively suppress phase separation and facilitate more uniform crystallization during thermal cycling.

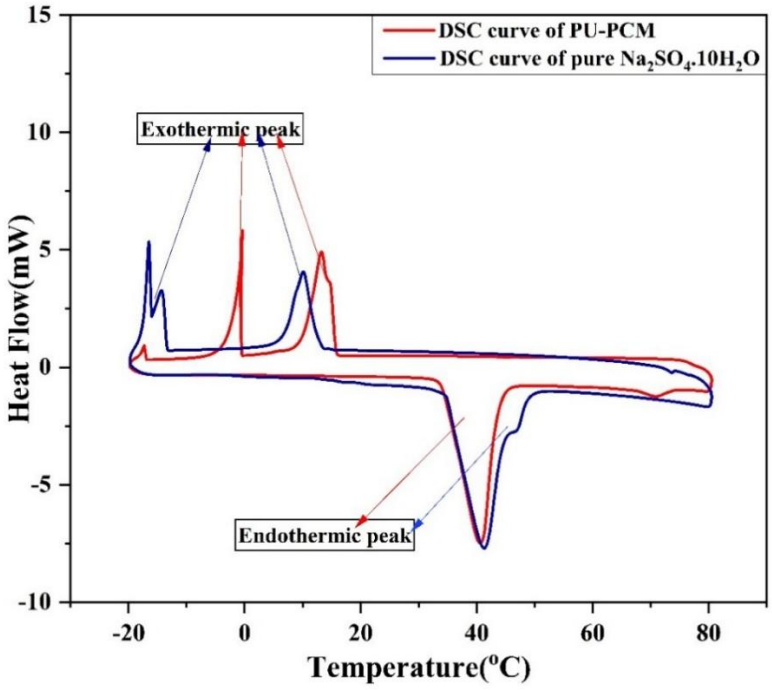

(a)

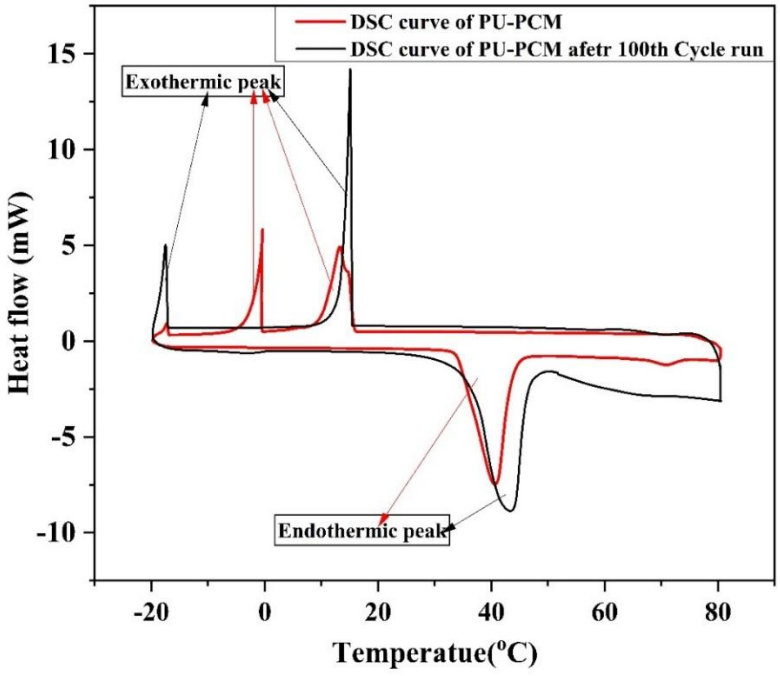

Figure 3.7 : DSC curve of **(a)** Pure Na2SO4.10H2O and PU-PCM composite **(b)** PU-PCM composite and same DSC PU-PCM composite after 100th cycle.

To examine long-term thermal durability, the PU-PCM composite was subjected to 100 consecutive heating-cooling cycles, and the resulting DSC curve (Figure 3.7(b)) was

compared with that of the initial sample. The primary melting peak remained near 34 °C, while the latent heat decreased slightly after 100th cycle. The exothermic peak during cooling, maintaining its sharpness with minimal broadening, confirming stable crystallization behaviour. The minimal change in transition temperature and peak profile after repeated cycling suggests that the composite retained its chemical integrity and phase transition reversibility. The slight reduction in enthalpy is likely due to minor water loss or partial redistribution of the hydrated salt within the PU pores during repeated melting-freezing cycles.

3.4.3 Thermal behaviour of a 600 mL reactor: computational vs experimental analysis

Figure 3.8 shows the temperature difference (T_2-T_1) between reactor's inner space and jacketed space and the chiller temperature over time for a 600 mL reactor. Validation of experimental results with the computational results using COMSOL 5.0 Multiphysics software. The solid continuous line represents the variation of chiller temperature, dotted line with square represents the temperature difference (T_2-T_1) variation over the time for experimental study and continuous line with triangle represent the temperature difference (T_2-T_1) variation over the time for computational study.

Initially, the whole reactor system was at 28 ℃ and chiller temperature was around 40 ℃, the reactor inner space is initially cooler than the outer space, therefore heat transfer take place from jacketed space to the inner space during first 20 minutes which leads to a temperature difference (T_2-T_1) to zero values. As the jacketed space temperature continued to decrease till it reached to 8 ℃, furthermore, temperature difference starts increasing. A maximum temperature difference was observed to be 12 ℃. If observed carefully, there is no sudden change in the temperature difference curve which attributes that there is no excess nucleation of $Na_2SO_4.10H_2O$. Moreover, a slight nucleation on the surface of the

PU fiber and continuous crystal growth can be expected as the temperature difference increases very smoothly.

The computational results showed similar trend with experimental data which closely follow each other, validating with an error of 0.5 ℃ (An average absolute percentage error (MAPE) of approximately 4.15%). Differences between simulation and experimental data may be due to the model assumptions, measurement errors, heat losses, and material property variations.

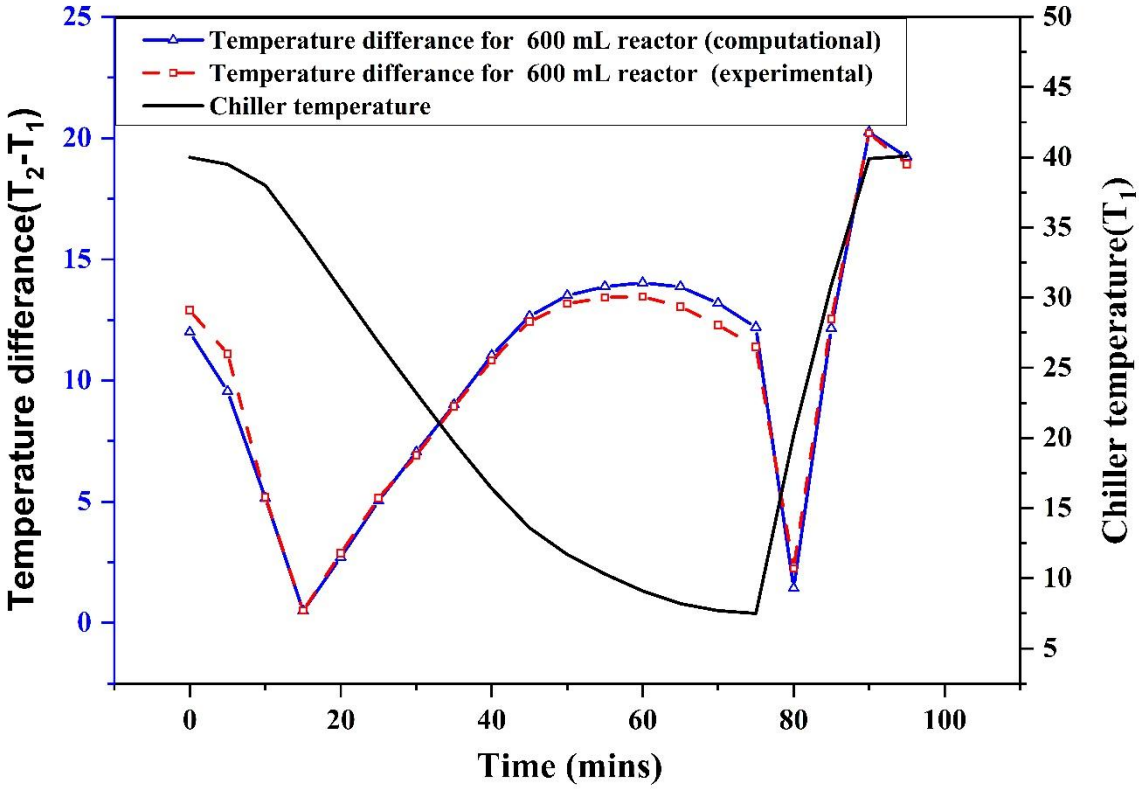

Figure 3.8 : Experimental and computational results for 600 mL reactor

3.4.4 3-D temperature distribution in the Reactors at t =0 min and t =95 min.

The energy storage experiments were performed in 600 mL (effective volume: 178 cm^3) reactor for different cycles as described in the section 3.4. The same experimental setup was modelled in COMSOL 5.0 Multiphysics software and exposed to the external temperature similar to experiments explained in section 3.4. Figure 3.9 shows the 3-D temperature distribution throughout the model 600 mL at time t=0 and t=95 mins.

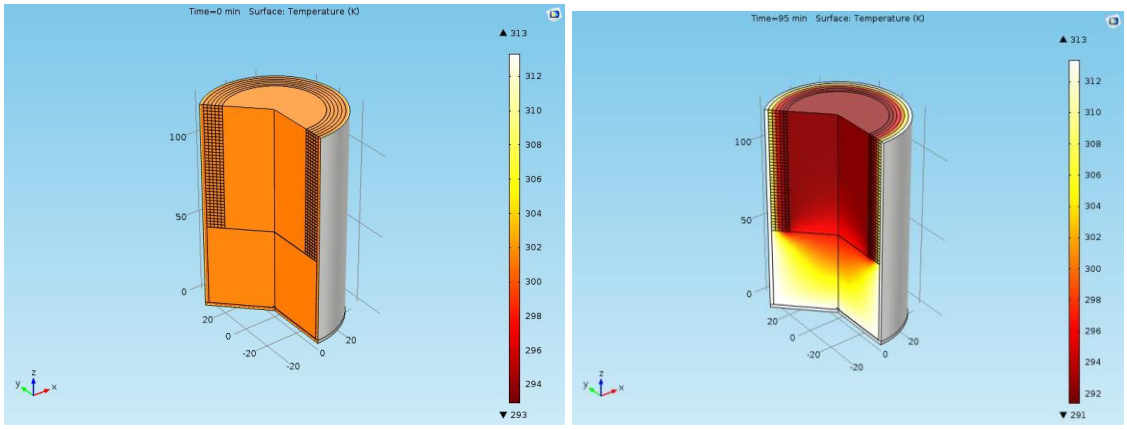

(a) (b)

Figure 3.9: 3-D temperature distribution in the reactors at t =0 min and t =95 min (with PU-PCM composite thickness of 10 mm).

At the beginning, the temperature recording point in the reactor is initially at a temperature of 28 °C (approx.). Figure 3.9 illustrate the heat variations in a model of a cylindrical element over a period of time. Figures 3.9 (a) indicate the temperature at 0 minute for 600 mL reactor which show a complete orange and red filling respectively. However, Figure 3.9 (b) gives the temperature distribution after duration of 95 minutes for both 600 mL reactor. The temperature values within the inner region of the cylinder are higher and progresses to hotter colours such as red and yellow.

The simulation perfectly illustrates the process of heat dissipation in a cylindrical structure, with a heating source located in the outer jacket and this heat slowly expanding over a period of time. This configuration is probably employed to study the evolution of temperature within hollow spaces exposed to outer heat sources over time.

3.4.5 Solid phase fraction for simulated model

Figure 3.10 is an illustration of how the "Solid Phase Fraction" of the material changes throughout the course of duration. It represent the quantity of crystals formed over time inside PU foam's pores. In the beginning, there is a growth phase that is monotonous and lasts for next thirty minutes, during which the solid phase fraction is virtually at zero. During the expansion phase, which lasts between thirty and seventy minutes, there is a significant increase in the solid phase fraction which may be connected to the variables of

nucleation and growth of crystal during cooling phase. The peak which occurs between 70 and 80 minutes, corresponds to the phase in which the solid phase fraction reaches its maximum attainable value; hence, the system contains the greatest quantity of solid crystal. During the depopulation phase, which lasts between 80 and 100 minutes, there is a significant fall in the proportion of solid phase, which indicates that the solid phase volume in the system has already reduced. This reduction in quantity may also be ascribed to the dissolution, retreat, or disintegration of crystal structure. To dissolve the crystals completely, the reactor will be exposed for some more time at 40 ℃.

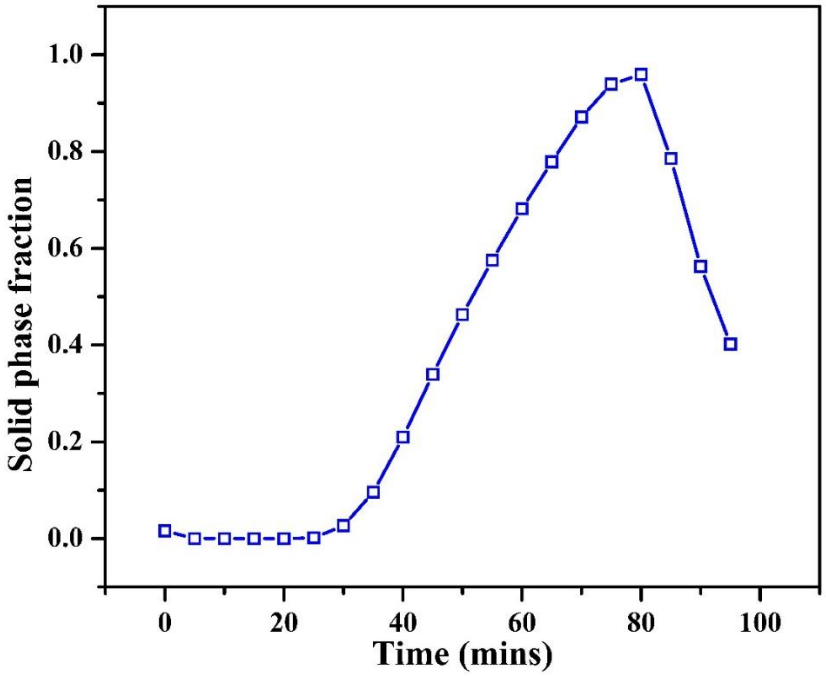

Figure 3.10 : Solid phase fraction

3.4.6 Mechanical properties of PU foam

Tensile tests were performed on a universal testing equipment to assess the mechanical characteristics of the PU foam by comparing its stress-strain responses. The image shows a stress-strain curve comparing the mechanical properties of polyurethane (PU) foam in two different states: one "Unused PU foam" and the other "after a week of use PU foam" is shown in Figure 3.11. Both unused and used foams exhibit similar elastic

behavior in the initial region. This indicates that the aging process mainly affects the foam's ability to bear greater loads rather than its initial flexibility. Table 3.4 presents the mechanical properties of unused and used polyurethane (PU) foam which are derived from stress and strain relation shown in Figure 3.11 The unused PU foam exhibits a slightly higher tensile strength (0.017 MPa) and strain at break (72%) compared to the used PU foam, which has a tensile strength of 0.015 MPa and strain at break of 70%. This is probably due to degradation, material fatigue and microstructural changes that occur over time.

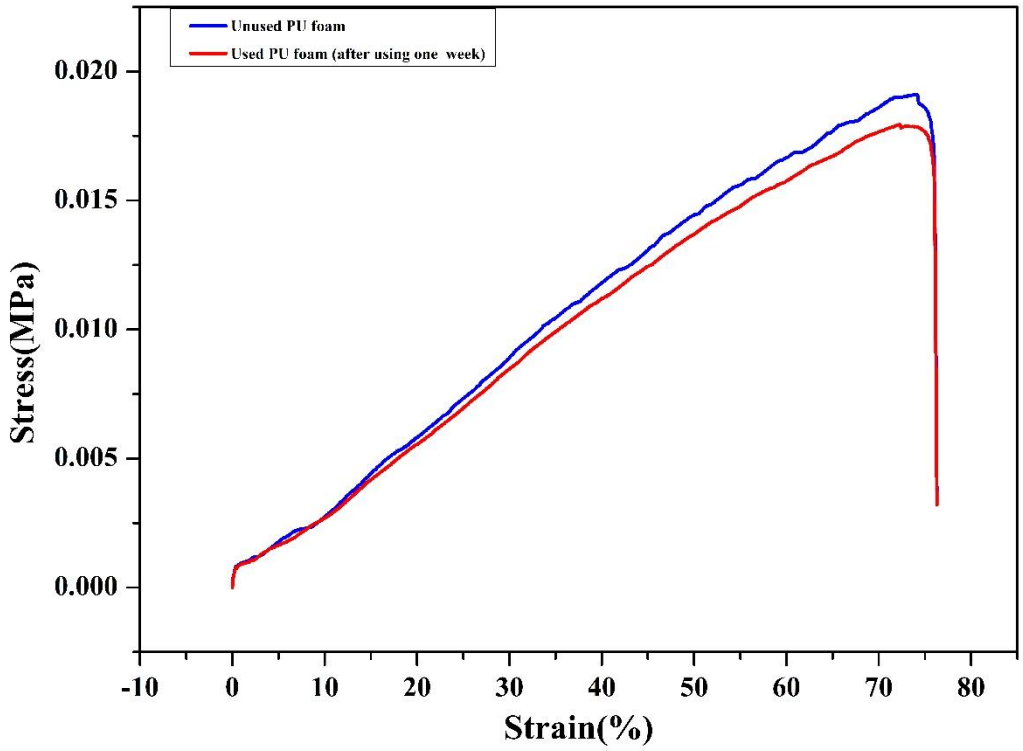

Figure 3.11 : Stress strain curve for PU-Foam

Table 3.4 : Properties from Stress strain curve for PU foam

	Ultimate tensile strength (MPa)	Strain at break (%)
Unused PU-Foam	0.017	72
Used PU-Foam	0.015	70

The overall mechanical performance of the PU foam degrades slightly after using one week as indicated by the lower stress response of the aged foam in both the yield and

ultimate strength regions. However, the degradation is not drastic, and the foam retains most of its elasticity and load-bearing capacity even after prolonged use.

3.5 Summary

This study presents a comprehensive experimental and numerical evaluation of the thermal performance of a sodium sulphate decahydrate ($Na_2SO_4 \cdot 10H_2O$)-based polyurethane foam composite for thermal energy storage applications. Differential Scanning Calorimetry (DSC) analysis confirmed that the PU-PCM composite retains the essential phase change characteristics of pure $Na_2SO_4 \cdot 10H_2O$, with only marginal variations in melting temperature and latent heat due to encapsulation within the polymer matrix. Furthermore, DSC results obtained after 100 thermal cycles demonstrated good thermal reliability of the composite, indicating negligible degradation in phase change enthalpy and thermal stability under repeated heating and cooling conditions.

The thermal behaviour of the PU-PCM composite was investigated using a 600 mL reactor under controlled boundary conditions. A detailed comparison between computational predictions and experimental measurements showed good agreement in temperature evolution during both charging and discharging processes, validating the accuracy of the numerical model with an error of 0.5 ℃ (An average absolute percentage error (MAPE) of approximately 4.15%). The small deviation between simulated and experimental results highlights the capability of the computational approach to reliably capture the transient heat transfer and phase change behaviour of the composite system.

Analysis of the solid phase fraction obtained from numerical simulations provided further insight into the melting and solidification dynamics of the PCM within the composite structure. The results revealed a gradual and uniform phase transition,

confirming effective heat storage and release characteristics, which are critical for practical thermal energy storage applications.

In addition to thermal performance, the mechanical integrity of the polyurethane foam was assessed. Mechanical testing showed that the PU foam maintained nearly identical properties before and after thermal cycling, demonstrating that PCM incorporation and repeated phase change processes do not adversely affect the structural stability of the composite material.

Overall, the combined DSC, thermal, numerical, and mechanical analyses confirm that $Na_2SO_4 \cdot 10H_2O$ based PU-PCM composite exhibit stable thermal performance, reliable phase change behaviour, and robust mechanical properties. The findings establish the proposed experimental-computational framework as an effective approach for evaluating salt hydrate-based PCM composite and support their potential application in building thermal energy storage and passive cooling systems. Future work may focus on long-term durability studies and optimization of composite configurations for enhanced thermal efficiency under real operating conditions.

Chapter-4

Performance analysis of a multi-scaled thermal energy storage system with varying volumes

4.1 Introduction

This chapter investigates the development, scale-up, and thermal performance of a sodium sulfate decahydrate ($Na_2SO_4 \cdot 10H_2O$) based polyurethane phase change material (PU-PCM) composite for thermal energy storage applications. The PU-PCM composite was synthesized by impregnating an aqueous $Na_2SO_4 \cdot 10H_2O$ solution into open-cell polyurethane foam, with Laponite® Gel and borax incorporated to enhance phase stability, reduce supercooling, and suppress phase segregation during repeated thermal cycling.

A key focus of this chapter is the systematic scale-up of the PU-PCM composite from a laboratory-scale 600 mL reactor to larger 2 L and 5 L reactors. The scale-up analysis demonstrates that maintaining consistent salt-to-solution ratios across different reactor volumes enables reliable estimation of composite volume and material requirements at higher scales. Initially, the 600 mL reactor was employed to evaluate the thermal energy storage capacity and insulation performance of the PU-PCM system. The composite was subsequently integrated into the inner walls of the 2 L and 5 L reactors to assess its thermal response under scaled conditions.

Transient thermal performance was evaluated experimentally, and numerical simulations were performed using COMSOL Multiphysics to determine the optimum PU-PCM composite thickness for each reactor size. The computational model was validated against experimentally measured temperature profiles and further utilized to examine the influence of phase change temperature range (ΔT) and latent heat (L) on the temperature difference

(T_2-T_1) across the reactor walls. The results confirm effective thermal buffering and delayed heat transfer introduced by the PU-PCM layer across all investigated scales.

Thermal cycling tests conducted over 100 repeated heating-cooling cycles demonstrated good thermal stability and repeatability of the PU-PCM composite. Overall, this chapter confirms that the scaled PU-PCM system provides effective thermal management and highlights its potential for integration into building envelopes and industrial thermal energy storage systems.

4.2 Methodology, Materials and Equipment

4.2.1 Methodology

The objective of this study is the optimization of the thickness of a PU-PCM composite that incorporates sodium sulphate decahydrate in 2 L and 5 L reactors for efficient TES. Optimizing the composite thickness is necessary for balancing the capacity of energy storage, thermal regulation, and efficiency of the system. The overall methodology adopted for this investigation is illustrated in Figure 4.1.

As shown in Figure 4.1, the study commenced with the preparation and characterization of the $Na_2SO_4 \cdot 10H_2O$ PCM and the fabrication of the PU-PCM composite. Differential Scanning Calorimetry (DSC) and material characterization were conducted to determine the thermal properties of the composite, followed by experimental investigations using a 600 mL reactor. These experiments were performed to acquire baseline data to understand key material properties such as thermal conductivity and phase transition behaviour for thickness optimization based on simulation.

To reduce the heat transfer to the inner space of reactor (inner space temperature, T_1) of the reactor from the outer jacket (jacketed space temperature, T_2), different PU-PCM composite thicknesses were used to attain temperature gradient (T_2-T_1) comparable to that observed in the 600 mL reactor. During the scale up to 2 L and 5 L, the objective was to

attain a similar temperature gradient (T_2-T_1) w.r.to time, as obtained for 600 mL reactor, for 2 L and 5 L with minimum PU-PCM composite thickness along with maximum heat transfer efficiency, hence minimum thermal losses. Preliminary conclusions from the 2 L reactor led to further scalability studies in a 5 L reactor. Actual conditions are validated experimentally to verify the optimal thicknesses and other parameters like temperature profile and energy storage efficiency.

The methodology integrates simulation and experimental approaches to refine the models and generate robust and scalable solutions. Furthermore, it determines the best suitable PU-PCM composite layer thickness for application such as reactors with enhanced TES, for industrial applications, for renewable energy technologies or for any form of thermal management technologies.

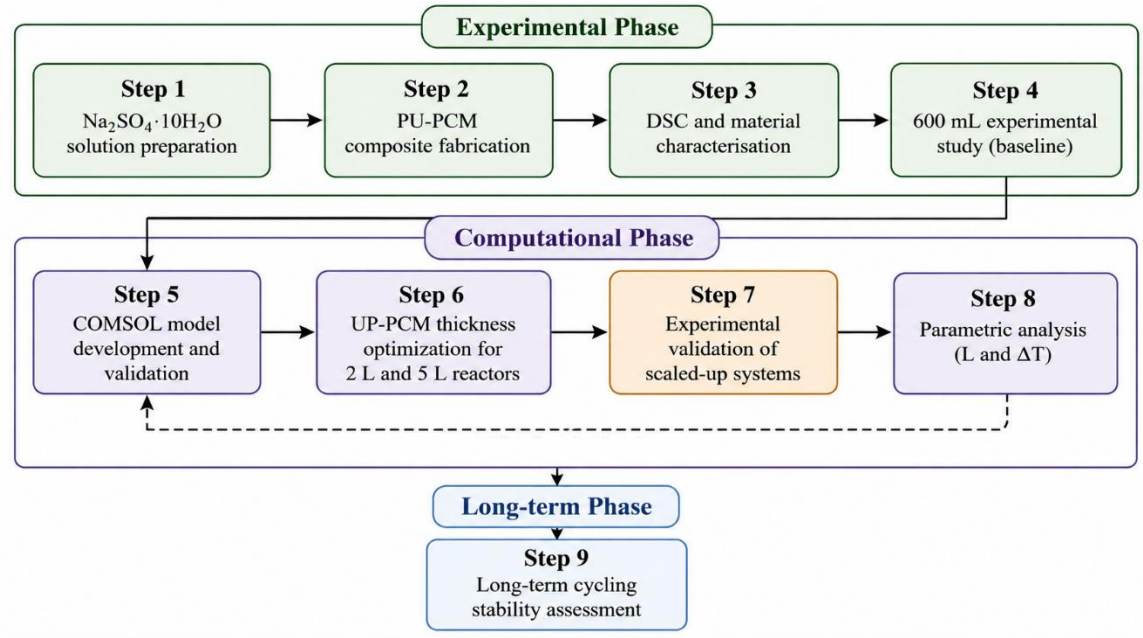

Figure 4.1: Overall methodology workflow for $Na_2SO_4 \cdot 10H_2O$ PCM scale-up study

4.2.2 Materials

Sodium sulphate decahydrate ($Na_2SO_4 \cdot 10H_2O$) was selected as phase change material for its high LHS capacity and thermal stability. To address the issue of the phase separation and supercooling commonly observed in inorganic salt hydrates. To mitigate supercooling

and phase separation, Laponite® Gel (1 wt%) was added as a stabilizing agent and borax (0.5 wt%) as a nucleating agent, Laponite®, a synthetic layered silicate, forms a gel-like network that inhibits phase separation by enhancing the viscosity of the molten hydrate phase and physically restricting the movement of salt and water molecules, thus maintaining homogeneity during phase transitions. Borax provides heterogeneous nucleation sites that facilitate crystallization of $Na_2SO_4 \cdot 10H_2O$, effectively reducing the degree of supercooling. Laponite® Gel also improves the dispersion and overall stability of the composite. Borax was preferred as nucleating agent for $Na_2SO_4 \cdot 10H_2O$. It can reduce the supercooling of $Na_2SO_4 \cdot 10H_2O$ [150]. PU foam served as a support matrix for PCMs, offering structural integrity and improved shape stability during phase transitions. Cellophane zipper pouch was used as an encapsulation technique to hold the PU-PCM Composite, which physically isolates the salt hydrate ($Na_2SO_4 \cdot 10H_2O$) from direct contact with the environment or structural materials. This method prevents leakage and corrosion related problem.

4.2.3 Equipment

For the experimental study, three different sizes of jacketed reactors (a 600 mL glass reactor, and 2 L and 5 L stainless steel reactors) were utilized to facilitate the scale-up study, each equipped with a jacketed space for temperature regulation. A 600 mL glass beaker was used for the preparation of saturated salt solutions, and a hot plate with magnetic stirrer was employed to ensure controlled heating and uniform mixing. Chiller with circulating fluid was utilized to maintain desired temperature in the jacketed space of reactors. Data logger with multichannel thermocouples were used to monitor and record the temperature at different reactors simultaneously.

4.3 Experimental Description

4.3.1 Methodology for Synthesis of $Na_2SO_4 \cdot 10H_2O$ for 600 mL, 2 L and 5 L reactors

The synthesis of sodium sulphate decahydrate was carried out following the methodology adapted from B.K. Purohit and Sistla [42], with appropriate calculations performed for reactor volumes of 600 mL, 2 L, and 5 L. The experimental conditions were determined based on the solubility phase diagram (Figure 4.2).

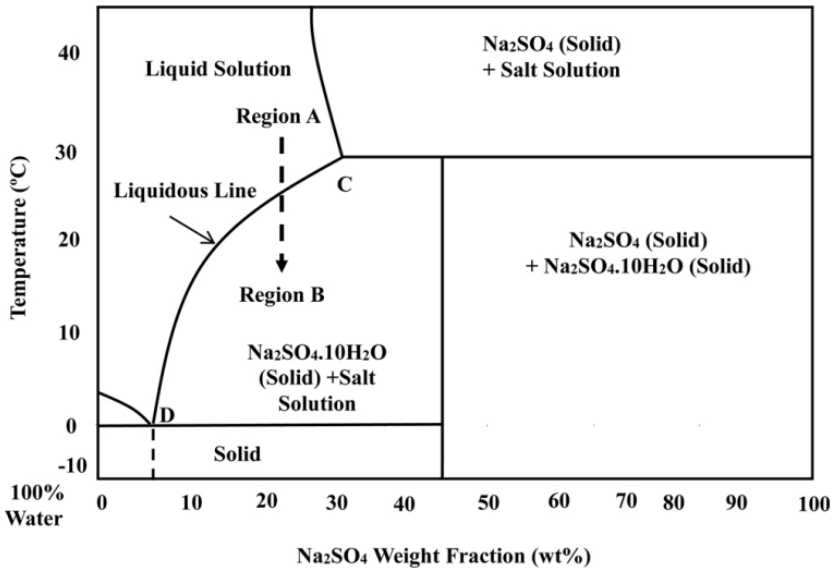

Figure 4.2 : Phase diagram for sodium sulphate [42]

64 g, 150 g and 450 g of anhydrous sodium sulphate (Na_2SO_4) were dissolved in 150 mL, 350 mL and 1050 mL of distilled water to prepare a 30% (by weight) sodium sulphate solution for 600 mL, 2 L and 5 L reactors respectively. Additionally, 1 g, 2 g and 5 g borax and 2 g, 5 g and 10 g Laponite® were also added to the respective solutions. The solutions were heated to 35 °C with continuous stirring to ensure complete dissolution. Undissolved particles were removed using a vacuum filtration unit, resulting in a clear solution of approximately 180 ml, 400 ml and 1225 ml for 600 mL, 2 L and 5 L reactors respectively. From these, 150 mL, 375 mL and 1085 mL was used for preparation of PU-PCM composite for 600 mL, 2 L and 5 L reactors respectively.

The melting and freezing enthalpy of the PU-PCM composite was measured through a differential scanning calorimeter DSC7020, HITACHI at RGIPT, Jais. For the DSC analysis, it was performed under a nitrogen environment at a flow rate of 50 mL/min. The programmed temperature range varied from -20 °C to 80 °C and was then cooled to -20 °C at a heating/cooling rate of 5 °C/min. Further details of analyses are being shown in Section 4.5.1.

4.3.2 Jacketed reactor setup preparation

In this experiment jacketed glass reactor (600 mL) and jacketed steel reactors (2 L and 5 L) were used to evaluate the thermal performance of the PU-PCM composite. The experimental configuration to study the thermal performance of the PU-PCM composite includes several equipment: a jacketed glass and steel reactors (600 mL, 2L and 5 L), a chiller (cooling- heating circulator), a hot plate with a magnetic stirrer and a vacuum filtration unit. In this study, 600 mL jacketed reactor made of glass have an internal diameter of 0.075 m and heights of 0.125 m, 2 L jacketed reactor which is made of steel have internal diameters of 0.140 m and heights of 0.140 m, while the steel 5 L jacketed reactors also made of steel have internal diameters of 0.180 m and heights of 0.180 m. For insulation support, open-cell PU foam sheets of 97% porosity with a density of 32 kg/m³ were used. The PU foam sheet used in the 600 mL reactor has dimensions of length of 0.235 m, height of 0.075 m, and thickness of 0.01 m (optimized thickness through simulation in COMSOL Multiphysics software), while for the 2 L reactor, the length is 0.44 m, height of 0.090 m and thickness of 0.01 m and for the 5 L reactor, the length is 0.56 m, height of 0.130 m and thickness of 0.02 m (optimized thickness through simulation in COMSOL Multiphysics software).

The PU-PCM composite was synthesized by infusing a saturated salt solution mixture (30 wt% Na_2SO_4 at 35 °C + Laponite ® + borax) into the porous structure of PU foam. To

prevent water evaporation or leakage of the viscous solution further, the composite was encapsulated within a thin cellophane pouch (0.01 mm thickness). This prepared PU-PCM composite was then affixed to the inner surface of the reactor's jacket, with the remaining volume inside the reactor filled with air. Temperature regulation within the reactor's jacketed space was achieved using a chiller, with water serving as the circulating fluid. To mitigate heat loss to the surroundings, insulation was applied to both the top and bottom of the reactor system. Additionally, a porous PU foam enclosed in a sealed zipper pouch was placed beneath the PU-PCM reactor system to further minimize thermal losses from the reactor base.

Figure 4.3 illustrates the design and experimental configuration of thermal regulation reactors with capacities of 600 mL, 2 L, and 5 L, incorporating a PU-PCM composite. Figures 4.3(a)(i), 4.3(b)(i) and 4.3(c)(i) show the glass (600 mL) and steel (2 L and 5 L) jacketed reactors each equipped with inlet and outlet ports for the circulation of heating or cooling fluids to regulate the reactor’s jacketed space temperature. Figures 4.3(a)(ii), 2(b)(ii) and 2(c)(ii) depict the same reactor with a PU-PCM composite lining its inner surface for insulation and thermal storage for 600 mL, 2 L and 5 L reactors, respectively. Finally, Figures 4.3(a)(iii), 4.3(b)(iii) and 4.3(c)(iii) present the complete experimental configuration featuring a thermocouple integrated within the composite for monitoring temperature of reactor’s inner space.

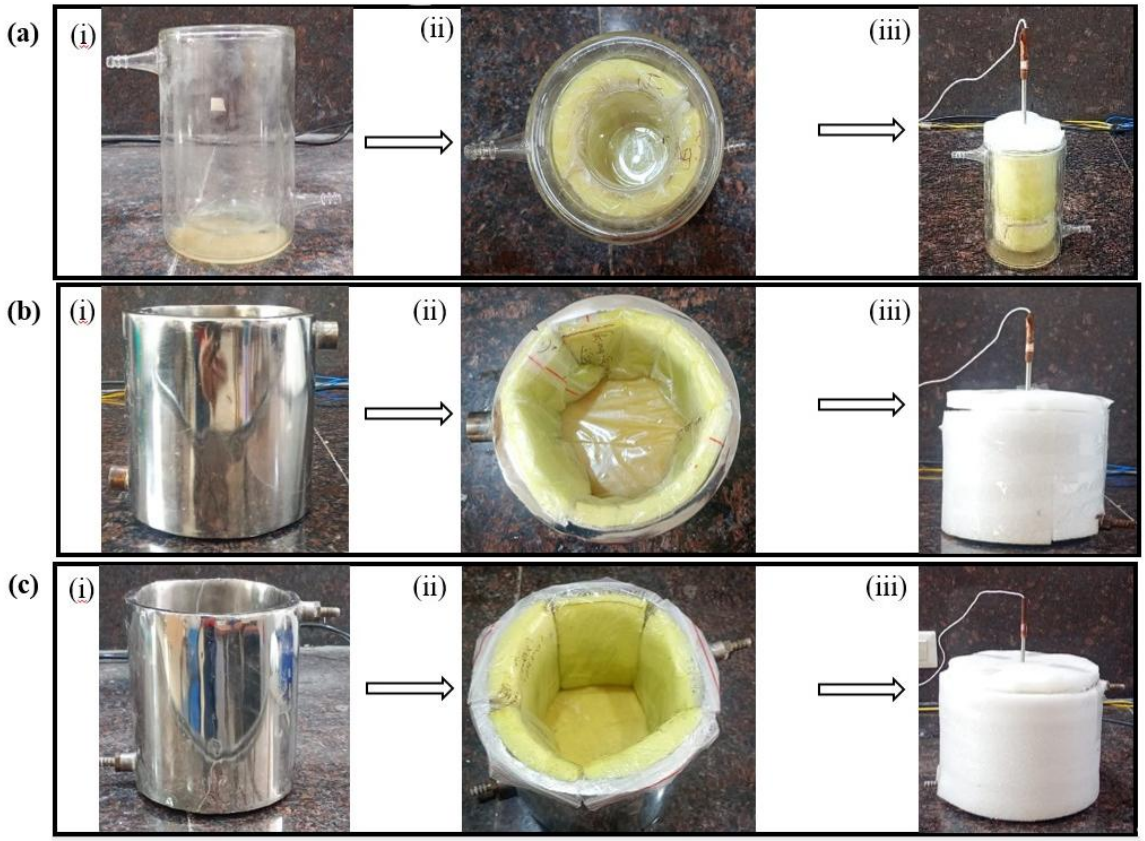

Figure 4.3 : Reactor setup for **(a)** 600 mL, **(b)** 2 L, and **(c)** 5 L reactors, showing **(i)** jacketed reactor, **(ii)** top view with PU-PCM, and **(iii)** complete reactor assembly

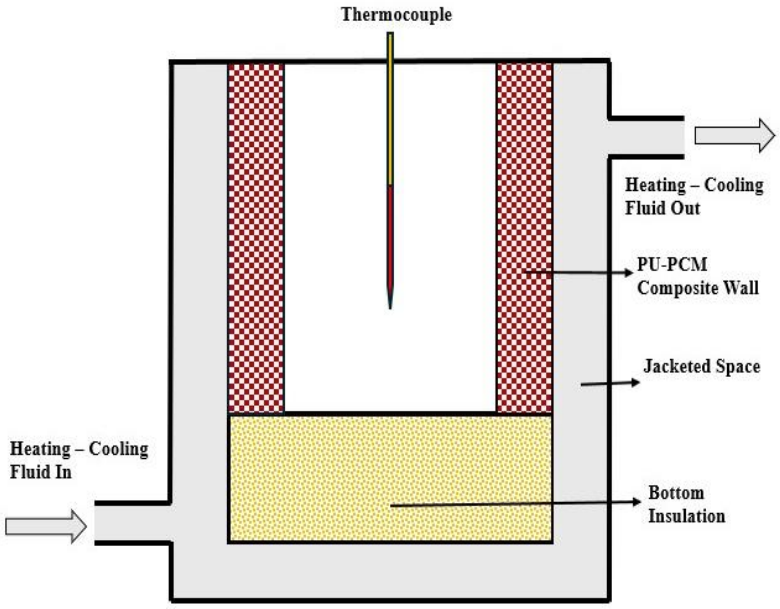

Figure 4.4 : Cross-sectional view of reactor set-up setup with PU-PCM composite

Figure 4.4 shows the cross-sectional view of the reactor, which includes the layers in the structure: PU-PCM composite walls, the jacketed space containing heating and cooling fluids, and bottom insulation to minimize heat loss. The experimental settings for heat transfer fluid flows are optimized to control the temperature precisely within the reactor. The PU and PCM composite wall store thermal energy by absorbing and releasing heat in the course of phase transitions, thus maintaining thermal stability. A thermocouple is placed inside the container to measure temperature fluctuations. The jacketed space around the container enables the flow of heating or cooling fluid, which enters through the inlet and exits through the outlet, thus facilitating efficient thermal regulation. In addition, bottom insulation increases energy efficiency as it reduces dissipation of heat. This type of experimental design is suitable to explore thermal behaviour under controlled heating and cooling environments and is applied for applications related to TES and temperature-controlled environments.

4.3.3 Experimental set-up for study of TES capability of PU-PCM composite

Figure 4.5 illustrates the experimental setup, which consists of three jacketed reactors of different sizes (600 mL, 2 L, and 5 L) connected in series and integrated with a chiller to regulate the temperature of the jacketed space. Temperature data was continuously recorded using data loggers. The experiment began by setting the jacket temperature to 40 °C and maintaining it for 30 minutes. The temperature was then slowly cooled down to 10 °C with a cooling rate of about 0.4 °C/min. It took around 75 minutes to attain the temperature. Then, with a heating rate of about 2 °C/min, the temperature was brought back up to 40 °C in 15 minutes through the heating cycle. The complete cooling-heating cycle of 40 °C to 10 °C and back to 40 °C took a total of 90 min. Upon cooling, the hydration reaction in the pores of the PU foam was evident and could be ascertained further from

DSC. This is to evaluate the thermal storage ability and insulation characteristics of the PU-PCM composite under controlled cyclic conditions.

Figure 4.5 : Experimental Setup for 600 ml, 2 L and 5 L reactors connected in series

4.3.4 Determination of the quantity of $Na_2SO_4.10H_2O$ used in reactors of different volumes

The Table 4.1 systematically outlines the quantity of $Na_2SO_4 \cdot 10H_2O$ required for reactors of various sizes, taking into account factors such as actual reactor volume, effective space for heating and cooling, and the ratio of actual to effective volume. For a 600 mL reactor, the effective space volume is 178 cm^3 with a ratio of 3.10, requiring 64 g of anhydrous Na_2SO_4 dissolved in 180 g of water. Similarly, a 2 L reactor has an effective volume of 1017 cm^3 and a ratio of 2.12, requiring 180 g of anhydrous Na_2SO_4in 500 g of water. For a 5 L reactor, the effective space volume is 2000 cm^3, with a ratio of 2.29. To maintain optimal conditions for PCM formation, this configuration requires 510 g of anhydrous Na_2SO_4 dissolved in 1400 g of water. This controlled formulation ensures the formation of $Na_2SO_4 \cdot 10H_2O$, a PCM that efficiently stores and releases thermal energy during phase transitions. By optimizing the hydration process, this setup enhances temperature stability within the reactor, making it suitable for TES applications. The Actual Volume is the physical volume of the reactor without any composite material inside and

effective Volume refers to the volume of space available for heating or cooling after applying the PU-PCM composite material inside the reactor.

Table 4.1 : Quantity of $Na_2SO_4 \cdot 10H_2O$ used in reactors of various sizes with effective space volume for heating/cooling

Actual volume of reactor	Effective space volume for heating/cooling inside the reactor	Ratio of Actual volume to effective volume	Quantity salt used Na_2SO_4 (anhydrous) (g)	Aqueous Na_2SO_4 solution used (g)
600 mL	178 cm^3	3.10	64 g	180 g
2 L	1017 cm^3	2.12	180 g	500 g
5 L	2000 cm^3	2.29	510 g	1400 g

4.4 COMSOL: Model development and computational study

4.4.1 Computational Model Assumptions

To make the computational model accurate and feasible, the following assumptions were made:

- PU foam was taken as a homogeneous material with constant porosity in its structure.
- The thermophysical properties of PCMs are constant in a single phase and do not depend on temperature difference.
- The temperature of the initial system is set to ambient conditions (28 ° C) before the start of thermal cycling.
- Volume expansion during phase transitions, especially solid-liquid transitions, is considered negligible.
- The upper boundary of the reactor is thermally insulated to reduce thermal loss to the surroundings and ensure an accurate thermal analysis.
- Leakage of water beyond the porous structure of PCM, salt solution or PU foam is considered insignificant.

- Residual mother liquors and PCMs remain confined within the foam pores, ensuring that there is no phase separation during multiple cooling-heating cycles.
- Surface effects due to heterogeneous crystallization of PCM are neglected, assuming a uniform phase transition occurs without interface irregularities.
- The PU foam matrix is assumed to be structurally stable, with no significant pore deformation or material degradation over repeated phase change cycles.
- Change in effective space volume due to change in PU-PCM thickness was considered negligible.

These assumptions provide a controlled computational setting for studying the thermal behavior of PU-PCM compounds and scalability in TES applications.

4.1.1 Model reactor development in COMSOL Multiphysics software

In the current computational analysis, 2-D an axisymmetric model in COMSOL Multiphysics was used. The model reactors were developed based on the dimensions of all the three reactors used in experimental set-up given in Figure 4.3 and Table 4.1. The models were developed with variable thickness of PU-PCM composite. Figure 4.6 (a) illustrates the dimensions taken in 2-D an axisymmetric model for 5 L reactor. The model consists of a PU-PCM composite layer developed from a porous PU foam infused with an inorganic PCM that usually is a solution of sodium sulfate injected into the pores of the foam, as shown in Figure 4.6. The composite layer is then encased in a thin cellophane zipper pouch having a thickness of 0.00006 m. For the 5 L model, the PU-PCM composite had height of 0.130, and simulations was carried out for thicknesses of 0.01 m, 0.015 m, 0.02 m, and 0.025 m. Below the PU-PCM layer, a highly porous (97%) PU foam insulation is used to minimize heat loss at the bottom of the reactor. The internal reactor volume is filled with air to simulate real thermal behaviour. In the jacketed reactor, a thermal cycling temperature profile (T_2) was applied on the jacketed space of the reactor to simulate heating and cooling

cycles, as shown in Figure 4.5, while the inner space temperature T_1 is monitored as a function of time using a thermocouple. Figure 4.6 (b) represents 2-D axis symmetry geometry in COMSOL Multiphysics software for simulation of 5 L reactor.

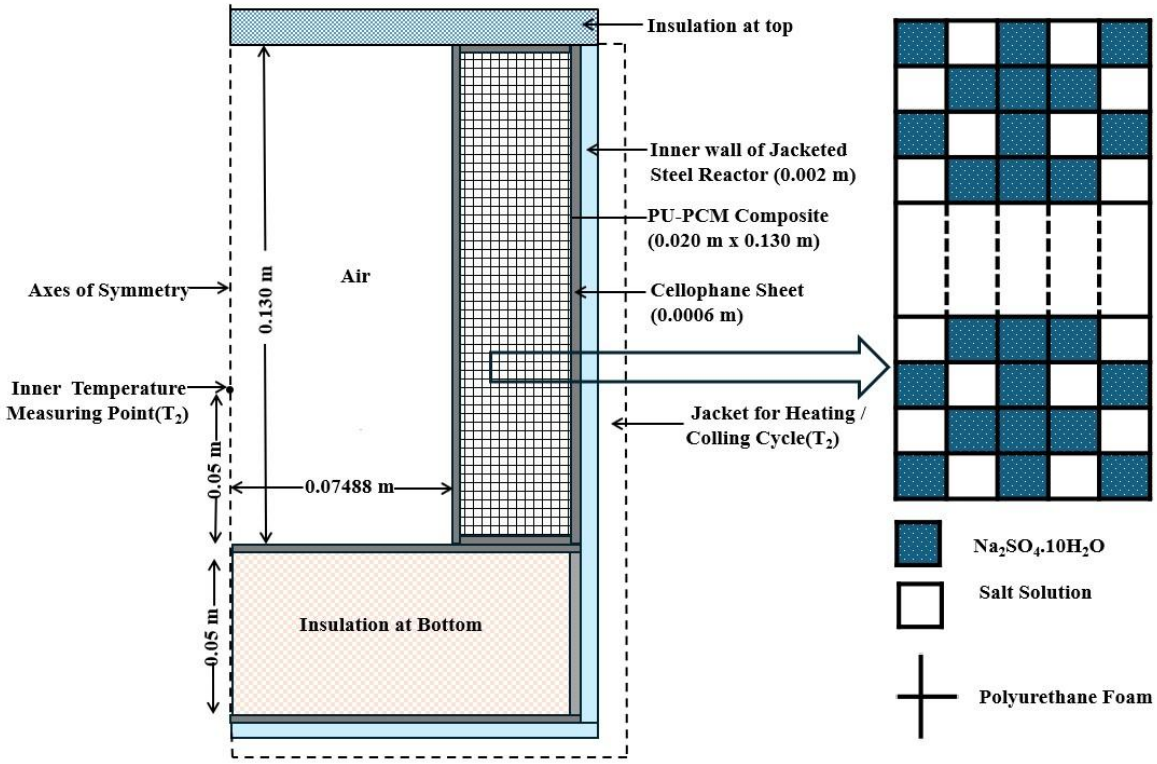

(a)

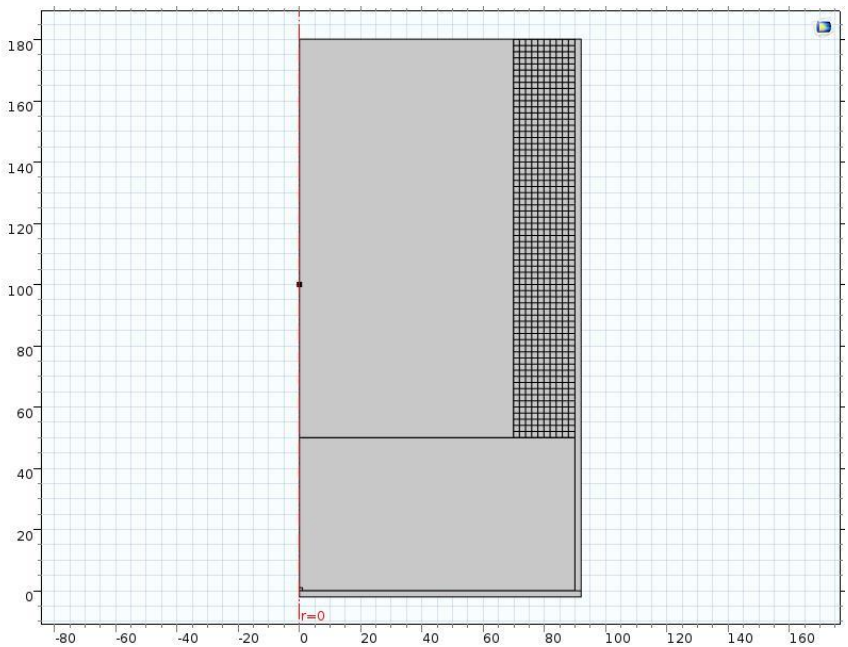

(b)

Figure 4.6 : (a): Description of cross-sectional view model for computational study for 5 L **(b):** 2-D axis symmetry geometry in COMSOL Multiphysics software for simulation of 5 L reactor

4.4.2 The model reactor thermal Simulation approach from experimental investigation

The computational analysis of the physical model was conducted using COMSOL Multiphysics software, which employs the finite element method for modelling and simulating complex physics-related phenomena. A time-dependent physical model was developed to simulate the crystallization process of sodium sulfate decahydrate ($Na_2SO_4 \cdot 10H_2O$) from an aqueous solution within the porous structure of PU foam over time. This model integrates heat transfer mechanisms in solids, fluids, and porous media while incorporating phase change heat transfer.

Development of Reactors in COMSOL Multiphysics software were done with the help of experimental reactors given in Figure 4.5. Experimentally, the void space within PU foam was determined to be 97%. During the preparation of the PU-PCM composite, it was assumed that PU foam occupied 3% of the total volume, while the remaining 97% was filled with an aqueous sodium sulfate solution, including minor additives such as Laponite® and borax nucleating agents (whose volume fractions were considered negligible). To computationally represent the PU-PCM composite's 97% void fraction, PU foam structures were arranged as linear elements occupying only 3% of the total area, with each line having a thickness of 0.0325 mm. The remaining 97% volume was designated for the salt solution, distributed within a structured 5×40 grid.

A prior computational and experimental study conducted by Purohit and Sistla [31] investigated a 600 mL reactor containing a 10 mm PU-PCM composite saturated with a 30 wt% sodium sulfate solution (185 g, corresponding to 150 mL). The solution was infiltrated into the PU foam pores, where crystallization occurred. The uncrystallised mother liquor

within the PU-PCM composite contained an 11 wt% sodium sulfate aqueous solution (~78 g), while the remaining mass (~105 g) was assumed to have crystallized as $Na_2SO_4 \cdot 10H_2O$. Similar initial and final concentrations of Na_2SO_4 in water were used in the present study for all the scales of reactors (600 mL, 2L and 5L). The salt solution and liquid $Na_2SO_4 \cdot 10H_2O$ were introduced in a 2:3 ratio as given in Table 4.2 ensuring uniform filling in all 200 pores. The phase change was confined exclusively to $Na_2SO_4 \cdot 10H_2O$. Figure 4.7 illustrates the structural arrangement of the 11 wt% sodium sulfate solution and $Na_2SO_4 \cdot 10H_2O$ within the PU-PCM composite layer in the 5 L model reactor.

Table 4.2 : Details of PU-PCM composition and salt distribution in different reactors

Parameter	600 mL Reactor	2 L Reactor	5 L Reactor
PU-PCM composite thickness	10 mm	10 mm	20 mm
Na_2SO_4 solution concentration	30 wt%	30 wt%	30 wt%
Total salt solution mass (g)	185	513	1440
Crystallized $Na_2SO_4 \cdot 10H_2O$ (g)	105	295	815
Uncrystallized 11 wt% solution(g)	78	218	625
PU foam void space	97%	97%	97%
PU foam solid volume	3%	3%	3%

The thermophysical properties of the saturated salt solution, $Na_2SO_4 \cdot 10H_2O$, glass, stainless steel, cellophane sheet, and PU foam are detailed in Tables 4.3 and 4.4. To determine the thermophysical properties of the 11 wt% sodium sulfate solution, an interpolation method was applied between the properties of pure water (ρ: 1000 kg/m³, C_P: 4186 J/kg·K, k: 0.6 W/m·K) and liquid $Na_2SO_4 \cdot 10H_2O$ (44 wt% Na_2SO_4). The latent heat (L) was taken as 240 J/g and phase change temperature range(ΔT) taken as 16 °C of PU-PCM composite for simulation.

Table 4.3 : Thermal properties of $Na_2SO_4 \cdot 10H_2O$ PCM [42]

Thermal properties	Solid $Na_2SO_4 \cdot 10H_2O$	Liquid $Na_2SO_4 \cdot 10H_2O$	Salt Solution (11 wt%) $Na_2SO_4 \cdot 10H_2O$
Density, ρ ($kg\ m^{-3}$)	1460	1330	1082.5
Heat Capacity, C_P ($J\ kg^{-1}\ K^{-1}$)	1920	3260	3491.5
Thermal Conductivity, K ($Wm^{-1}\ K^{-1}$)	0.544	0.544	0.597

Table 4.4 : Thermal properties of glass, stainless steel, cellophane sheet and PU foam [42]

Thermal properties	Glass	Stainless Steel	Cellophane Sheet	Polyurethane Foam
Density, ρ ($kg\ m^{-3}$)	2203	7850	1460	32
Heat Capacity, C_P ($J\ kg^{-1}\ K^{-1}$)	703	475	1440	2700
Thermal Conductivity, K ($Wm^{-1}\ K^{-1}$)	1.38	44.5	0.0035	0.048

The system was subjected to dynamic outer boundary temperature, which remained constant at any given time step, consistent with the experimental conditions. The temperature variations at a selected inner point within the reactor (depicted in Figure 4.5) were simulated with COMSOL Multiphysics software and the results are discussed in Sections 4.5.3 and 4.5.4.

The variation in temperature difference (T_2-T_1) profile with respect to change in latent heat(L) of melting and phase change temperature range (ΔT) was also analysed and the results are discussed in section 4.5.7 and 4.5.8.

4.4.3 The governing equations for numerical model

In COMSOL Multiphysics, the melting and solidification of $Na_2SO_4.10H_2O$ are described by the general heat transfer equation, as shown in Equation (4.1):

$$\rho C_P \frac{\partial T}{\partial t} + \rho C_P v.\nabla T = \nabla.(k\nabla T) + Q + Q_{vd} + Q_P \quad (\mathbf{4.1})$$

By Ignoring viscous dissipation (Q_{vd}) and pressure work (Q_P) and neglecting heat transfer through convection and radiation, the heat equation simplifies to a more familiar form, equation (4.2):

$$\rho C_P \frac{\partial T}{\partial t} + \rho C_P v.\nabla T = \nabla.(k\nabla T) + Q \quad (\mathbf{4.2})$$

Further simplification by setting the velocity v = 0 to result in equation (4.3), which governs only conductive heat transfer:

$$\rho C_P \frac{\partial T}{\partial t} + \nabla.(-k\nabla T) = Q \quad (\mathbf{4.3})$$

The COMSOL phase change model applies melting and solidification of pure substances, where the phase change occurs smoothly over a phase change temperature range (ΔT) centered around the phase change temperature (Tm). Within this interval, the phase fraction θ changes from 0 (solid) to 1 (liquid), as defined in equation (4.4):

$$\theta = [0 \quad -1 \quad 1] \begin{cases} T < \left(T_m - \frac{\Delta T}{2}\right) \\ \left(T_m + \frac{\Delta T}{2}\right) \leq T \leq \left(T_m - \frac{\Delta T}{2}\right) \\ T > \left(T_m + \frac{\Delta T}{2}\right) \end{cases} \quad (\mathbf{4.4})$$

During Heat transfer with phase change, the effective material properties such as density (ρ), specific heat capacity (C_P), effective thermal conductivity (k), and the effective specific enthalpy (H) of PCM are given by equations (4.5) - (4.8))

$$\rho = \theta\rho_L + (1-\theta)\rho_S \quad (\mathbf{4.5})$$

$$C_P = \frac{1}{\rho}\left(\theta\rho_L C_{P,L} + (1-\theta)\rho_S C_{P,S}\right) + L\frac{\partial \alpha_m}{\partial T} \quad (\mathbf{4.6})$$

$$k = \theta k_L + (1-\theta)k_S \quad (\mathbf{4.7})$$

$$\rho H = \theta\rho_L H_L + (1-\theta)\rho_S H_S \quad (\mathbf{4.8})$$

Where the function for thermal diffusivity (α_m) in Equation (6) is defined as:

$$\alpha_m = \frac{1}{2}\frac{(1-\theta)\rho_L - \theta\rho_S}{2\theta_S + (1-\theta)\rho_L} \quad (\mathbf{4.9})$$

For porous materials (Porous PU foam insulation), heat transfer is govern by the Equations (4.10) - (4.12):

$$(\rho C_P)_{eff}\frac{\partial T}{\partial t} + \rho C_P v \cdot \nabla T = \nabla \cdot \left(k_{eff}\nabla T\right) + Q \quad (\mathbf{4.10})$$

$$(\rho C_P)_{eff} = \theta_P \rho_\rho C_{P,P} + (1-\theta_P)\rho_{FM} C_{P,F} \quad (\mathbf{4.11})$$

$$k_{eff} = \theta_P k_P + (1-\theta_P)k_F \quad (\mathbf{4.12})$$

4.4.4 Different arrangements for salt solutions and $Na_2SO_4 \cdot 10H_2O$ within PU-PCM

To study the PU-PCM composite stability over the repeated heating and cooling cycles, six distinct spatial configurations for distribution of sodium sulfate decahydrate ($Na_2SO_4 \cdot 10H_2O$) and saturated salt solution in the PU-PCM composite (illustrated in Figure 4.7(a-f)) were studied. These distributions are expected to happen during different heating and cooling cycles. These configurations are designated as PCM1, PCM2, PCM3, PCM4, PCM5, and PCM6.

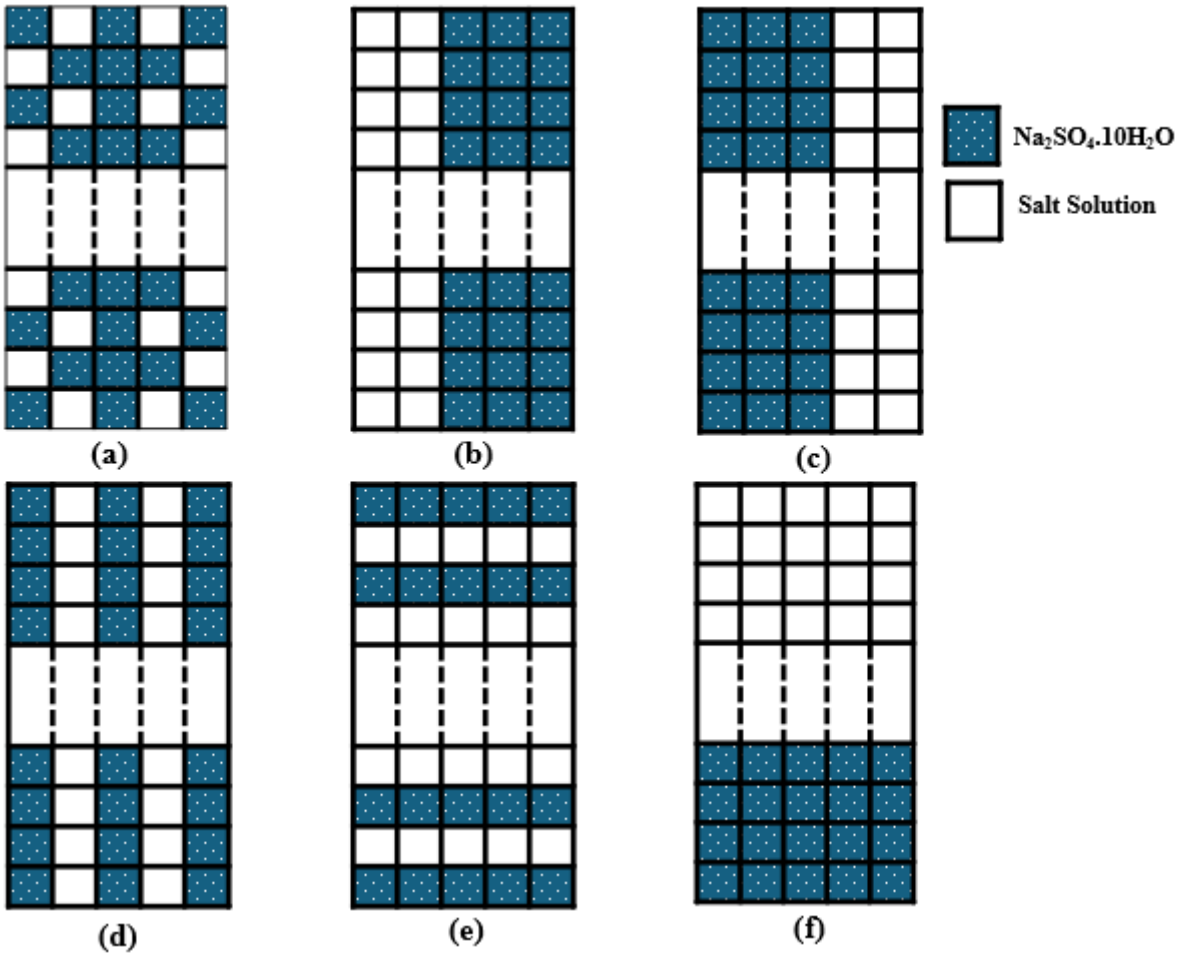

Figure 4.7 : Different arrangements for salt solutions and $Na_2SO_4 \cdot 10H_2O$ within PU-PCM **(a)** PCM1 **(b)** PCM2 **(c)** PCM3 **(d)** PCM4 **(e)** PCM5 **(f)** PCM6

Figure 4.7 (a) (PCM1) $Na_2SO_4 \cdot 10H_2O$ crystals or salt solution was distributed in a scattered manner throughout with alternating regions of both in the upper and lower sections of the composite into the PU matrix. In Figure 4.7 (b) (PCM2) The salt solution is concentrated on the left side, while $Na_2SO_4 \cdot 10H_2O$ occupies the right half, creating a vertically segregated arrangement similar previous case. In Figure 4.7 (c) (PCM3) The salt solution is concentrated on the right side, while $Na_2SO_4 \cdot 10H_2O$ occupies the left side, creating a vertically segregated arrangement. In Figure 4.7 (d) (PCM4) the salt solution and $Na_2SO_4 \cdot 10H_2O$ was arranged in alternate uniform vertical layers left to right of the PU-PCM composite. In Figure 4.7 (e) (PCM5) The salt solution and $Na_2SO_4 \cdot 10H_2O$ was arranged in alternate uniform horizontal layer from top to bottom of the PU-PCM

composite. In Figure 4.7 (f) (PCM6) the lower section of the PU-PCM composite is entirely filled with $Na_2SO_4 \cdot 10H_2O$, while the upper section remains occupied by the salt solution, forming a two-layer system. PCM6 configuration is the most practical case after using the PU-PCM composite for several days, due to gravity $Na_2SO_4 \cdot 10H_2O$ tries to segregate at the lower portion of the PU-PCM composite.

4.5 Results and discussion

4.5.1 DSC thermal analysis of PU-PCM composite

DSC is an essential technique used to examine the thermal properties of PU-PCM composite. DSC is also used to evaluate material stability by analyzing melting temperature and enthalpy, as well as recrystallization temperature and enthalpy, under various heating and cooling cycles. PU-PCM composite can absorb and release thermal energy during phase transitions. The DSC results over 10 cycles for same PU-PCM composite sample, as illustrated in Figure 4.8, presents the temperature profile (dotted line) and the DSC signal (solid line), which represents the heat flow associated with phase transitions in the Na_2SO_4-based PU-PCM composite. In each cycle during the heating phase, the temperature increases from -20°C to 80°C, and during the cooling phase, the temperature decreases from 80°C to -20°C. Sharp endothermic and exothermic peaks were observed alternatively in each cycle on DSC curve (Figure 4.8).

In the first cycle during heating from -20°C to 80°C (dotted line) at 5 °C/min, two distinct melting peaks appeared at temperature 0ºC and 30ºC. The melting peak at 0ºC indicates the presence of free water and the peak at 30ºC confirms the melting of $Na_2SO_4.10H_2O$. During cooling from 80°C to -20ºC (dotted line) with a cooling rate of 5°C/min, two exothermic peaks observed at temperature nearly 8ºC and 10ºC. First exothermic peak belongs to the partial crystallization of Na_2SO_4 solution as a mixture and the second peak is attributed to the complete crystallization of remaining Na_2SO_4 solution.

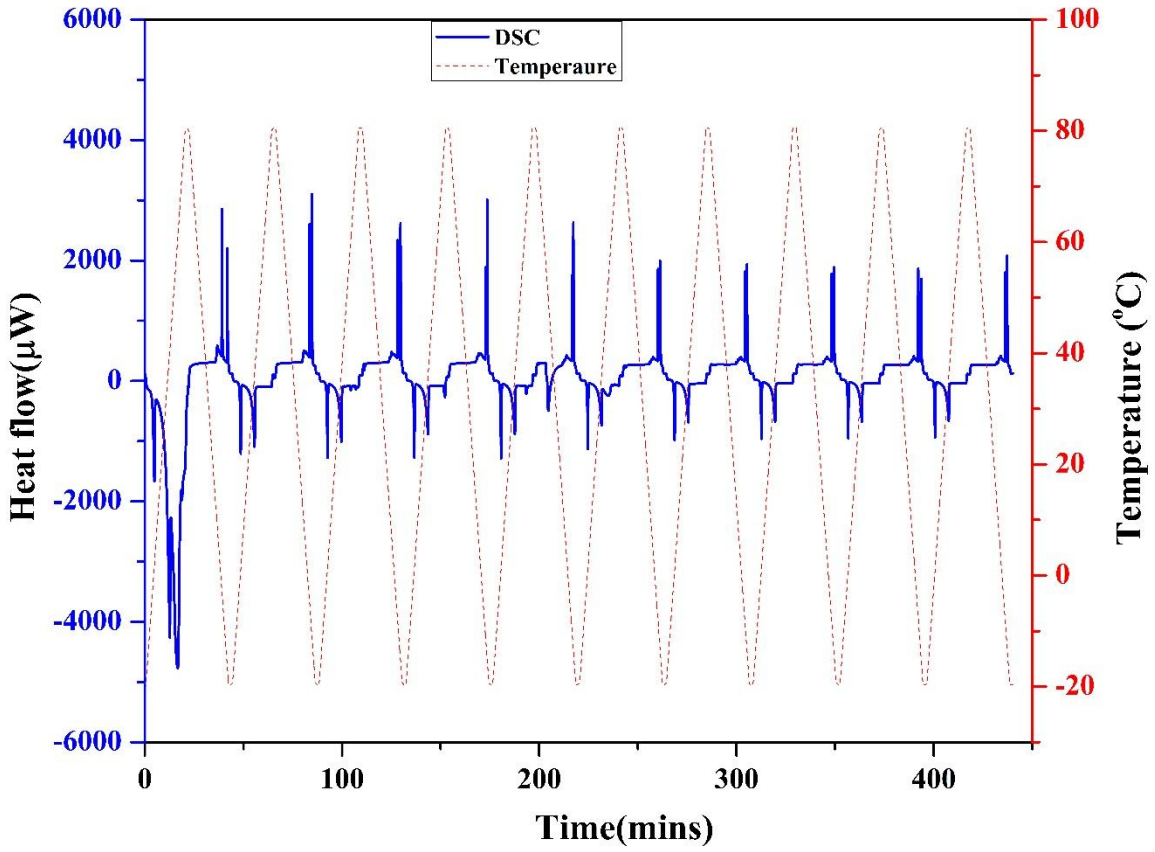

Figure 4.8 : DSC curve for $Na_2SO_4 \cdot 10H_2O$ - Based PU-PCM composite for 10 cycles

It was observed that in subsequent cycles the peak areas (endothermic and exothermic) and corresponding melting/freezing enthalpies varied in every cycle. This variation may be due to changes in PU-PCM composite properties during repeated melting and crystallization cycles in presence of Nitrogen carrier gas.

4.5.2 Experimental results for 600 mL Reactor

Figure 4.9 depicts the temperature difference (T_2-T_1) between reactor jacketed space temperature and inner space temperature alongside the jacketed space temperature over time for a 600 mL reactor. The experimental results were juxtaposed with computational simulations performed using COMSOL Multiphysics software. In the figure, the solid continuous line illustrates the fluctuations in chiller temperature, the dotted line with squares represents the temporal variation of the temperature difference (T_2-T_1) in the

experimental study, and the continuous line with triangles denotes the corresponding variation in the computational study.

At the outset, the reactor system was at 28 ℃, whereas the jacketed space temperature was roughly 40 ℃. The reactor's interior was cooler than the surrounding jacketed space, resulting in heat transfer from the jacket to the reactor. In the initial 20 minutes, this process eliminated the temperature differential (T_2-T_1). As the jacketed space cooled to 8 ℃, the temperature differential increased, peaking at 12 ℃. The gradual progression of the temperature differential curve implies a lack of sudden fluctuations, signifying the absence of excessive nucleation of $Na_2SO_4 \cdot 10H_2O$. Rather, minor nucleation on the PU fiber surface and ongoing crystal growth are anticipated as the temperature differential progressively rises.

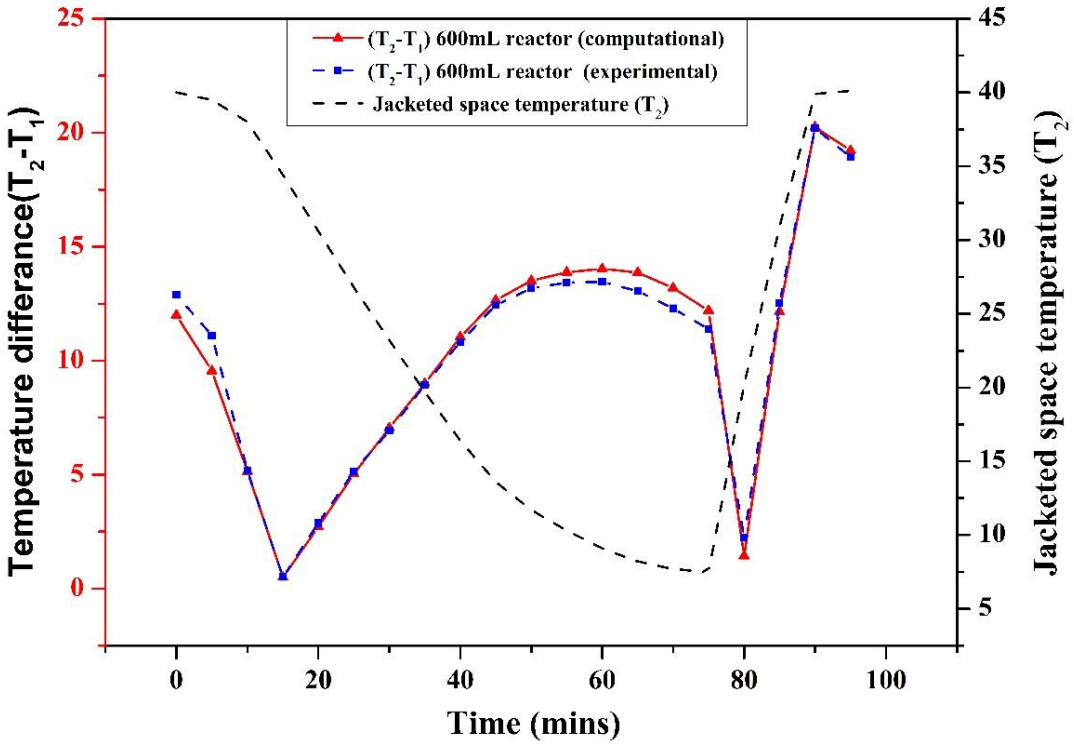

Figure 4.9 : Experimental results for 600 mL Reactor

The computational results closely aligned with the experimental trend, exhibiting a maximum deviation of 0.5 ℃, thereby validating the simulation. Minor discrepancies

between the experimental and computational data may be ascribed to model assumptions, measurement inaccuracies, thermal losses, and fluctuations in material properties.

4.5.3 Comparison of Computational results for 2L and 5L Reactor for different-different PU-PCM thickness with 600 mL reactor result

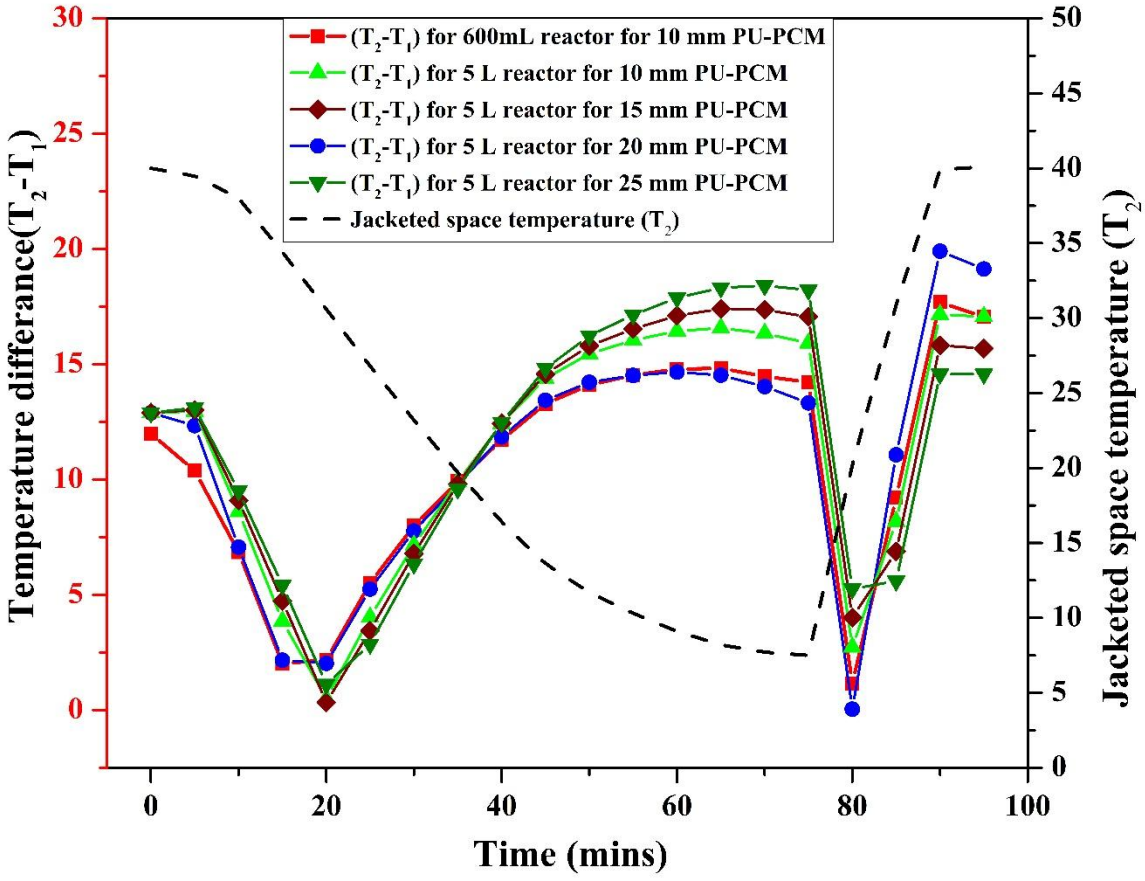

Figure 4.10 : Comparison of Computational results of 2L and 5L reactors for different-different PU-PCM Thickness with 600 mL reactor result

Figure 4.10 presents a comparison of computational results for 5 L reactor with different PU-PCM) thicknesses against the reference 600 mL reactor. This comparison aims to determine the optimal PU-PCM thickness for TES or insulation. In Figure 4.10 the jacketed space temperature (dashed line) follows a cooling and heating cycle, dropping from 40 °C to 10 °C in 75 minutes, then rising back to 40°C in 15 minutes. The temperature

difference (T_2-T_1) curves are plotted for various PU-PCM thicknesses. The line with squares represents the temperature difference (T_2-T_1) curves for 600 mL reactor (reference data curve).

Figure 4.10 the lines with circles, up triangles, down triangles, and diamonds represents the temperature difference (T_2-T_1) curves for 5 L reactor with 10 mm, 15 mm, 20 mm, and 25 mm PU-PCM thicknesses, respectively. The temperature differences (T_2-T_1) for 10 mm, 15 mm and 25 mm PU-PCM are higher, while the 20 mm PU-PCM thickness closely follows the 600 mL reactor's temperature differences (T_2-T_1) behaviour with respective to time. The absolute average error for 10 mm, 15 mm, 20 mm and 25 mm PU-PCM thickness compared to the 600 mL reference reactor is 1, 1.5, 0.25 and 2.5 respectively. The largest deviation occurs between 40 and 80 minutes, possibly due to increased salt solution content and reduced effective chamber volume caused by PU-PCM thickness. Among the tested PU-PCM thicknesses, 20 mm for 5 L reactor was the most suitable choice, as it maintains temperature variations closest to the 600 mL reference reactor. The same was considered to check the 5L reactor performance experimentally as shown in Figure 4.11.

4.5.4 Comparison of results for experimental and Computational models for 2L and 5L Reactors

The optimum PU-PCM thickness obtained through simulation using COMSOL Multiphysics software for 2 L and 5 L reactors, as discussed in the previous Section 4.4.2, was used for the experimental study. The experimental validation of simulation results obtained from model 2 L and 5 L reactors was also done. In Figure 4.11, the primary Y-axis represents the temperature difference (T_2-T_1), while the secondary Y-axis indicates the jacketed space temperature (T_2), with time plotted on the X-axis. The line with triangles and squares corresponds to computational and experimental results for a 2 L reactor with

10 mm PU-PCM, while the line with circles and diamonds represents computational and experimental data for a 5 L reactor with 20 mm PU-PCM. Additionally, the dashed black line shows the jacketed space temperature variation over time.

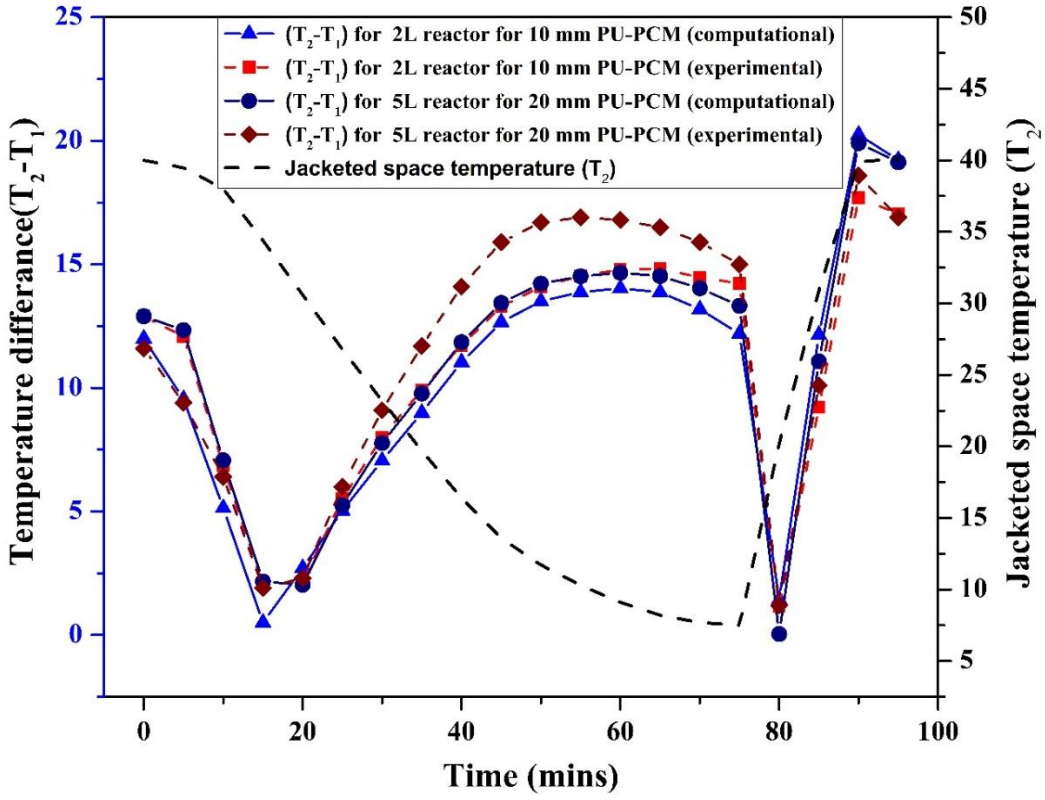

Figure 4.11 : Comparison of experimental and computational results for 2 L and 5 L reactors

The close alignment between experimental and computational results for 2 L and 5 L was observed, which validates the accuracy of the computational model in predicting the thermal behavior of PU-PCM-integrated reactors with an error of 0.5°C for 2 L and 0.75°C for 5 L. Multiple intrinsic factors in the experimental configuration and computational modeling procedure can account for this discrepancy. Heat loss may occur from the experimental apparatus to the surrounding environment, as perfect insulation is often impractical. Despite attempts to control environmental conditions such as temperature fluctuations and insulation levels, some degree of heat loss is inevitable. This loss can lead to discrepancies between the actual temperature inside the reactor and the temperature

being measured or simulated. The error might have been caused by differences in the thermal properties of the PU-PCM composite used in the simulation model compared to the real thing. Even when trying to model the material properties accurately in the simulation model, variations may occur due to differences in material composition, production process, or environmental conditions.

4.5.5 Comparison of salt quantity and salt solutions used in 600 mL, 2 L and 5 L reactors

Comparisons of actual and effective volumes, as well as salt and salt solution amounts for the 600 mL, 2 L, and 5 L reactors shown in Figure 4.3 are presented in Table 4.5 and illustrate the consistency and scalability of PCM preparation based on sodium sulphate decahydrate. Scaling factors for increasing reactor volumes are 3.90, 8.33, and 2.12, and effective volumes scale by 5.70, 11.20, and 2.55, indicating higher thermal efficiency in larger systems. The usage of anhydrous Na_2SO_4 increased from 64 g to 510 g, and the salt solution from 180 g to 1400 g, for 600 mL to 5 L reactor (as mentioned in Table 4.1) with scaling factors suggesting better phase change performance. PU-PCM composite volume ratios (2.24, 4.16, 1.85) show that insulation and PCM do not increase linearly with volume, with better thermal retention and reduced material costs. overall, large reactor provided superior heat transfer, lower unit volume cost, and higher energy storage efficiency, which makes them suitable for extensive thermal management applications.

Table 4.5 : Ratio of various parameters of various reactors

Comparison between reactors	Ratio of Actual Volume	Ratio of Effective volume	Ratio of Quantity Salt Used	Ratio of Aqueous Na_2SO_4 solution used	Volume ratios of PU-PCM composite for both reactors
2 L and 600 mL	3.90	5.70	2.81	2.77	2.24
5 L and 600 mL	8.33	11.20	7.96	7.77	4.16
5 L and 2 L	2.12	2.55	2.83	2.83	1.85

It has also been observed that all three reactors (600 mL, with 10 mm PU-PCM thickness, 2 L with 10 mm PU-PCM thickness and 5 L with 20 mm PU-PCM thickness) have exhibited similar temperature difference (T_2-T_1) profile trends along with time (given in Figure 4.9 and Figure 4.11). Based on the computational the actual volume ratio, effective volume ratio, required quantity of salt ratio and required quantity of salt solution ratio were calculated and presented in Table 4.5.

An intriguing observation from Table 4.5 is that, when comparing the ratios for (2 L and 600 mL), (5 L and 600 mL) and (5 L and 2 L) most ratios (such as effective and actual volume) varied irregularly. However, ratios for the required quantity of salt and salt solution are similar. This suggests that, based on simulation result, the ratio of salt and salt solution could potentially be used to estimate the volume of the PU-PCM composite and subsequently the overall reactor size. This insight will guide future developments in this research.

4.5.6 Comparison of simulation results for different arrangements of PU-PCM Composite

Simulation results were obtained using COMSOL Multiphysics software by considering various possible arrangements of the salt solution and $Na_2SO_4 \cdot 10H_2O$ within the PU-PCM composite, as discussed in the section associated with Figure 4.7. The computational results obtained for arrangements PCM 1, PCM 2, PCM 3, PCM 4, PCM 5, and PCM 6 (Figure 4.7) are shown in Figure 4.11. The temperature difference profiles observed for all arrangements exhibited similar trends. It was assumed that, upon the initiation of cooling from the left side of the composite, the phase transformation inside all the pores began from the left side and continued until complete solidification of $Na_2SO_4 \cdot 10H_2O$ was achieved.

For PCM 2 and PCM 3, though the quantity of phase change was identical, the heat flow from the outside was dependent on time. As the distance from the crystallization/phase change region increased, more heat was transferred into the vessel, resulting in an increased temperature difference profile compared to arrangement PCM 1. A similar trend of an increased temperature difference profile was also observed for PCM 4. In contrast, the temperature difference profile for PCM 5 almost coincided with that of PCM 1. However, as shown in Figure 4.12, a decrease in the temperature difference profile was observed for PCM 6. With a smaller phase change area, the heat resistance was reduced, resulting in a smaller temperature gap due to PCM phase segregation in PU-PCM composite.

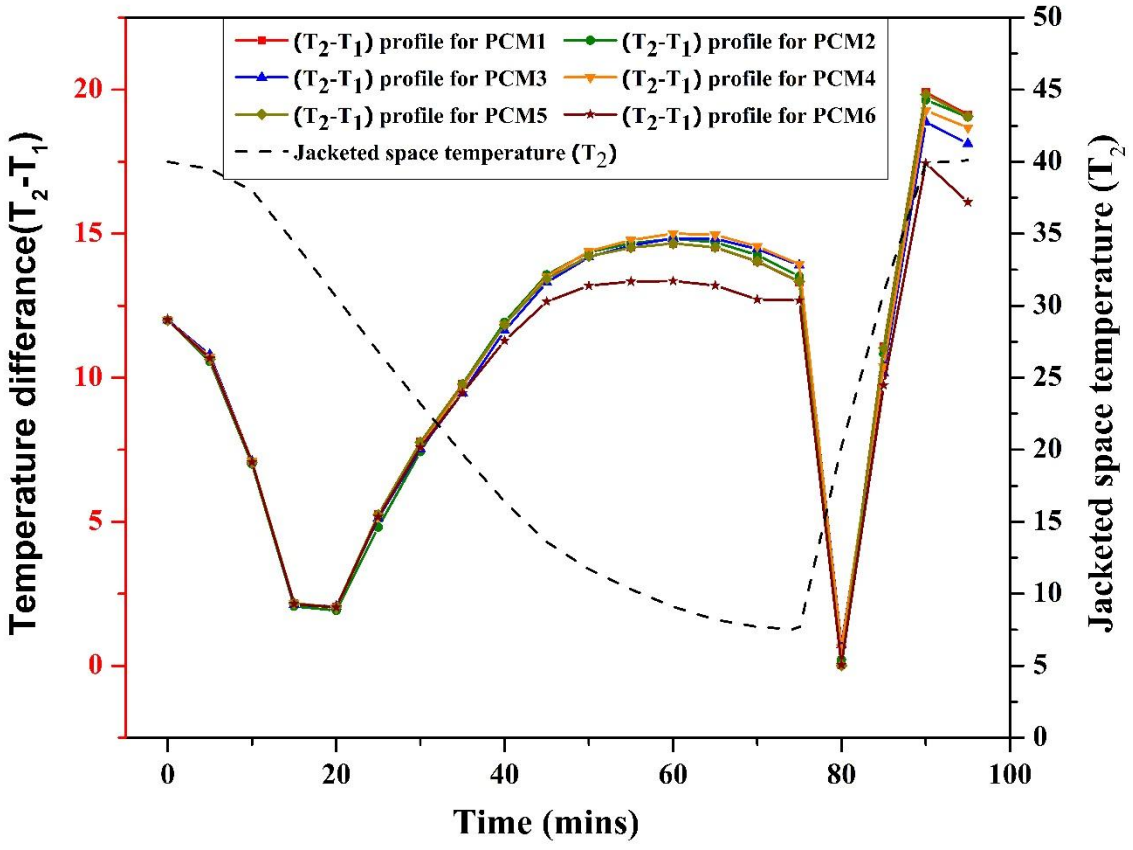

Figure 4.12 : Effect of different arrangements of PU-PCM Composite

4.5.7 Effect of latent heat (L) of PU-PCM composite on temperature difference (T_2-T_1) profile

For computational simulation, the latent heat (L) was taken as 240 J/g for validation of the experimental data, as discussed in section 4.4.2. $Na_2SO_4 \cdot 10H_2O$ crystallization is heterogeneous, and surface-based heterogeneous crystallization may have differences in melting enthalpy from homogeneous crystallization. Literature showed that the melting enthalpy of $Na_2SO_4 \cdot 10H_2O$ fell between 180 and 240 J/g. To investigate the effect of the latent heat (L) value on the temperature difference profile (T_2-T_1), the latent heat (L) of the PCM material was changed in computational simulation. Keeping phase change temperature range(ΔT) as 16 °C and PU-PCM arrangement PCM1 (given in Figure 4.7 (a)), latent heat of fusion for $Na_2SO_4.10H_2O$ PCM was changed with values 180, 240 and 300 J/g and temperature difference profile (T_2-T_1) observed as shown in Figure 4.13.

Figure 4.13, which has a line with a square, triangle and circle, shows the temperature difference profile (T_2-T_1) for 180, 240 and 300 J/g latent heat, respectively. The results show a similar trend in all the simulated temperature difference profiles (T_2-T_1), with a slight deviation observed between 45 and 75 minutes. For latent heat 180 J/g, the maximum temperature difference (T_2-T_1) was observed to be 14.5°C at the 60^{th} minute. For latent heat of 240 and 300 J/g, the maximum temperature differences were approximately 14°C and 15°C, respectively, at almost the same time point. Since the phase change temperature range (ΔT) was similar for all the three cases, the complete crystallization time would be similar. An increase in the latent heat of PCM, a greater amount of heat was absorbed during its phase transition. As a result, decrease in inner temperature (T_1) was delayed leading in the increased temperature difference profile (T_2-T_1).

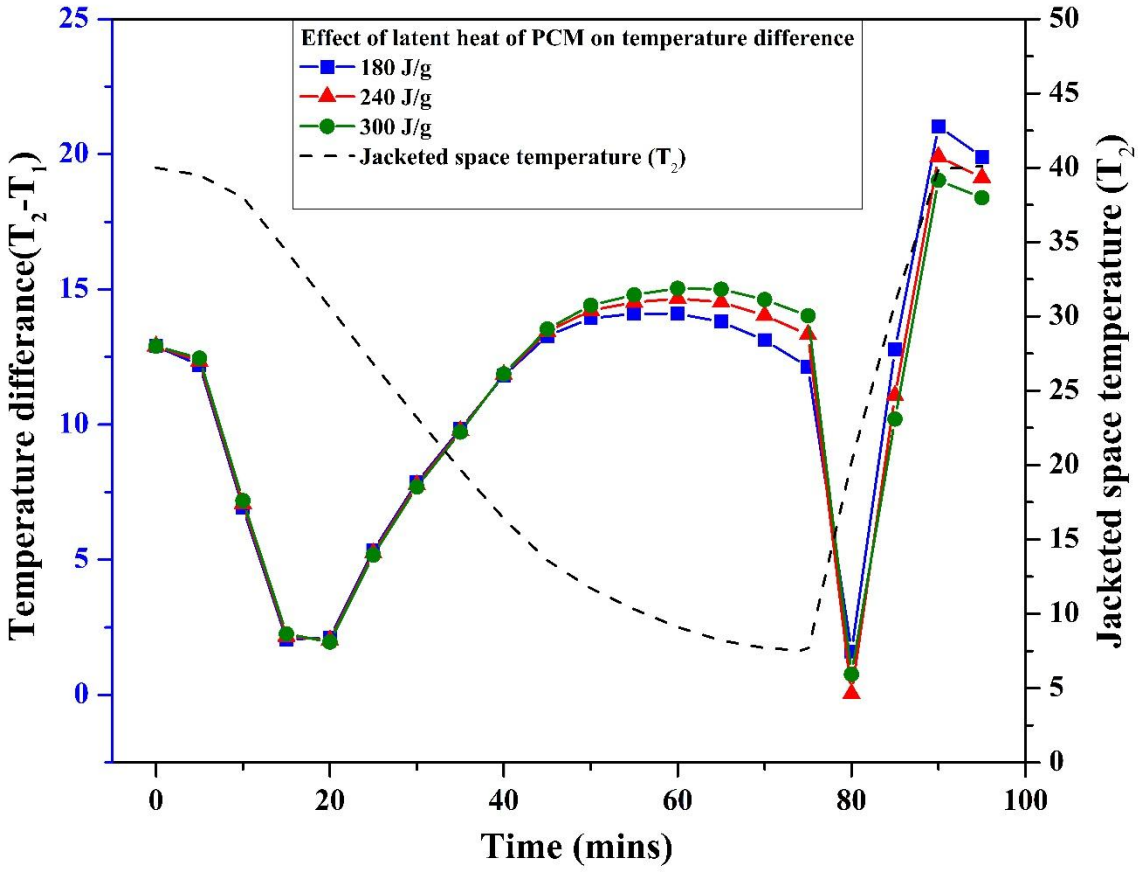

Figure 4.13 : Effect of latent heat (L) of PU-PCM composite on temperature difference profile (T_2-T_1)

4.5.8 Effect of phase change temperature range (ΔT) of PU-PCM composite on temperature difference (T_2-T_1) profile

A computational analysis was conducted to examine how variations in the phase change temperature range (ΔT) influence the temperature difference profile (T_2-T_1). In this study, the latent heat (L) of the PCM material was fixed at 240 J/g and PU-PCM arrangement PCM1 (given in Figure 4.7 (a)), while phase change temperature range (ΔT) was adjusted to 12°C, 18°C, and 24°C. Figure 4.14, illustrate line with a square, triangle and circle, shows the temperature difference profile (T_2-T_1) for 12 °C, 18 °C and 24 °C phase change temperature range (ΔT) respectively. The results show a similar trend in all the simulated temperature difference profiles (T_2-T_1).

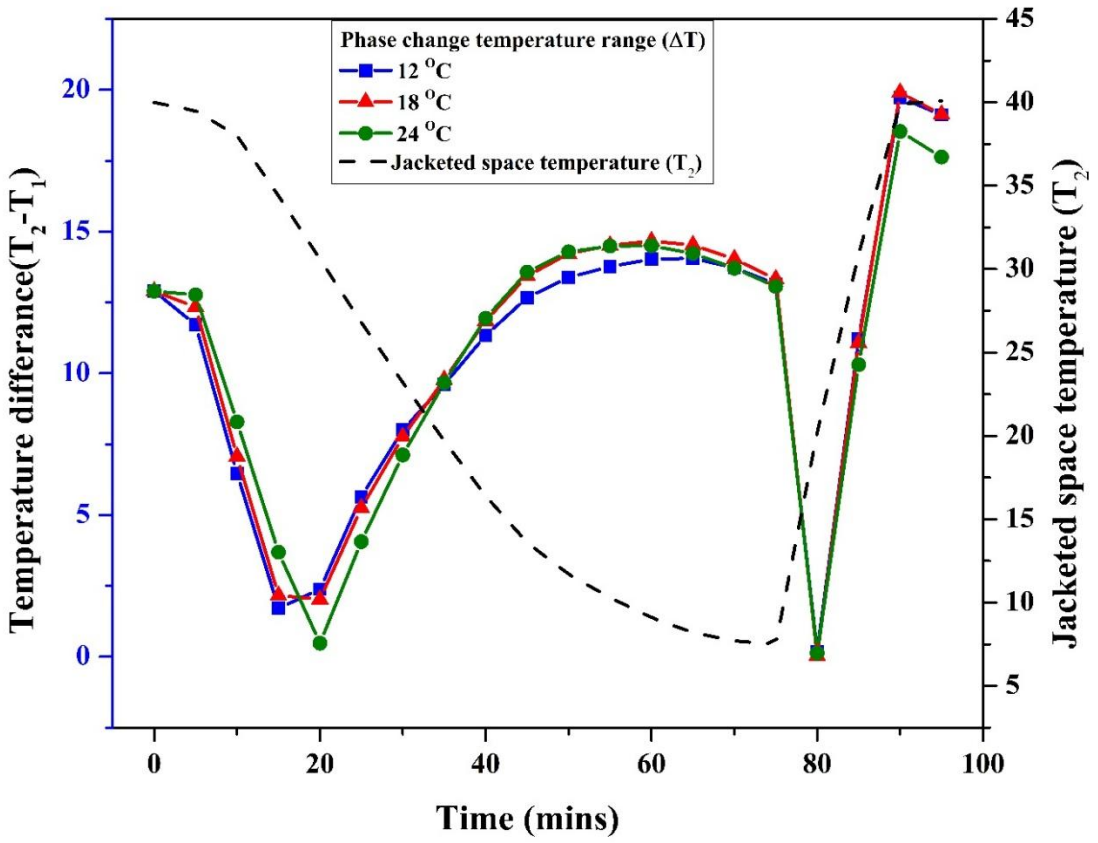

Figure 4.14 : Effect of phase change temperature range (ΔT) of PCM on temperature difference (T_2-T_1) profile

Figure 4.14 reveals that as ΔT increases from 12°C to 24°C, the area under the curves expands. The temperature difference profile (T_2-T_1) profile for ΔT = 24°C, represented by line with circles, appears broader than the others. This phenomenon can be attributed to the extended time required for the system to achieve thermal equilibrium, delaying the complete solidification of the PCM. As a result, the energy release within the PU-PCM composite is prolonged, maintaining a larger temperature difference over time.

4.5.9 Thermal performance and Stability for repeated cycles

Figure 4.15 illustrated the experimental results (as give in experimental setup Figure 4.4) temperature difference (T_2-T_1) profile for various cycles (1st, 10th, 25th, and 100th) over time, along with the jacketed space temperature(T_2) for 5 L reactor. The dotted lines with circle, square, diamond, and triangle represent the temperature difference profile for

1st, 10th, 25th, and 100th cycles respectively. The results show a similar trend for temperature difference profiles (T_2-T_1) in all the cycles.

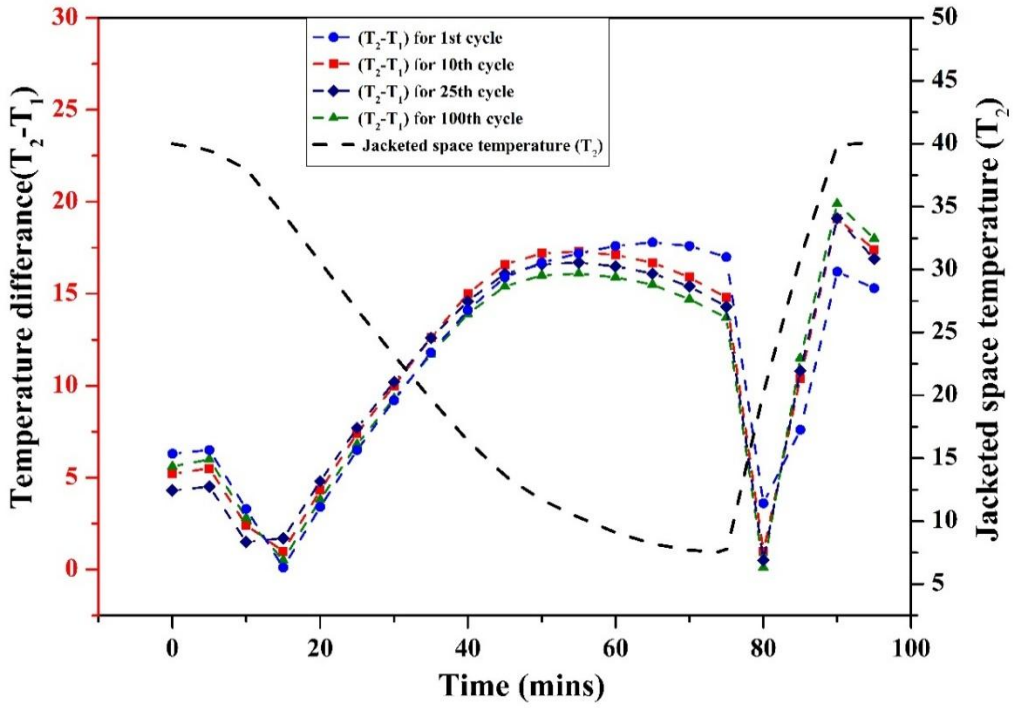

Figure 4.15 : Temperature difference profile (T_2-T_1) repeated cycles

It was observed from Figure 4.15 that there is slight variation in temperature difference profiles (T_2-T_1) from 1st cycle to 100th cycle. These variations may have occurred due to changes in properties of PU-PCM composite such as specific heat and viscosity which might change over time due to phase segregation, foam degradation, or aging. These changes could have affected heat transfer rates and resulted in decreased temperature difference (T_2-T_1). Overall, for initial 100th cycles, the system was found to be thermally stable with variation of temperature difference profile with error of 1 °C. This may have been due to $Na_2SO_4 \cdot 10H_2O$ settle down at the lower portion of the PU-PCM composite due to gravity in long term use. Furthermore, the results 25th, 50th and the 100th cycle may be compared with one of the simulation results given in Figure 4.12 for PU-PCM to understand reason for the variation in thermal insulation performance may be found easily.

4.6 Summary

This study investigated the scale-up of sodium sulfate decahydrate-based phase change material (PCM) for TES systems, expanding from a 600 mL reactor to 2 L and 5 L reactors. Experimental data from the 600 mL reactor served as a baseline for evaluating larger systems. Optimal PU-PCM thicknesses (10 mm for the 2 L and 20 mm for the 5 L reactor) were determined through simulation using COMSOL Multiphysics. The simulation results closely matched experimental observations, validating the thermal response across all reactor sizes.

DSC confirmed the thermal stability of the PU-PCM composite over multiple cycles, showing consistent melting temperature and latent heat values. Simulation was also conducted analyses of the thermal performance of different PU-PCM composite arrangements, as well as the effects of latent heat (L) of PCM and phase change temperature range (ΔT) on the temperature difference (T_2-T_1) profile. Long-term cycling test confirmed consistent energy storage and release behaviour.

The simulation results indicate that the ratios of salt and salt solution between the reactors can serve as a reliable parameter for estimating the PU-PCM composite volume, and further the overall reactor size. This insight provides valuable guidance for future scale - up related research. Overall, the findings demonstrate the feasibility of scaling sodium sulfate decahydrate-based TES systems by using COMSOL Multiphysics software. Extension of current work need to focus on enhancing thermal conductivity, refining reactor geometry, and integrating advanced heat management strategies to support efficient large-scale thermal storage systems.

The scaled-up PU-PCM system developed in this study is designed to function as a thermal buffer in external walls and ceilings of buildings exposed to variable solar radiation. By embedding the sodium sulphate decahydrate-based composite within building

components, heat is stored during peak solar gain and released during cooling demand periods, thereby reducing temperature swings and shifting energy usage away from peak hours. This approach supports passive heating in cold climates and hybrid cooling in hot regions.

Chapter-5

Performance Evaluation and Integration of Salt Hydrate-Based PCMs with Wall Materials for Cooling of Buildings

5.1 Introduction

The present study numerically investigates the thermal performance of a brick wall integrated with a polyurethane-based phase change material (PU-PCM) composite for passive cooling applications. A PU-PCM composite incorporating sodium sulfate decahydrate ($Na_2SO_2 \cdot 10H_2O$) as the latent heat storage medium was developed and positioned as an interlayer between two brick wall sections to regulate indoor thermal conditions. $Na_2SO_2 \cdot 10H_2O$ was selected due to its appropriate phase transition temperature, high latent heat capacity, non-flammability, and cost-effectiveness, making it suitable for building envelope integration.

A transient finite element model was developed using COMSOL Multiphysics to simulate heat transfer through the PCM-integrated wall under realistic outdoor temperature variations. The model accounts for conduction, phase change behavior, and temperature-dependent material properties. Differential Scanning Calorimetry (DSC) was performed to experimentally determine the melting temperature and latent heat of the PU-PCM composite, and the obtained thermal properties were incorporated into the numerical model to improve prediction accuracy.

Simulation results indicate that the inclusion of the PU-PCM layer significantly enhances the thermal inertia of the wall system. Compared to a conventional brick wall, the PCM-integrated configuration reduced peak indoor surface temperature by approximately 3-5 °C and introduced a noticeable time lag in heat transfer. This delay effectively shifts thermal

loads to off-peak periods, contributing to improved indoor thermal comfort and reduced cooling demand.

The findings demonstrate that $Na_2SO_2 \cdot 10H_2O$ -based PU-PCM composite are effective for passive thermal regulation in buildings and can be feasibly integrated into brick wall assemblies. The study provides valuable insights for the design and optimization of scalable PCM-based thermal storage systems, particularly for energy-efficient buildings in hot and arid climatic regions.

5.2 Materials and Methods

5.2.1 Selection of PCM

$Na_2SO_2 \cdot 10H_2O$ (sodium sulphate decahydrate) was selected as the phase change material for this study owing to its thermophysical properties that are well suited for passive summer cooling applications in buildings. It exhibits a melting temperature of approximately 32 °C, which closely matches the typical indoor comfort range and enables effective absorption of excess heat during peak daytime conditions. In addition, its high latent heat of fusion, around 250 kJ/kg, provides a high thermal energy storage density, allowing substantial heat absorption within a relatively small material volume. Furthermore, sodium sulphate decahydrate is non-flammable and significantly more cost-effective than organic PCMs such as paraffins, making it a safer and economically attractive option for large-scale building integration.

5.2.2 Fabrication Composite PCM

A saturated sodium sulphate solution was prepared by dissolving 64 g of anhydrous Na_2SO_4 in 150 mL of distilled water, producing a 30 wt.% Na_2SO_2 solution with an approximate final volume of 175 mL. The solution was heated to 35 °C and continuously stirred to ensure complete dissolution of the salt. It was subsequently clarified by vacuum filtration to remove any remaining undissolved particles. From the filtered solution, 150 mL was

collected for further use. This clear sodium sulphate solution was then impregnated into the interconnected pore network of polyurethane (PU) foam sheets to fabricate PU-PCM composite sheets, as illustrated in Figure 5.1. The porous PU matrix effectively retains the hydrate and suppresses leakage during the melting process. To prevent the solution from evaporation/leakage prepared PU-PCM composite was finally cast into sheets with thicknesses of 0.00006 m for integration within wall assemblies.

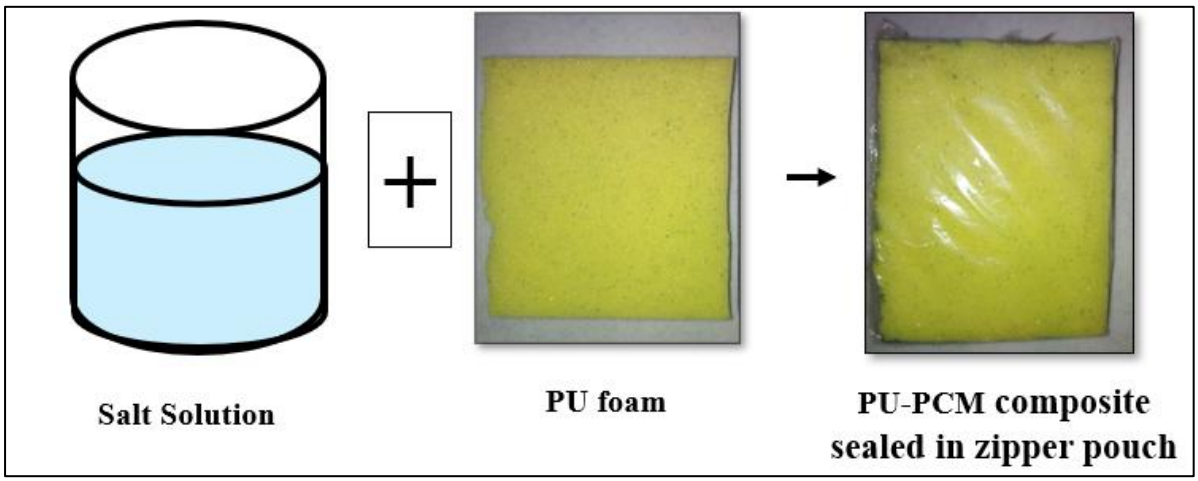

Figure 5.1: Development of PU-PCM composite

5.2.3 Thermal Characterization

Differential Scanning Calorimetry (DSC): The melting enthalpy of the PU-PCM composite was measured through a differential scanning calorimeter DSC7020, HITACHI at RGIPT, Jais. For the DSC analysis, it was performed under a nitrogen environment at a flow rate of 50 mL/min. The programmed temperature range varied from -20 °C to 80 °C at a heating rate of 5 °C/min.

Thermal conductivity measurement: The thermal conductivity of the prepared nanocomposite PCM was determined using a Linseis THB-100 thermal conductivity analyzer operating on the transient hot-wire principle. Measurements were performed at

room temperature (25 °C). The instrument provides a measurement uncertainty of ±5% and a timing accuracy of ±0.1 s for transient measurements.

5.3 Wall Assembly

A composite wall representative of a typical Indian residential building was considered in this study. The base configuration comprised a 90 mm thick brick wall with 20 mm plaster layers on both the inner and outer surfaces. To evaluate the influence of PCM integration on thermal performance, this baseline wall was systematically modified by introducing a 10 mm thick PCM composite layer at different locations within the wall assembly.

The resulting wall configurations, illustrated in Figure 5.2, are designated as Module 0, Module 1, Module 2, and Module 3. Module 0 corresponds to the conventional brick wall and serves as the reference case, where heat transfer occurs solely through sensible heat storage, resulting in limited thermal inertia and a rapid response to outdoor temperature variations.

In Module 1, the PCM composite layer is positioned on the external side of the wall, immediately after the outer plaster layer, enabling it to absorb a substantial portion of incoming solar and ambient heat before it reaches the brick core. Module 2 places the PCM composite layer on the internal side, just before the inner plaster layer, allowing direct interaction with the indoor environment. Module 3 embeds the PCM composite layer at the mid-plane of the brick wall, forming a symmetric sandwich structure that acts as a thermal buffer by moderating heat transfer from both exterior and interior directions.

Overall, these configurations enable a systematic assessment of how PCM placement within the wall assembly influences heat storage, time lag, and passive cooling effectiveness, thereby guiding optimal design strategies for energy-efficient building envelopes.

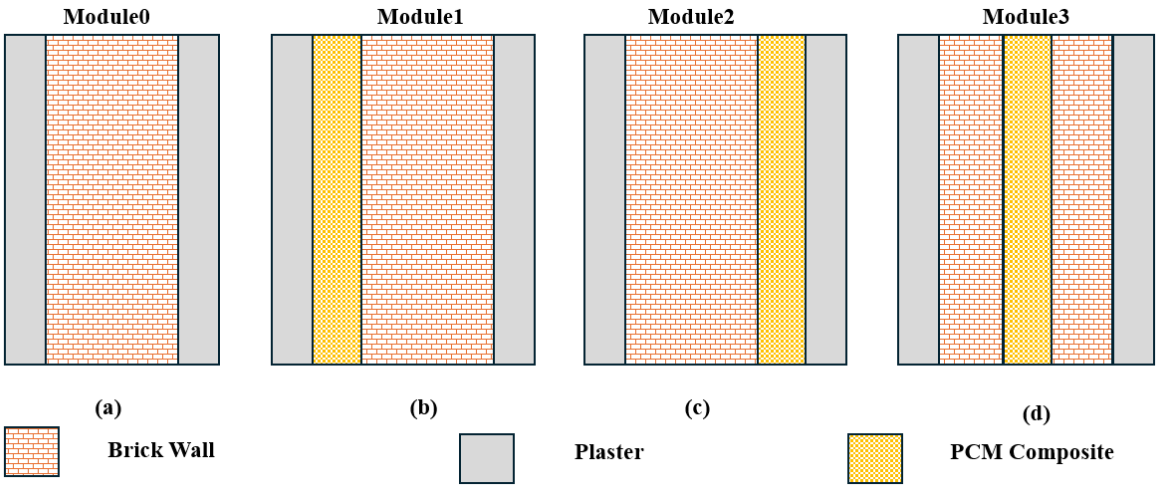

Figure 5.2 : Different configurations of wall **(a)** Brick wall plaster at inner and outer side **(b)** PCM Composite Integration after outer plaster (c) PCM Composite integration before inner plaster **(d)** PCM composite integration at the middle of brick wall

5.4 Numerical Modelling and Simulation

5.4.1 3-D model development for Heat Transfer through Walls

A three-dimensional room model with dimensions of 4 m × 4 m × 4 m was developed using COMSOL Multiphysics**,** as shown in Figure 5.3 (a), to investigate transient heat transfer through the wall assemblies. The model incorporated the various wall configurations, with and without the PCM-integrated layers, to evaluate their thermal performance under realistic boundary conditions. Particular emphasis was placed on assessing the effect of the $Na_2SO_4 \cdot 10H_2O$ based PU-PCM composite interlayer in moderating indoor temperature fluctuations.

The computational domain was discretized using the finite element method (FEM). To ensure accuracy, a non-uniform mesh was applied: coarser elements were used in bulk regions of the brick and plaster layers, while a normal mesh (as shown in Figure 5.3 (b)) was generated within the PCM composite region to capture the sharp thermal gradients associated with phase change. The generated mesh provided a good balance between computational efficiency and numerical accuracy, ensuring stability during transient simulations.

The simulations were conducted in a time-dependent mode over a 24-hour cycle corresponding to the atmospheric temperature profile of 2 June 2025, as shown in Figure 5.4. A time step of 60 s was employed to accurately capture the transient heat transfer and phase change behaviour of the PCM while maintaining numerical stability and reasonable computational cost. The time step was selected based on preliminary trials to ensure convergence and to resolve the rapid temperature variations occurring during the melting and solidification processes.

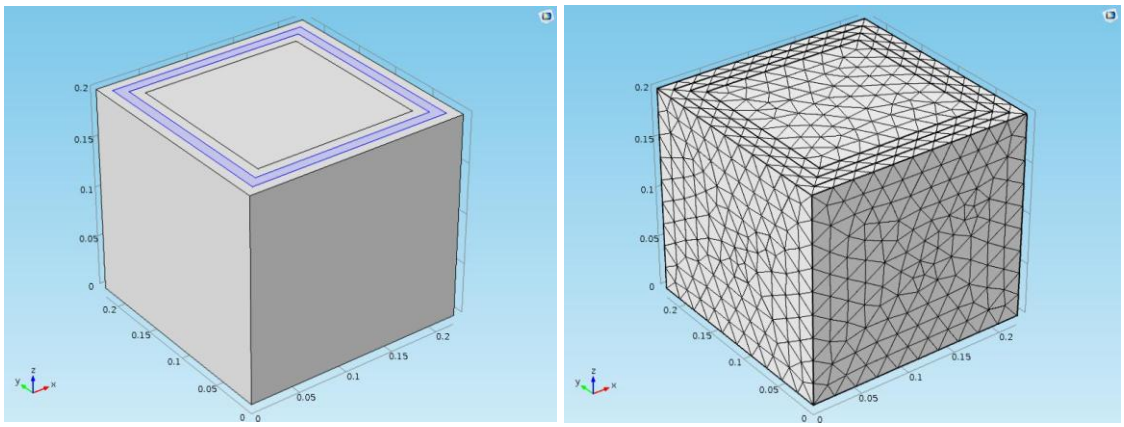

(a) **(b)**

Figure 5.3 : (a) 3-D- model developed in COMSOL **(b)** model with normal mesh

5.4.2 Assumptions used for computational study

To simplify the heat transfer model, the following assumptions are applied:

- The heat transfer is primarily one-dimensional across wall thickness.
- The convection effect in the molten PCM was neglected.
- The thermophysical properties of the materials were constant except the specific heat capacity of the PCM during the melting and freezing processes.
- All the materials were assumed to be isotropic media.
- The initial Temperature of the whole system was assumed to be 32℃.
- For simplification of simulation temperature of the outer wall is assumed to be same their surrounding temperature.

5.4.3 Governing Equations and Boundary Conditions

5.4.3.1 Governing Equations

A one-dimensional transient heat conduction model is used to describe heat transfer through the multi-layer wall or roof assembly, including the PCM layer. For non-PCM layers, the governing equation is the standard heat diffusion equation in Cartesian coordinates:

$$\rho C_P \frac{\partial T}{\partial t} + \nabla.(-k.\nabla T) = Q \qquad (\mathbf{5.1})$$

where ρ is the density (kg m^{-3}), C_p is the specific heat capacity (J kg^{-1} K^{-1}), k is the thermal conductivity (W m^{-1} K^{-1}), T is the temperature (K), and t is time (s).

5.4.3.2 Boundary Conditions

The external wall surface was subjected to time-dependent ambient temperature conditions corresponding to the climatic data of 2 June 2025, along with convective heat transfer with the surrounding air. The boundary condition at the exterior surface is given by:

$$-k\nabla T \cdot \mathrm{n} = h_o(T - T_{amb}) \qquad (\mathbf{5.2})$$

here $h_o$is the outdoor convective heat transfer coefficient (W m^{-2} K^{-1}) and T_{amb} is the ambient air temperature (K).

The interior wall surface was modeled using an indoor convective boundary condition to represent heat exchange with the room air:

$$-k\nabla T \cdot \mathrm{n} = h_i(T - T_{in}) \qquad (\mathbf{5.3})$$

where $h_i$is the indoor convective heat transfer coefficient (W m^{-2} K^{-1}) and $T_{in}$is the indoor air temperature (K).

All other surfaces of the computational domain were assumed to be adiabatic, neglecting lateral heat losses.

5.4.4 Variation of outdoor air temperature for different regions and different Seasons of India

In the present study, the initial analysis focused on Delhi**,** for which outdoor air temperature data were collected over a four-day period from 1 June to 4 June 2025 and employed as the external thermal boundary conditions in the numerical simulations. This period corresponds to peak summer conditions in Delhi and captures pronounced diurnal temperature variations, as illustrated in Figure 5.4(a). To extend the analysis and enable a broader climatic assessment, outdoor temperature profiles were subsequently considered for four major Indian cities—Delhi, Mumbai, Chennai, and Kolkata, representing distinct climatic zones.

Furthermore, seasonal variability was incorporated by using temperature data corresponding **to** three representative seasons, namely winter (January), summer (June), and monsoon (September), as illustrated in the Figures 5.4 (b).

The inclusion of multi-city and multi-season temperature profiles enables a comprehensive evaluation of the thermal response of PCM-integrated building envelopes under diverse and extreme climatic conditions, thereby providing a robust basis for assessing the effectiveness of passive cooling strategies.

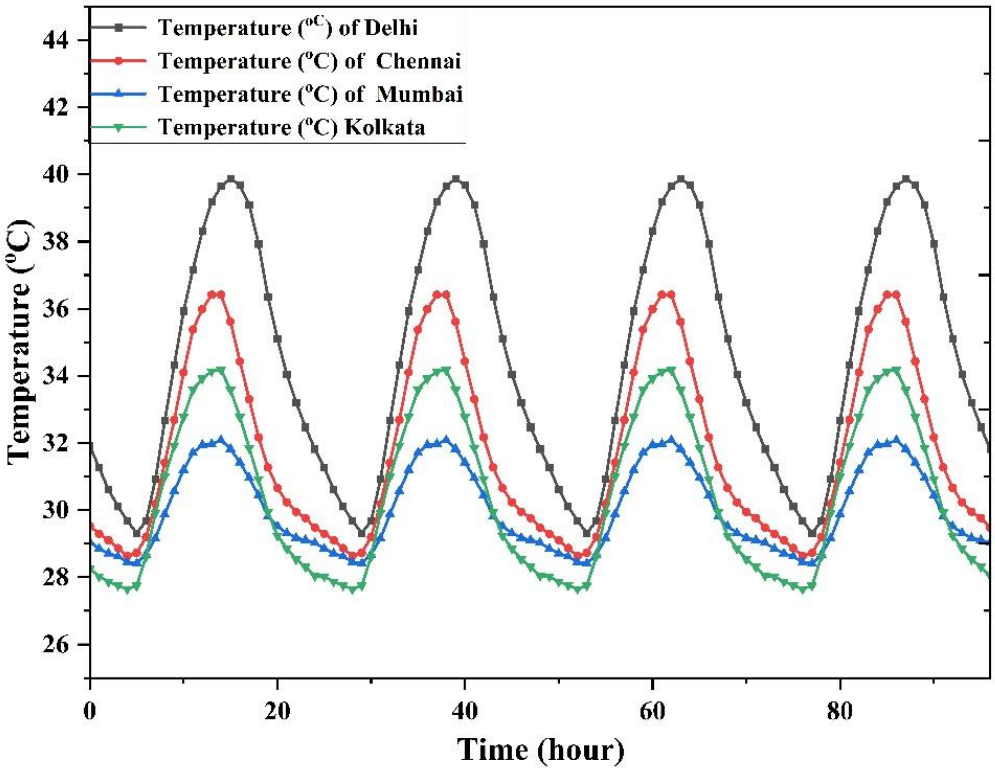

(a)

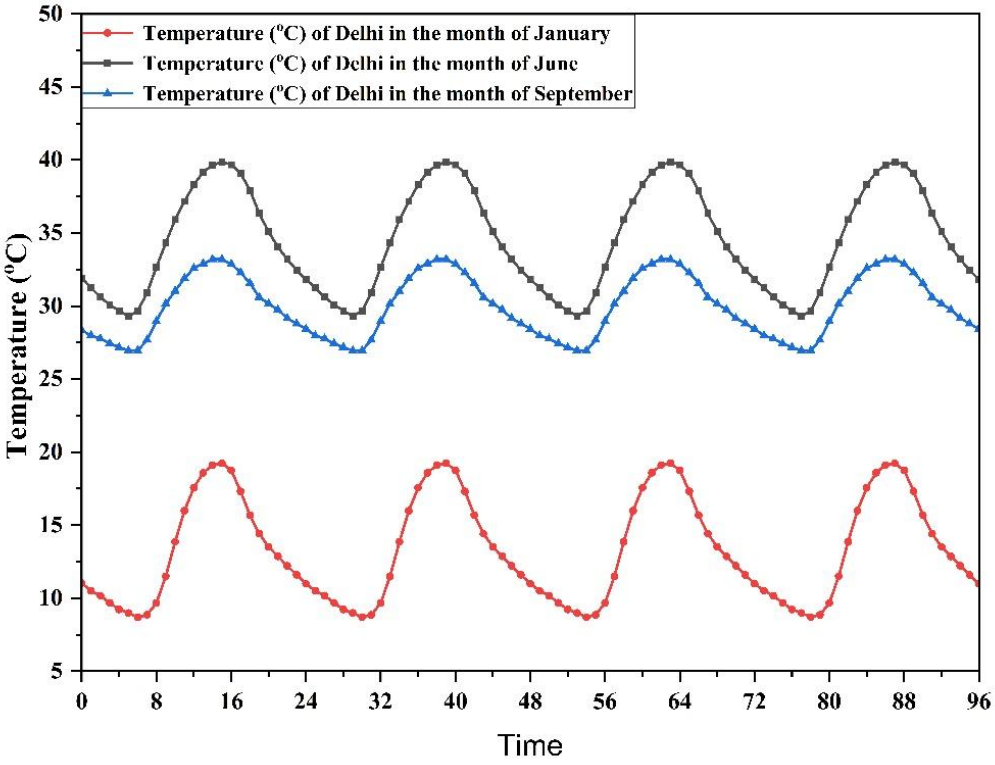

Figure 5.4 : Variation of outdoor air temperature with time for different **(a)** Cities and **(b)** Seasons of India

5.4.5 Materials Properties

Table 5.1 presents the thermophysical properties of the wall constituent materials used in the simulations, including brick, plaster, and the PCM in both solid and liquid states. These properties such as density, specific heat capacity, and thermal conductivity govern the heat storage and transfer within the wall assembly and are essential inputs for accurately predicting the thermal response of PCM-integrated building envelopes.

Table 5.1 : Thermophysical parameters of wall materials [42]

Thermal properties	**Brick**	**Plaster**	**PCM Solid**	**PCM Liquid**
Density, ρ (kg m^{-3})	2000	1300	1460	1330
Heat capacity, C_P (J kg^{-1} K^{-1})	900	1620	1920	3260
Thermal conductivity, K (Wm^{-1} K^{-1})	0.5	0.35	0.544	0.544

5.5 Results and Discussion

5.5.1 DSC Analysis: Melting Temperature and Latent Heat

The Differential Scanning Calorimetry (DSC) results, shown in Figure 5.5, provide clear insight into the thermal storage capability and phase change behaviour of the developed PU-PCM composite. The DSC thermogram reveals a distinct melting peak at 31.8 °C, which lies well within the targeted indoor thermal comfort range for passive cooling applications in buildings (22-35 °C). This confirms that the selected salt hydrate $Na_2SO_2 \cdot 10H_2O$ based PCM is thermally well matched to building envelope requirements, enabling it to effectively absorb excess heat during daytime temperature rise.

The measured latent heat of fusion of the PU-PCM composite was 233 kJ/kg, which is in close agreement with the reported latent heat values of pure $Na_2SO_4 \cdot 10H_2O$ (230-250 kJ/kg). This indicates that incorporation of the salt hydrate into the polyurethane matrix does not significantly compromise its heat storage capacity. The high latent heat ensures

that a substantial amount of thermal energy can be absorbed during the phase transition process, thereby reducing heat transfer to the indoor environment and enhancing thermal buffering of the wall system.

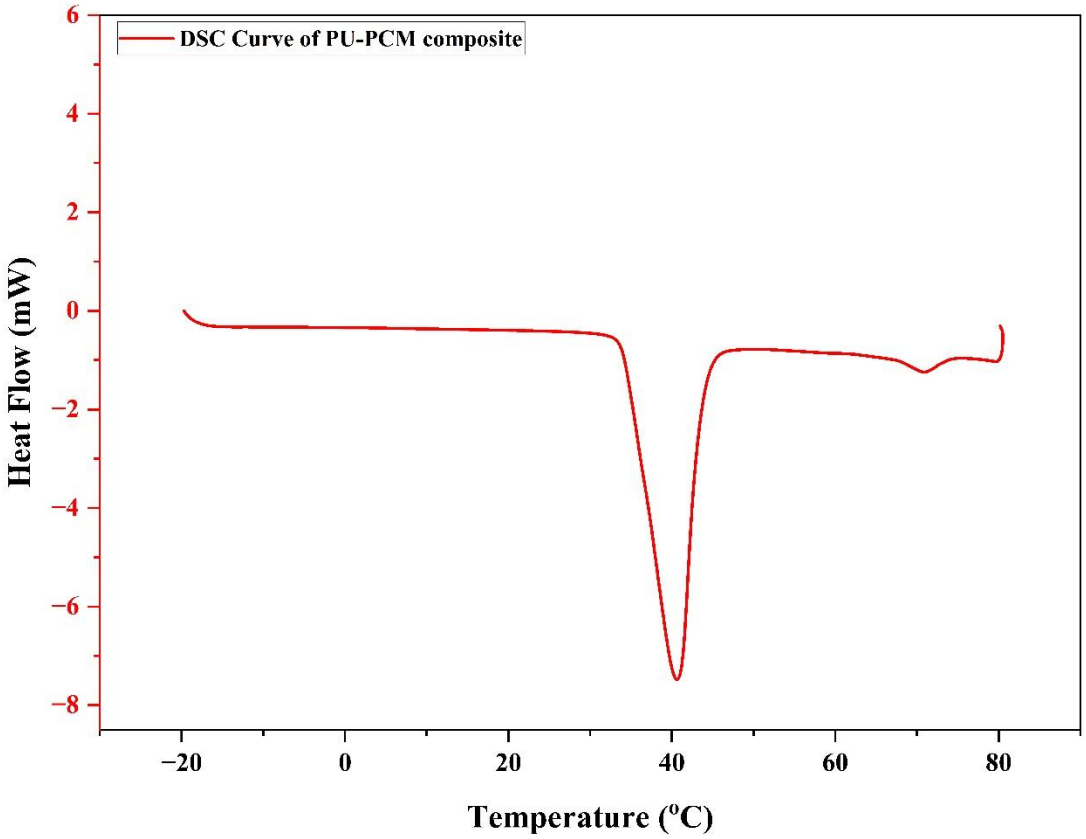

Figure 5.5 : DSC Analysis on PU-PCM Composite

5.5.2 Thermal Properties Analysis of PU-PCM Composite

The thermal performance of PU-PCM composite is governed by key properties such as thermal conductivity, specific heat capacity, thermal penetration depth, and thermal diffusivity, which collectively influence heat transfer efficiency, energy storage capability, and transient thermal response. These properties were experimentally evaluated at room temperature using a THB-100 (Linseis) thermal analyzer, ensuring reliable measurements through optimized sensor contact and automated data acquisition. Incorporation of Laponite® and Borax into the PU-PCM matrix resulted in enhancements in thermal conductivity, and heat storage capacity. This enhancement is attributed to improved heat-

transfer pathways and reduced interfacial thermal resistance, leading to superior thermal response and stability of the PU-PCM composite under cyclic thermal loading. Thermal properties measured are shown in Table 5.2.

Table 5.2 : Measured Thermal Properties of PU-PCM Composite with and without Additives

Material	K Thermal conductivity (W/mK)	Cp Specific heat (J/gK)
PU-PCM Composite without additive	0.506	1860
PU-PCM Composite with additives	0.554	1950

5.5.3 Comparison of indoor thermal behaviour of a PCM-incorporated wall with a conventional wall

Figure 5.6 illustrates the transient variation of outdoor air temperature and the corresponding indoor temperature for the conventional wall (Module 0) and the PCM-integrated wall (Module 1) over a 96-hour period. The outdoor temperature exhibits pronounced diurnal fluctuations, with peak values approaching 40 °C during daytime and minimum values of approximately 29-30 °C during nighttime. In contrast, the indoor temperature responses show moderated behaviour due to the thermal inertia of the wall assemblies.

For the conventional wall (Module 0), the indoor temperature closely follows the outdoor temperature trend, with relatively high peak values and limited attenuation. Peak indoor temperature reach approximately 38-39 °C during daytime hours, indicating rapid heat transfer through the wall and limited thermal buffering capacity.

In comparison, the PCM-integrated wall (Module 1) demonstrates a noticeable reduction in peak indoor temperature, with maximum values lowered by approximately 2-3 °C relative to the conventional wall. This reduction is attributed to the latent heat absorption of the PCM during the melting process, which effectively stores excess thermal energy and

delays its transmission to the indoor space. As a result, indoor temperature remain comparatively lower during periods of peak outdoor heat load.

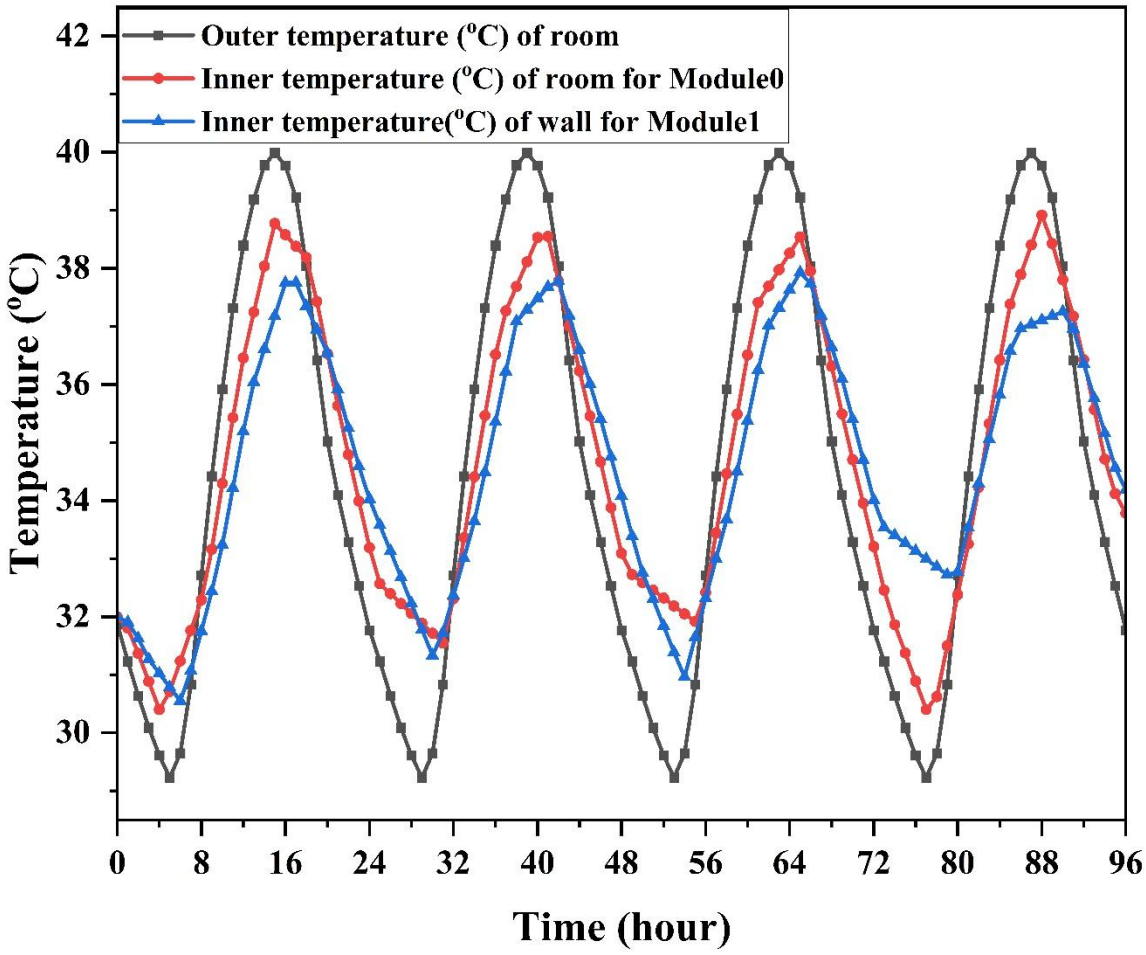

Figure 5.6 : Comparison of indoor thermal behaviour of a PCM-incorporated wall with a conventional wall

Additionally, the PCM wall exhibits a clear time lag in the occurrence of peak indoor temperature. The indoor temperature maximum for Module 1 is shifted several hours later compared to the outdoor peak, indicating effective phase-shifting behavior. This thermal lag helps postpone indoor heat gain to later hours when outdoor temperature begin to decline, thereby improving indoor thermal comfort.

Furthermore, the amplitude of indoor temperature fluctuations is significantly reduced for the PCM-integrated wall. Compared to the conventional configuration, the PCM wall

shows a damped temperature swing, leading to a more stable indoor thermal environment over the daily cycle. This reduction in temperature amplitude highlights the enhanced thermal inertia provided by the PCM layer and its ability to smooth out extreme temperature variations.

Overall, the results presented in Figure 5.6 confirm that incorporation of the PU-PCM composite layer substantially improves wall thermal performance by reducing peak indoor temperature, increasing thermal lag, and attenuating temperature fluctuations, thereby enhancing the passive cooling effectiveness of the building envelope.

5.5.4 Investigation of the optimum location of PU-PCM

Figure 5.7 compares the transient variation of inner wall temperature for different PCM-integrated wall configurations over a 96-hour period. The results clearly highlight the influence of PCM placement and quantity on the thermal performance of the wall assembly.

Module 0, which does not incorporate any PCM, exhibits the highest and earliest peak inner wall temperature, clearly reflecting the limited thermal buffering capacity of a conventional brick-plaster wall. The rapid rise in inner surface temperature indicates that heat is transmitted directly through the wall with minimal attenuation or delay. In contrast, the incorporation of PCM in Module 1 and Module 2 significantly reduces peak inner wall temperature, demonstrating the effectiveness of latent heat absorption in moderating heat transfer through the wall assembly.

Among the PCM-integrated configurations, Module 3—featuring two PCM layers—shows a marginally improved performance compared to Module 2, where the PCM is placed closer to the inner wall. This improvement can be attributed to the increased PCM content and enhanced distribution of latent heat storage within the wall, which allows for more effective absorption and redistribution of thermal energy. Notably, Module 1, in which the PCM layer is positioned closer to the outer wall, delivers the most substantial reduction in inner

wall temperature, on the order of approximately 3-4 °C. This superior performance arises because the PCM intercepts and absorbs the incoming heat flux earlier in the daily heating cycle, thereby preventing excessive heat penetration into the interior.

Overall, these results confirm that both the quantity and the strategic placement of PCM layers play a critical role in improving wall thermal performance. Increasing PCM content and positioning it nearer to the heat-exposed side of the wall enhances thermal stability, delays heat transfer, and significantly improves the passive cooling effectiveness of the building envelope.

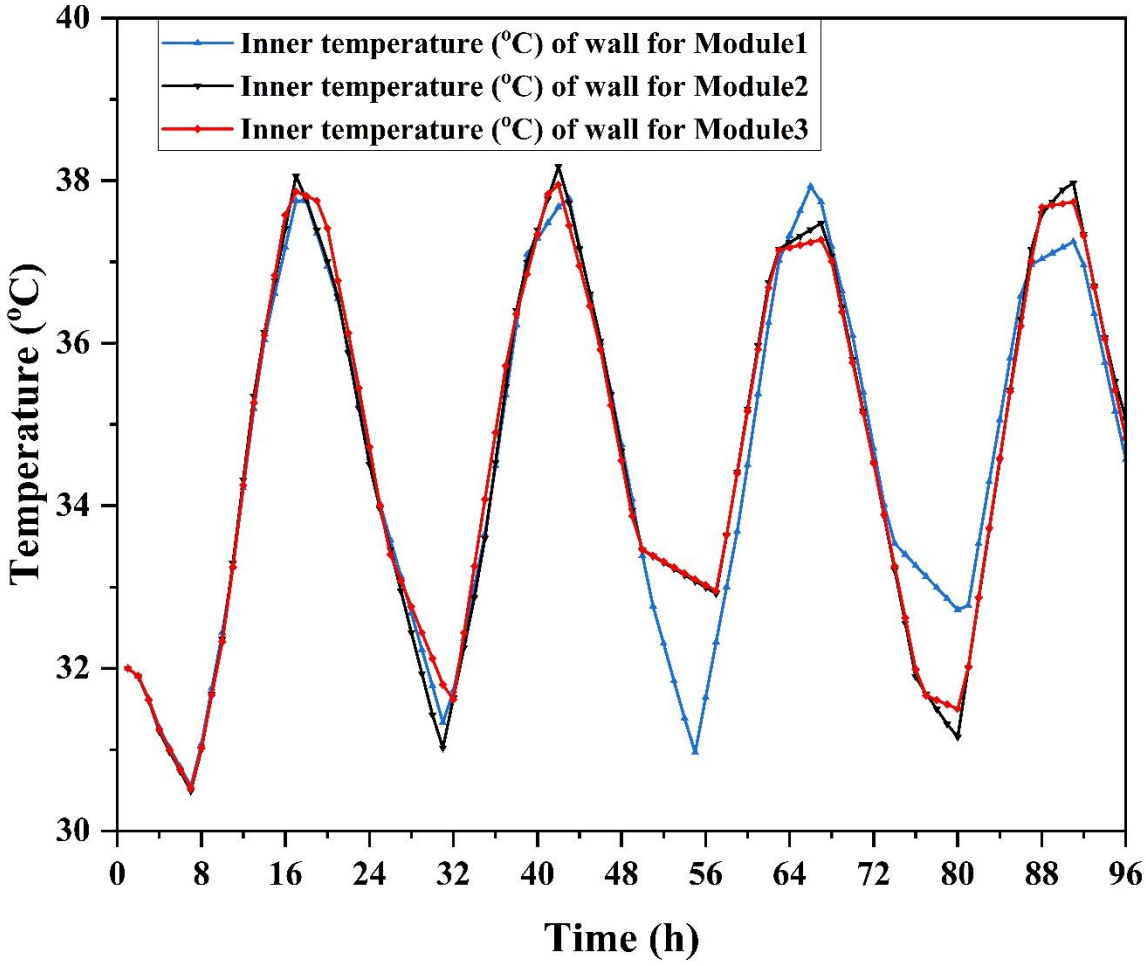

Figure 5.7 : Variation of inner temperature for different module

5.5.5 Effect of PU-PCM composite thickness on the optimal wall location

Figure 5.8 illustrates the effect of PU-PCM composite layer thickness on the transient inner wall temperature. As the PU-PCM layer thickness increases from 10 mm to 20 mm, a progressively larger fraction of the incoming heat flux is absorbed during the phase change process, leading to a noticeable reduction in inner wall temperature. Among the configurations studied, the 20 mm PU-PCM layer exhibits the most effective attenuation of temperature peaks, lowering the maximum inner wall temperature by approximately 1.5-2 °C compared to the 10 mm configuration during periods of peak external heat load. This behavior highlights the improved ability of thicker PCM layers to store thermal energy temporarily rather than allowing it to be transmitted into the indoor space.

In addition to peak temperature suppression, thicker PU-PCM layers introduce enhanced thermal inertia, which is evident from the increased time lag in heat propagation through the wall. The 20 mm PCM layer shows a clear delay in the occurrence of peak inner wall temperature relative to thinner layers, indicating effective phase-shifting of heat flow. This delay is particularly advantageous for building applications, as it shifts heat release to later hours when outdoor temperature decline and cooling demand is reduced.

During nighttime conditions, the inner wall temperature profiles for all PCM thicknesses tend to converge, suggesting that the stored latent heat is fully released and the PCM returns to its initial thermal state. Despite this convergence, thicker PCM layers continue to provide superior daytime thermal buffering by limiting temperature rise over extended periods.

Overall, the combined effects of enhanced peak temperature reduction, increased thermal lag, and effective daily charge-discharge behavior confirm that the 20 mm PU-PCM layer offers the most robust thermal performance among the configurations studied.

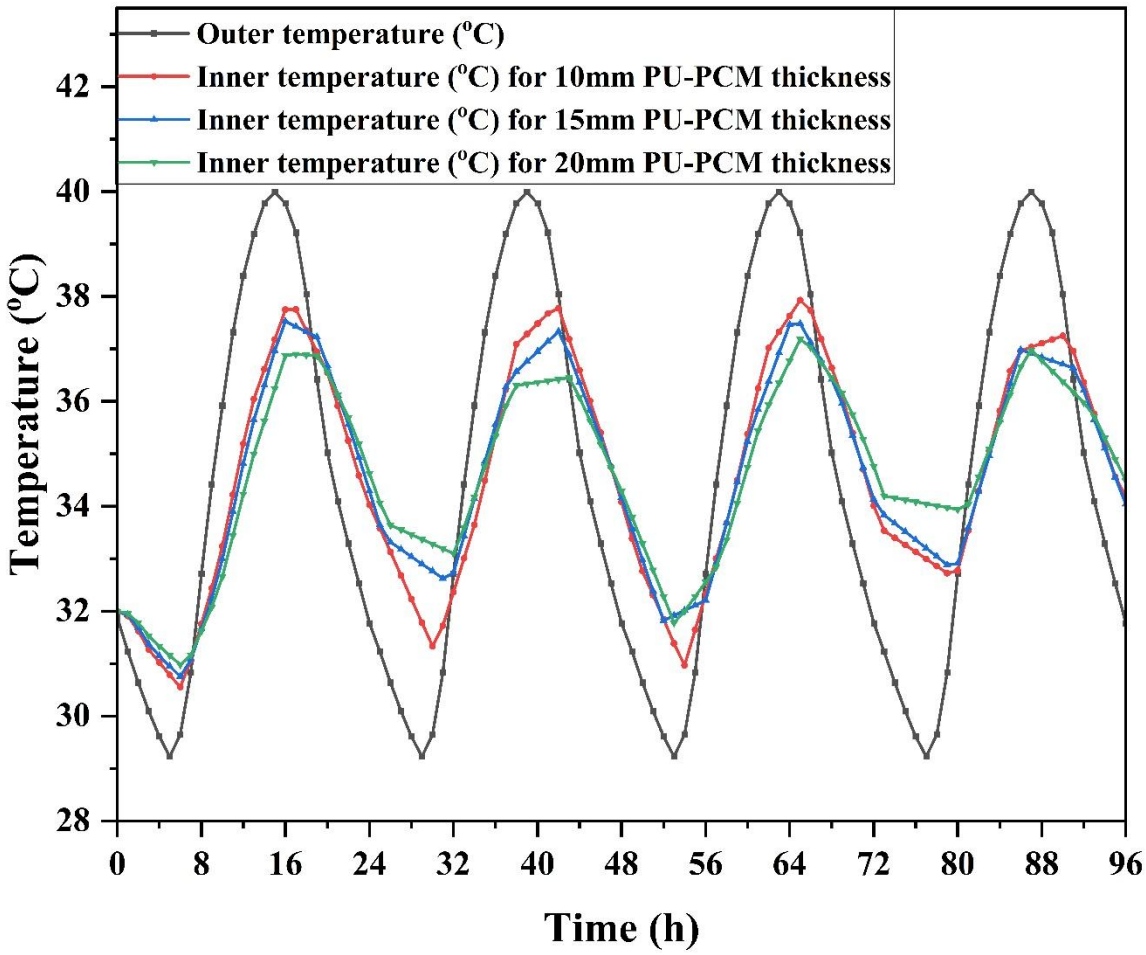

Figure 5.8 : Variation of inner temperature for different PU-PCM thickness

5.5.6 PCM effectiveness across different climatic zones of India

The variation of indoor and outdoor air temperature over a continuous four-day (96 h) period in June for four major Indian cities Delhi, Chennai, Mumbai, and Kolkata representing distinct climatic zones for 20 mm PU-PCM thickness at optimal place (module 1) are presented in Figure 5.9. Across all locations, the outdoor temperature profiles exhibit pronounced diurnal fluctuations, while the corresponding indoor temperature responses show reduced amplitude and a clear time lag, demonstrating the moderating influence of the PCM-integrated building envelope.

For Delhi, the outdoor temperature varies approximately between 29-40 °C, reflecting severe summer conditions. In contrast, the indoor temperature remains within a narrower

band of about 32-37 °C. A clear reduction in peak temperature of roughly 3-4 °C is observed, along with a time lag of several hours between outdoor and indoor temperature maxima. This delay confirms effective latent heat absorption during daytime PCM melting and subsequent heat release during nocturnal cooling, resulting in significant damping of thermal oscillations.

In Chennai, outdoor temperature fluctuate between approximately 28-36.5 °C, while indoor temperature are constrained to about 30-34 °C. Although the peak temperature reduction (≈2-3 °C) is lower than that observed in Delhi, the indoor temperature profile remains smoother, with reduced amplitude and delayed peaks. The comparatively smaller diurnal temperature range and higher nighttime temperature limit complete PCM solidification, thereby reducing the overall cooling potential.

A similar trend is observed for Kolkata, where outdoor temperature range from about 29-40 °C and indoor temperature are maintained between 32-37 °C. The PCM-integrated wall reduces peak indoor temperature by approximately 3 °C and moderates temperature swings, though the effectiveness is slightly constrained by humid conditions and elevated nocturnal temperature.

In Mumbai, characterized by a coastal climate, outdoor temperature variation is minimal (≈28-32 °C). Consequently, the indoor-outdoor temperature difference is smaller, with indoor temperature fluctuating within a narrow range of about 29-32 °C. Despite the limited diurnal variation, the PCM layer still provides noticeable damping and maintains a more uniform indoor thermal profile.

Overall, the results demonstrate that PCM integration effectively reduces peak indoor temperature, attenuates daily temperature fluctuations, and introduces thermal time lag

across all climatic conditions, with maximum performance observed in regions experiencing larger diurnal temperature variations.

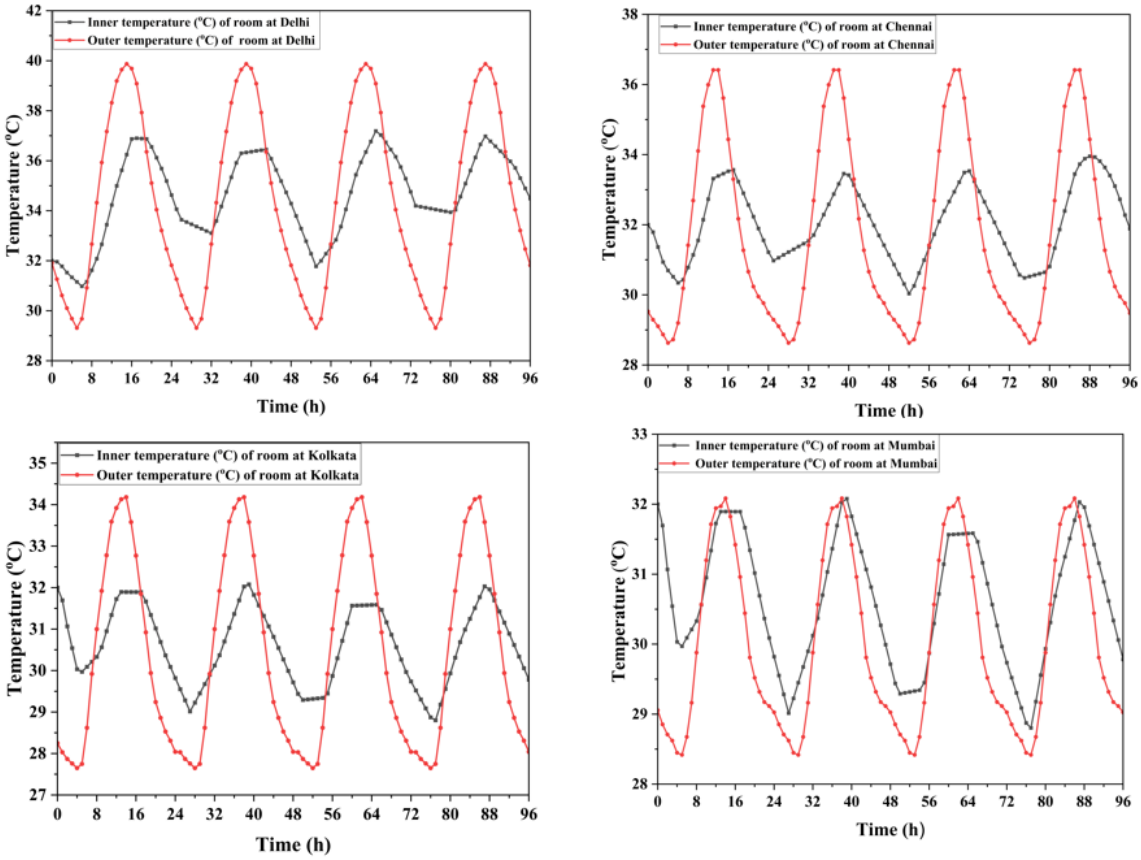

Figure 5.9 : PCM effectiveness across different climatic zones of India

5.5.7 The effectiveness of PCM integration performance in different seasons (summer, autumn, winter)

Figure 5.10 presents the indoor and outdoor air temperature variations over a 96 h period for Delhi during winter (January) and fall/monsoon (September), enabling a seasonal assessment of the thermal performance of the 20 mm PU-PCM thickness at optimal place (module 1) integrated building envelope. The results clearly indicate that the effectiveness of PCM-based thermal regulation is strongly dependent on ambient temperature levels relative to the PCM phase change range.

During January, outdoor temperature fluctuate approximately between 8-19 °C, remaining well below the melting temperature of the PCM. Under these conditions, the indoor

temperature varies within a narrower range of about 10-16 °C but closely follows the outdoor trend with limited phase shift. The absence of significant peak reduction and time lag suggests that the PCM does not undergo phase change and primarily behaves as a sensible heat storage medium. Consequently, the latent heat contribution to thermal regulation is minimal during winter conditions.

In September, outdoor temperature ranges from approximately 28-31.5 °C, which partially overlaps with the PCM melting range. The indoor temperature is maintained within a broader but moderated band of about 27-33.5 °C. Compared to outdoor conditions, the indoor temperature profile exhibits reduced amplitude and a noticeable delay in peak occurrence. Peak indoor temperature is reduced by approximately 1.5-2.5 °C, indicating partial melting and solidification of the PCM during daily cycles. This behavior demonstrates the PCM's ability to damp temperature fluctuations and enhance thermal stability during transitional seasons.

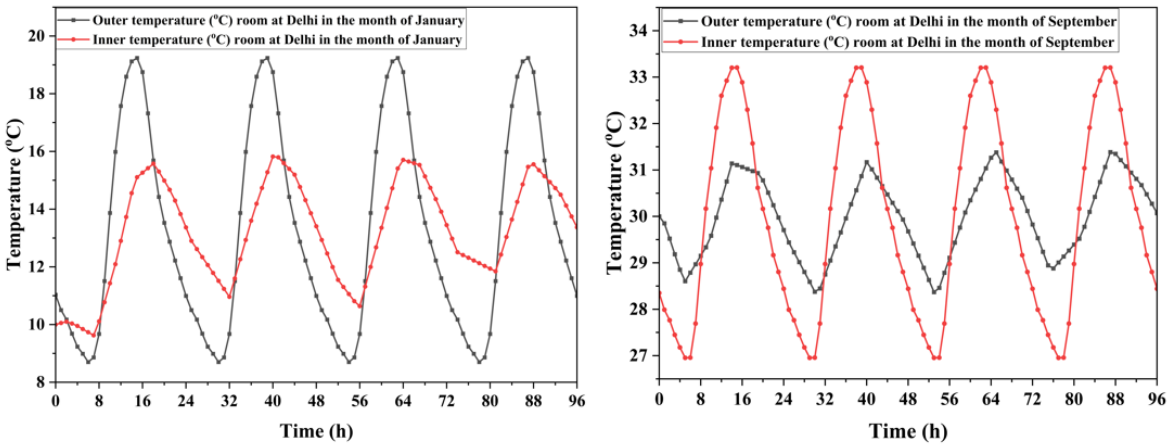

Figure 5.10 : PCM integration performance in different seasons (summer, autumn, winter)

When compared with summer performance (discussed previously), the September results show reduced but still meaningful thermal regulation, while the January results confirm minimal PCM activity. Overall, the seasonal comparison highlights that the PCM-

integrated envelope performs most effectively when ambient temperature frequently crosses the PCM phase change range, offering maximum benefit in summer, moderate benefit in fall, and limited benefit in winter conditions.

5.6 Summary

This study systematically evaluated the thermal performance and building integration potential of a salt hydrate-based phase change material (PCM) incorporated within a polyurethane (PU) composite layer for passive cooling of buildings. Differential Scanning Calorimetry (DSC) analysis confirmed that the $Na_2SO_4 \cdot 10H_2O$-based PCM exhibits a melting temperature of 31.8 °C, well aligned with the indoor thermal comfort range (22-35 °C), and a high latent heat of fusion of approximately 233 kJ kg^{-1}, validating its suitability for building envelope applications. The PU-PCM composite demonstrated effective thermal storage and dynamic response, enabling efficient absorption and release of heat during daily thermal cycles.

Numerical simulations showed that PCM-integrated walls significantly outperform conventional brick-plaster walls. Peak indoor temperature was reduced by approximately 2-4 °C, while diurnal temperature fluctuations were attenuated by up to 40-50%. In addition, PCM integration introduced a beneficial thermal time lag of about 2-4 hours, delaying indoor temperature peaks relative to outdoor maxima and thereby improving indoor thermal comfort during peak heat periods.

A parametric analysis of PCM thickness revealed that increasing the PU-PCM layer thickness from 10 mm to 20 mm enhanced thermal buffering performance. The 20 mm PCM layer achieved an additional peak inner wall temperature reduction of approximately 1.5-2 °C compared to the 10 mm configuration and exhibited a more pronounced thermal lag due to increased latent heat storage capacity. Furthermore, PCM placement was found to be critical; positioning the PCM layer closer to the heat-exposed (outer) side of the wall

resulted in the greatest thermal benefit, with peak inner wall temperature reductions of up to 3-4 °C, as the incoming heat flux was intercepted earlier in the daily heating cycle.

Climatic assessment across major Indian cities Delhi, Chennai, Kolkata, and Mumbai demonstrated that PCM-based walls are most effective in regions with high diurnal temperature variation. In Delhi, peak indoor temperature reductions of 3-5 °C were observed, whereas in hot-humid and coastal climates, reductions of 1-3 °C were achieved alongside improved thermal stability. Seasonal analysis indicated that PCM integration is most effective during summer, moderately effective during fall/monsoon conditions, and least effective during winter due to limited phase-change activity.

Overall, the findings confirm that salt hydrate-based PU-PCM composite walls represent a scalable and energy-efficient passive cooling solution for buildings in warm and tropical climates, with optimal performance achieved through appropriate PCM selection, thickness, and placement.

Chapter-6

Summary, Conclusions and Future Scope

6.1 Summary

This thesis presents a comprehensive experimental and numerical investigation into the development, stabilization, characterization, scale-up, and building integration of a salt hydrate-based phase change material (PCM) composite for passive cooling of buildings. The work is organized across five chapters and addresses the full chain from material stabilization to wall-level thermal performance. A brief summary of each chapter is provided below.

Chapter 1 establishes the motivation for the research, highlighting the growing cooling energy demand in buildings under hot climatic conditions, the limitations of conventional insulation, and the potential of latent heat thermal energy storage using PCMs, classification of PCMs and the use of salt hydrates as PCMs.

In Chapter 2, a systematic review of existing literature is presented covering stabilization strategies for salt hydrates, and their application in building envelopes. The review identifies key research gaps, particularly the lack of multi-scale experimental validation and the insufficient consideration of scalability and wall-level integration of salt hydrate-based composite. The research gap, objectives, scope, and thesis organization are presented.

Chapter 3 presents the experimental and computational methodology adopted to evaluate the thermal performance of the $Na_2SO_4 \cdot 10H_2O$-based PU-PCM composite. The chapter describes the preparation of the salt hydrate solution and PU-PCM composite, experimental setup configuration, material characterization (DSC and TGA), and thermal cycling procedures in a 600 mL jacketed reactor. A COMSOL Multiphysics model was developed

and validated using experimental data to investigate heat transfer and phase-change behaviour within the composite.

Chapter 4 presents the scale-up investigation of the $Na_2SO_4 \cdot 10H_2O$-based PU-PCM thermal energy storage system from 600 mL to 2 L and 5 L reactors. Experimental and COMSOL simulation studies were conducted to optimize the PU-PCM composite thickness, evaluate thermal storage performance, and validate heat transfer behaviour under cyclic heating-cooling conditions. The chapter further examines the effects of reactor scale, latent heat, phase change temperature range, and PCM distribution on thermal regulation and insulation performance. The results demonstrate that the scaled-up PU-PCM system provides effective thermal buffering, stable cyclic performance, and significant potential for building thermal energy storage applications.

Chapter 5 investigates the integration of a $Na_2SO_4 \cdot 10H_2O$-based PU-PCM composite within building wall assemblies for passive cooling using experimental characterization and COMSOL-based numerical simulations. PCM-integrated walls consistently exhibited reduced inner wall temperature, enhanced thermal damping, and a measurable time lag in heat transfer. The placement of the PCM layer closer to the outer surface and increasing PCM thickness both improved daytime passive cooling performance.

6.2 Conclusions

Based on the experimental investigations, numerical simulations, and building-scale analyses conducted in this study, the following conclusions are drawn:

1. $Na_2SO_4 \cdot 10H_2O$ **was identified as a suitable inorganic PCM** for passive cooling applications due to its favourable phase transition temperature (32-34 °C), high latent heat capacity (>230 J g^{-1}), non-flammability, wide availability, and lower cost compared with organic PCMs.

2. **A stable PU-PCM composite was successfully developed** by impregnating a $Na_2SO_4 \cdot 10H_2O$ solution into an open-cell polyurethane (PU) foam matrix. The incorporation of Laponite® Gel and borax effectively minimized phase segregation and supercooling, resulting in improved thermal reliability.
3. **DSC analysis confirmed excellent thermal storage characteristics**, with a sharp and repeatable melting peak near 34 °C and a latent heat of approximately 233 J g^{-1}. The PU matrix preserved the intrinsic heat storage capacity of the salt hydrate while enhancing operational stability.
4. **The developed PU-PCM composite demonstrated excellent scalability**, maintaining consistent melting-solidification behaviour and reproducible charging-discharging cycles across reactor volumes ranging from 600 mL to 5 L.
5. **Long-term thermal cycling tests confirmed the durability of the composite**, with negligible degradation in latent heat storage performance after more than 100 thermal cycles, indicating good long-term stability for practical applications.
6. **The COMSOL Multiphysics model accurately predicted the thermal behaviour of the PCM system**, with simulated temperature profiles closely matching experimental results and deviations generally within ±1-2 °C.
7. **Parametric numerical analysis identified key design parameters influencing thermal performance**, showing that PCM thickness, latent heat (L), and phase change temperature range (ΔT) significantly affect thermal buffering capacity and charging-discharging characteristics.
8. **Integration of the PU-PCM composite into brick wall assemblies significantly improved thermal performance**, reducing peak inner wall surface temperature by approximately 3-5 °C compared with conventional wall systems.

9. **PCM-integrated walls introduced a beneficial thermal time lag of several hours**, delaying heat transfer to indoor spaces and thereby improving thermal comfort during periods of peak outdoor temperature.
10. **The optimum wall configuration was achieved when the PCM layer was positioned closer to the exterior wall surface**, enabling earlier absorption of incoming heat flux and maximizing passive cooling effectiveness.
11. **Increasing PCM layer thickness enhanced thermal damping and temperature stabilization**, resulting in lower indoor temperature fluctuations and improved daytime thermal regulation, provided complete nighttime discharge was achieved.
12. **Seasonal analysis demonstrated that PCM effectiveness is climate dependent**, with maximum benefits observed during summer conditions, moderate performance during transitional seasons, and limited effectiveness during winter when ambient temperature remain below the PCM melting range.
13. **The developed $Na_2SO_4 \cdot 10H_2O$-based PU-PCM system successfully bridges the gap between material development and practical building applications**, demonstrating high latent heat storage capacity, thermal stability, scalability, and compatibility with conventional construction materials.
14. **The proposed PCM-integrated building envelope offers a sustainable passive cooling strategy**, capable of reducing peak indoor temperature, delaying heat transfer, smoothing temperature fluctuations, lowering cooling energy demand, and mitigating peak electrical loads in buildings.
15. **The findings of this research provide practical design guidelines and performance benchmarks** for the development and deployment of PCM-enhanced building envelopes in energy-efficient and climate-responsive buildings.

6.3 Limitations and Future Scope

While this research establishes the technical feasibility and building-level effectiveness of $Na_2SO_4 \cdot 10H_2O$-based PU-PCM composite, the following limitations and future research directions are identified:

Thermal conductivity enhancement: The developed composite exhibits moderate thermal conductivity, which may limit heat charging and discharging rates, particularly in thicker PCM layers. Future studies should investigate the incorporation of high-conductivity additives such as graphene, expanded graphite, carbon-based materials, or metal oxide nanofillers. Their influence on thermal performance, viscosity, mechanical integrity, and economic feasibility should also be evaluated.

Development of advanced PCM formulations: The present study focuses on a single salt hydrate PCM system. Future investigations should explore eutectic and blended salt hydrate systems (e.g., Na_2SO_4–$MgSO_4$ and Na_2SO_4–Na_2HPO_4 mixtures) to broaden the operational temperature range, improve thermal reliability, and enhance adaptability to different climatic conditions.

Optimization of PCM-integrated wall systems: Additional studies are required to optimize PCM layer thickness, placement, and distribution within building envelopes. The performance of multiple PCM layers, graded PCM configurations, and hybrid PCM–insulation wall assemblies should be examined. Furthermore, climate-specific design guidelines incorporating solar radiation, building orientation, and occupancy patterns should be developed.

Full-scale implementation and field validation: The thermal performance of the PU–PCM composite was evaluated at the wall-module level under controlled boundary conditions. Long-term field studies in residential and commercial buildings are required to

validate thermal performance, energy-saving potential, and indoor thermal comfort under real operating conditions.

• **Mechanical, fire, and environmental assessment:** Comprehensive investigations of the mechanical durability, fire resistance, and long-term environmental impacts of PU–PCM composites are necessary to ensure compliance with building safety standards and to support sustainable large-scale deployment.

• **Long-term thermal cycling stability:** Although the composite exhibited stable thermal performance during the investigated cycles, extended melt–freeze cycling tests (exceeding 100 cycles) are required to quantify degradation mechanisms, evaluate long-term reliability, and establish maintenance requirements for practical building applications.

• **Hybrid cooling and advanced energy management systems:** Future research should explore the integration of PCM-based passive cooling with active cooling technologies to enhance overall thermal management. The combined effects of hybrid cooling systems, multilayer PCM configurations, and long-term thermal cycling on building energy performance should also be investigated.

• **Techno-economic analysis:** A detailed techno-economic assessment comparing PCM-integrated building envelopes with conventional insulation and HVAC systems is required. Such analyses should consider installation costs, operational energy savings, maintenance requirements, and payback periods to facilitate commercialization and large-scale adoption.

Addressing these research directions will further advance the development, optimization, and practical implementation of salt hydrate-based thermal energy storage systems for energy-efficient and sustainable buildings.

References

[1]. Blackley E, Lai T, Odukomaiya A, Tabares-velasco PC, Wheeler LM, Woods J. Surface-Modified Compressed Expanded Graphite for Increased Salt Hydrate Phase Change Material Thermal Conductivity and Stability. 2023;

[2]. Report GS. Not just another brick in the wall. 2024;

[3]. González-torres M, Pérez-lombard L, Coronel JF, Maestre IR, Yan D. A review on buildings energy information : Trends , end-uses , fuels and drivers. Energy Reports [Internet]. 2022;8:626–37. Available from: https://doi.org/10.1016/j.egyr.2021.11.280

[4]. Grubler A, Wilson C, Bento N, Boza-Kiss B, Krey V, McCollum DL, et al. A low energy demand scenario for meeting the 1.5 °c target and sustainable development goals without negative emission technologies. Nat Energy [Internet]. 2018;3(6):515–27. Available from: http://dx.doi.org/10.1038/s41560-018-0172-6

[5]. Ni N, Shafique M, Zhou X, Zheng Z. Case Studies in Construction Materials Net zero carbon buildings : A review on recent advances , knowledge gaps and research directions. Case Stud Constr Mater [Internet]. 2025;22(January):e04200. Available from: https://doi.org/10.1016/j.cscm.2024.e04200

[6]. Ayalew BS, Andrzejczyk R. Recent Advancements in Latent Thermal Energy Storage and Their Applications for HVAC Systems in Commercial and Residential Buildings in Europe—Analysis of Different EU Countries' Scenarios. Energies. 2025;18(15):1–35.

[7]. Woldekidan K, Bianchi C, Fallahi Z, LaClair TJ. Techno-Economic Analysis for the Addition of Thermal Energy Storage to a Campus With Existing Battery Storage. ASME J Eng Sustain Build Cities. 2025;6(2):1–12.

[8]. Ürge-vorsatz D, Cabeza LF, Serrano S, Barreneche C. Heating and cooling energy trends and drivers in buildings. Renew Sustain Energy Rev [Internet]. 2015;41:85–98. Available from: http://dx.doi.org/10.1016/j.rser.2014.08.039

[9]. Crawley DB, Hand JW, Kummert M, Griffith BT, Hand JW, Kummert M, et al. Crawley , D . B . and Hand , J .* and Kummert , M . and Griffith , B . T . (2008) Contrasting the capabilities of building energy performance simulation programs . Building and Environment , 43 (4). pp . 661-673 . ISSN 0360-1323 Strathprints is design. 2008;43.

[10]. Lund H, Werner S, Wiltshire R, Svendsen S, Eric J, Hvelplund F, et al. 4th Generation District Heating (4GDH) Integrating smart thermal grids into future sustainable energy systems. Energy [Internet]. 2014;68:1–11. Available from: http://dx.doi.org/10.1016/j.energy.2014.02.089

[11]. Arteconi A, Hewitt NJ, Polonara F. State of the art of thermal storage for demand-side management. Appl Energy [Internet]. 2012;93:371–89. Available from: http://dx.doi.org/10.1016/j.apenergy.2011.12.045

[12]. Santamouris M. Cooling the buildings – past , present and future. Energy Build [Internet]. 2016;128:617–38. Available from:

http://dx.doi.org/10.1016/j.enbuild.2016.07.034

[13]. Cabeza LF, Castell A, Barreneche C, De Gracia A, Fernández AI. Materials used as PCM in thermal energy storage in buildings: A review. Renew Sustain Energy Rev [Internet]. 2011;15(3):1675–95. Available from: http://dx.doi.org/10.1016/j.rser.2010.11.018

[14]. Sharma A, Tyagi V V., Chen CR, Buddhi D. Review on thermal energy storage with phase change materials and applications. Renew Sustain Energy Rev. 2009;13(2):318–45.

[15]. Rosen MA. Thermal Energy Thermal Energy. 2011;

[16]. Zalba B, Cabeza LF, Mehling H. Review on thermal energy storage with phase change: materials, heat transfer analysis and applications. Vols. 250–253, Advanced Materials Research. 2003. 3541–3544 p.

[17]. Zalba B, Marín JM, Cabeza LF, Mehling H. Free-cooling of buildings with phase change materials. Int J Refrig. 2004;27(8):839–49.

[18]. Cabeza LF, Castell A, Barreneche C, Gracia A De, Fernández AI. Materials used as PCM in thermal energy storage in buildings : A review. Renew Sustain Energy Rev [Internet]. 2011;15(3):1675–95. Available from: http://dx.doi.org/10.1016/j.rser.2010.11.018

[19]. Kuznik F, David D, Johannes K, Roux JJ. A review on phase change materials integrated in building walls. Renew Sustain Energy Rev. 2011;15(1):379–91.

[20]. Ismail MM, Dincer I, Bicer Y, Saghir MZ. Nanoparticles enhanced phase change materials for thermal energy storage applications : An assessment. Int J Thermofluids [Internet]. 2025;27(April):101207. Available from: https://doi.org/10.1016/j.ijft.2025.101207

[21]. Farid MM, Khudhair AM, Razack SAK, Al-Hallaj S. A review on phase change energy storage: Materials and applications. Energy Convers Manag. 2004;45(9–10):1597–615.

[22]. Alva G, Lin Y, Fang G. An overview of thermal energy storage systems. Energy [Internet]. 2018;144:341–78. Available from: https://doi.org/10.1016/j.energy.2017.12.037

[23]. N'Tsoukpoe KE, Schmidt T, Rammelberg HU, Watts BA, Ruck WKL. A systematic multi-step screening of numerous salt hydrates for low temperature thermochemical energy storage. Appl Energy [Internet]. 2014;124:1–16. Available from: http://dx.doi.org/10.1016/j.apenergy.2014.02.053

[24]. Cot-Gores J, Castell A, Cabeza LF. Thermochemical energy storage and conversion: A-state-of-the-art review of the experimental research under practical conditions. Renew Sustain Energy Rev [Internet]. 2012;16(7):5207–24. Available from: http://dx.doi.org/10.1016/j.rser.2012.04.007

[25]. Yu N, Wang RZ, Wang LW. Sorption thermal storage for solar energy. Prog Energy Combust Sci. 2013;39(5):489–514.

[26]. Scapino L, Zondag HA, Van Bael J, Diriken J, Rindt CCM. Sorption heat storage for long-term low-temperature applications: A review on the advancements at

material and prototype scale. Appl Energy [Internet]. 2017;190:920–48. Available from: http://dx.doi.org/10.1016/j.apenergy.2016.12.148

[27]. De Gracia A, Cabeza LF. Phase change materials and thermal energy storage for buildings. Energy Build [Internet]. 2015;103:414–9. Available from: http://dx.doi.org/10.1016/j.enbuild.2015.06.007

[28]. Sari A, Alkan C, Karaipekli A, Önal A. Preparation, characterization and thermal properties of styrene maleic anhydride copolymer (SMA)/fatty acid composites as form stable phase change materials. Energy Convers Manag. 2008;49(2):373–80.

[29]. Zhou D, Zhao CY, Tian Y. Review on thermal energy storage with phase change materials (PCMs) in building applications. Appl Energy [Internet]. 2012;92:593–605. Available from: http://dx.doi.org/10.1016/j.apenergy.2011.08.025

[30]. Abhat A. Low temperature latent heat thermal energy storage: Heat storage materials. Sol Energy. 1983;30(4):313–32.

[31]. Kenisarin M, Mahkamov K. Salt hydrates as latent heat storage materials:Thermophysical properties and costs. Sol Energy Mater Sol Cells [Internet]. 2016;145:255–86. Available from: http://dx.doi.org/10.1016/j.solmat.2015.10.029

[32]. Gil A, Medrano M, Martorell I, Lázaro A, Dolado P, Zalba B, et al. State of the art on high temperature thermal energy storage for power generation. Part 1-Concepts, materials and modellization. Renew Sustain Energy Rev. 2010;14(1):31–55.

[33]. Sharma SD, Sagara K. Latent Heat Storage Materials and Systems: A Review. Int J Green Energy. 2005;2(1):1–56.

[34]. Raaj R V, Sharma A, Kothadia H. Experimental Study of Different Factors Influencing Supercooling in Phase Change Material – Sodium Acetate Trihydrate Experimental Study of Different Factors Influencing Supercooling in Phase Change Material – Sodium Acetate Trihydrate. Heat Transf Eng [Internet]. 2025;0(0):1–11. Available from: https://doi.org/10.1080/01457632.2025.2452745

[35]. Raju KVLN, Kumar GN, Ram VV, Parameshwaran R. Preparation, thermal and structural properties of n-octadecane/melamine formaldehyde nanocapsules embedded cement mortar for energy storage application in buildings. Mater Today Proc [Internet]. 2022;56:1424–31. Available from: https://doi.org/10.1016/j.matpr.2021.11.645

[36]. Bo H, Gustafsson EM, Setterwall F, Dixit P, Reddy VJ, Dasari A, et al. Thermal Properties and Reliabilities of Lauric Acid-Based Binary Eutectic Fatty Acid as a Phase Change Material for Building Energy Conservation. J Energy Storage [Internet]. 2020;13(18):1907–21. Available from: https://doi.org/10.1016/j.solmat.2018.09.016

[37]. Chen K, Yu X, Tian C, Wang J. Preparation and characterization of form-stable paraffin/polyurethane composites as phase change materials for thermal energy storage. Energy Convers Manag [Internet]. 2014;77:13–21. Available from: http://dx.doi.org/10.1016/j.enconman.2013.09.015

[38]. Sun X, Lee KO, Medina MA, Chu Y, Li C. Melting temperature and enthalpy variations of phase change materials (PCMs): a differential scanning calorimetry

(DSC) analysis. Phase Transitions [Internet]. 2018;91(6):667–80. Available from: https://doi.org/10.1080/01411594.2018.1469019

[39]. Fan Z, Zhao Y, Liu X, Shi Y, Jiang D. Thermal Properties and Reliabilities of Lauric Acid-Based Binary Eutectic Fatty Acid as a Phase Change Material for Building Energy Conservation. ACS Omega. 2022;7(18):16097–108.

[40]. Wu M, Liu C, Rao Z. Experimental study on lauryl alcohol/expanded graphite composite phase change materials for thermal regulation in building. Constr Build Mater [Internet]. 2022;335(January):127400. Available from: https://doi.org/10.1016/j.conbuildmat.2022.127400

[41]. Pielichowska K, Pielichowski K. Phase change materials for thermal energy storage. Prog Mater Sci [Internet]. 2014;65:67–123. Available from: http://dx.doi.org/10.1016/j.pmatsci.2014.03.005

[42]. Purohit BK, Sistla VS. Studies on solution crystallization of Na2SO4·10H2O embedded in porous polyurethane foam for thermal energy storage application. Thermochim Acta [Internet]. 2018;668(August):9–18. Available from: https://doi.org/10.1016/j.tca.2018.08.005

[43]. Uttam A, Kumar B, Sistla VS. Performance analysis of a multi-scale thermal energy storage system with varying volumes using polyurethane-encapsulated sodium sulphate decahydrate for building applications. Energy Build [Internet]. 2025;347(PB):116390. Available from: https://doi.org/10.1016/j.enbuild.2025.116390

[44]. Liu L, Li J, Deng Y, Yang Z, Huang K, Zhao S. Optimal design of multi-layer structure composite containing inorganic hydrated salt phase change materials and cement: Lab-scale tests for buildings. Constr Build Mater [Internet]. 2021;275:122125. Available from: https://doi.org/10.1016/j.conbuildmat.2020.122125

[45]. Rezvanpour M, Borooghani D, Torabi F, Pazoki M. Using CaCl2·6H2O as a phase change material for thermo-regulation and enhancing photovoltaic panels' conversion efficiency: Experimental study and TRNSYS validation. Renew Energy [Internet]. 2020;146:1907–21. Available from: https://doi.org/10.1016/j.renene.2019.07.075

[46]. Xie N, Gao X, Zhong Y, Ye R, Chen S, Ding L, et al. Enhanced thermal performance of Na2HPO4·12H2O composite phase change material supported by sepiolite fiber for floor radiant heating system. J Build Eng [Internet]. 2022;56(June):104747. Available from: https://doi.org/10.1016/j.jobe.2022.104747

[47]. Lee M, Dahlhauser SD, Lucci C, Donohoe BS, Allen RD, Rorrer NA. Shape-Stabilization of Phase Change Materials with Carbon-Conscious Poly(hydroxy)Urethane Foams. Adv Funct Mater. 2025;35(24):1–13.

[48]. Man X, Lu H, Xu Q, Wang C, Ling Z. Review on the thermal property enhancement of inorganic salt hydrate phase change materials. J Energy Storage [Internet]. 2023;72(PE):108699. Available from: https://doi.org/10.1016/j.est.2023.108699

[49]. Lak SN, Hsieh C min, Almahbobi L, Wang Y, Chakraborty A, Yu C, et al. Printing Composites with Salt Hydrate Phase Change Materials for Thermal Energy Storage. 2023;

[50]. Gupta N, Kumar A, Dhasmana H, Kumar V, Kumar A, Shukla P, et al. Enhanced thermophysical properties of Metal oxide nanoparticles embedded magnesium nitrate hexahydrate based nanocomposite for thermal energy storage applications. J Energy Storage [Internet]. 2020;32(August):101773. Available from: https://doi.org/10.1016/j.est.2020.101773

[51]. Dixit P, Jagadeeswara V, Parvate S, Balwani A, Singh J, Kanti T, et al. Salt hydrate phase change materials : Current state of art and the road ahead. J Energy Storage [Internet]. 2022;51(November 2021):104360. Available from: https://doi.org/10.1016/j.est.2022.104360

[52]. Bouhal T, Meghari Z, Fertahi S ed D, El Rhafiki T, Kousksou T, Jamil A, et al. Parametric CFD analysis and impact of PCM intrinsic parameters on melting process inside enclosure integrating fins: Solar building applications. J Build Eng. 2018;20(August):634–46.

[53]. Khudhair AM, Farid MM. A review on energy conservation in building applications with thermal storage by latent heat using phase change materials. Energy Convers Manag. 2004;45(2):263–75.

[54]. Purohit BK, Sistla VS. Inorganic salt hydrate for thermal energy storage application: A review. Energy Storage. 2021;3(2):1–26.

[55]. Li Y, Li C, Lin N, Xie B, Zhang D, Chen J. Review on tailored phase change behavior of hydrated salt as phase change materials for energy storage. Mater Today Energy [Internet]. 2021;22:100866. Available from: https://doi.org/10.1016/j.mtener.2021.100866

[56]. Zhao BC, Li TX, Gao JC, Wang RZ. Latent heat thermal storage using salt hydrates for distributed building heating : A multi-level scale-up research. 2020;121(January).

[57]. Cui H, Zhang W, Yang H, Zou Y, Liu J, Yan J. Preparation and investigation of a prefabricated salt hydrate phase change material partition for passive solar buildings. Energy [Internet]. 2024;303(December 2023):132010. Available from: https://doi.org/10.1016/j.energy.2024.132010

[58]. Xie N, Huang Z, Luo Z, Gao X, Fang Y, Zhang Z. Inorganic salt hydrate for thermal energy storage. Appl Sci. 2017;7(12).

[59]. Prakash R, Meenakshipriya B, Kumaravelan R, Vijayan S. Preparation and study on thermophysical properties of inorganic salt hydrate as energy storage materials. Mater Today Proc [Internet]. 2020;42:450–6. Available from: https://doi.org/10.1016/j.matpr.2020.10.171

[60]. Yu K, Liu Y, Yang Y. Review on form-stable inorganic hydrated salt phase change materials : Preparation , characterization and effect on the thermophysical properties. Appl Energy [Internet]. 2021;292(March):116845. Available from: https://doi.org/10.1016/j.apenergy.2021.116845

[61]. Clark RJ, Gholamibozanjani G, Woods J, Kaur S, Odukomaiya A, Al-Hallaj S, et al. Experimental screening of salt hydrates for thermochemical energy storage for building heating application. J Energy Storage [Internet]. 2022;51(November 2021):104415. Available from: https://doi.org/10.1016/j.est.2022.104415

[62]. Tanwar S, Kaur R. Fabrication and evaluation of polyurethane supported form-stable PCMs. Energy Storage. 2024;6(2):1–9.

[63]. Xie N, Niu J, Zhong Y, Gao X, Zhang Z, Fang Y. Development of polyurethane acrylate coated salt hydrate/diatomite form-stable phase change material with enhanced thermal stability for building energy storage. Constr Build Mater [Internet]. 2020;259:119714. Available from: https://doi.org/10.1016/j.conbuildmat.2020.119714

[64]. Purohit BK, Sistla VS. Crystallization of inorganic salt hydrates in polymeric foam for thermal energy storage application. J Energy Storage [Internet]. 2017;12:196–201. Available from: http://dx.doi.org/10.1016/j.est.2017.05.001

[65]. Bennacef C, Desobry-Banon S, Probst L, Desobry S. Alginate Core-Shell Capsules Production through Coextrusion Methods: Principles and Technologies. Mar Drugs. 2023;21(4).

[66]. Akeiber HJ, Wahid MA, Hussen HM, Mohammad AT. Review of development survey of phase change material models in building applications. Sci World J. 2014;2014(Figure 1).

[67]. Faraj K, Khaled M, Faraj J, Hachem F, Castelain C. A Summary Review on Experimental Studies for PCM Building Applications: Towards Advanced Modular Prototype. Energies. 2022;15(4):1–43.

[68]. Nair AM, Wilson C, Huang MJ, Griffiths P, Hewitt N. Phase change materials in building integrated space heating and domestic hot water applications: A review. J Energy Storage [Internet]. 2022;54(July):105227. Available from: https://doi.org/10.1016/j.est.2022.105227

[69]. Chen Z, Zhang X, Ji J, Lv Y. A review of the application of hydrated salt phase change materials in building temperature control. J Energy Storage [Internet]. 2022;56(PC):106157. Available from: https://doi.org/10.1016/j.est.2022.106157

[70]. Kenisarin M, Mahkamov K. Solar energy storage using phase change materials. Renew Sustain Energy Rev. 2007;11(9):1913–65.

[71]. Dixit P, Reddy VJ, Parvate S, Balwani A, Singh J, Maiti TK, et al. Salt hydrate phase change materials: Current state of art and the road ahead. J Energy Storage [Internet]. 2022;51(March):104360. Available from: https://doi.org/10.1016/j.est.2022.104360

[72]. Zhang X, Tan Z, Geng L, Zhao J, Liu C. Experimental study on supercooling performance optimization of sodium acetate trihydrate phase change energy storage materials. J Energy Storage [Internet]. 2024;99(PA):113345. Available from: https://doi.org/10.1016/j.est.2024.113345

[73]. Liu Y, Li X, Xu Y, Xie Y, Hu T, Tao P. Carbon-Enhanced Hydrated Salt Phase Change Materials for Thermal Management Applications. 2024;

[74]. Tao W, Kong X, Bao A, Fan C, Zhang Y. Preparation and phase change performance of graphene oxide and silica composite Na2So4·10H2O phase change materials (PCMs) as thermal energy storage materials. Materials (Basel). 2020;13(22):1–12.

[75]. Jay Thakkar, Sai Bhargav Annavajjala MJS and JK. Influence of Carboxymethyl Cellulose as a Thickening Agent for. 2024;

[76]. Lin N, Li C, Zhang D, Li Y, Chen J. Emerging phase change cold storage materials derived from sodium sulfate decahydrate. Energy [Internet]. 2022;245:123294. Available from: https://doi.org/10.1016/j.energy.2022.123294

[77]. Li C, Zhang B, Xie B, Zhao X, Chen J. Tailored phase change behavior of Na2SO4·10H2O/expanded graphite composite for thermal energy storage. Energy Convers Manag [Internet]. 2020;208(November 2019):112586. Available from: https://doi.org/10.1016/j.enconman.2020.112586

[78]. Chen Z, Zhang X, Ji J, Lv Y. Review article A review of the application of hydrated salt phase change materials in building temperature control. J Energy Storage [Internet]. 2022;56(PC):106157. Available from: https://doi.org/10.1016/j.est.2022.106157

[79]. Shao F, Wang L, Luo R, Yu W, Xie H. Shape-Stable Hybrid Emulsion Gel with Sodium Acetate Trihydrate and Paraffin Wax for Efficient Solar Energy Storage and Building Thermal Management. 2023;

[80]. Zhang X, Tan Z, Geng L, Zhao J, Liu C. Experimental study on supercooling performance optimization of sodium acetate trihydrate phase change energy storage materials. 2024;99(March).

[81]. Turnaoglu T, Kumar N, Hirschey J, Li Y, Akamo DO, Tim J, et al. Proceedings of the ASME 2023 17. 2023;1–5.

[82]. Damilola O, Li Y, Keffer DJ, Rios O, Gluesenkamp R, Laclair TJ, et al. iScience ll Stabilization of low-cost phase change materials for thermal energy storage applications for thermal energy storage applications. ISCIENCE [Internet]. 2023;26(7):107175. Available from: https://doi.org/10.1016/j.isci.2023.107175

[83]. Wang C, Liu P, Cheng X, Zhang Y, Wang Z. Preparation and thermal properties of a new hydrated salt phase change material without phase separation. Materialia [Internet]. 2025;42:102462. Available from: https://doi.org/10.1016/j.mtla.2025.102462

[84]. He Z, Ma H, Lu S. Preparation and thermal performance study of a novel hydrated salt composite PCM for space heating. J Energy Storage [Internet]. 2024;90(PA):111906. Available from: https://doi.org/10.1016/j.est.2024.111906

[85]. Akamo DO, Kumar N, Li Y, Pekol C, Li K, Goswami M, et al. Stabilization of low-cost phase change materials for thermal energy storage applications. iScience [Internet]. 2023;26(7):107175. Available from: https://doi.org/10.1016/j.isci.2023.107175

[86]. Amidu MA, Ali M, Alkaabi AK, Addad Y. OPEN A critical assessment of nanoparticles enhanced phase change materials (NePCMs) for latent heat energy storage applications. Sci Rep [Internet]. 2023;(0123456789):1–13. Available from: https://doi.org/10.1038/s41598-023-34907-0

[87]. Hayat MA. NOVEL NANO-ENHANCED PHASE CHANGE MATERIALS FOR THERMAL ENERGY STORAGE By Author ’ s Declaration. 2024;(July).

[88]. Phukaokaew W, University KK, Amnart -.University KKS, Wongwuttanasatian T. Thermal Management of Photovoltaic Module Using Affordable Organic Phase Change Material Combined with Nano Metal Oxide Particles Enhancer.

[89]. Prashant RV, Ch S, Mohanavel V, Veerababu K. Effect of paraffin with salt hydrates PCM and hybrid - Al 2 O 3 / Tio 2 nanofluid on thermal and energy storage characteristics of solar thermal heat exchanger. J Therm Anal Calorim [Internet]. 2025;150(10):8029–42. Available from: https://doi.org/10.1007/s10973-025-14224-6

[90]. Rajagopalan KK, Haney S, Shamberger PJ, Sukhishvili SA. Hybrid Polymer Salogels for Reversible Entrapment of Salt-Hydrate- Based Thermal Energy Storage Materials. 2024;

[91]. Tang Z, Gao H, Chen X, Zhang Y, Li A, Wang G. Advanced multifunctional composite phase change materials based on photo-responsive materials. Nano Energy [Internet]. 2021;80(September 2020):105454. Available from: https://doi.org/10.1016/j.nanoen.2020.105454

[92]. Wang H, Chen Y, Li J, Guo L, Fang M. Review of Encapsulated Salt Hydrate Core-Shell Phase Change Materials †. 2020;37(37):85–96.

[93]. Graham M. Encapsulated Salt Hydrate Phase Change Materials for Thermal Energy Storage. 2017;(September).

[94]. Sharma J, Polizos G, Jafta CJ, Datta S, Gluesenkamp KR, Nawaz K. A Novel Approach for Microencapsulating Salt Hydrate-Based Phase Change Materials. 2025;1–15.

[95]. Xianliang H, Donghuan X, Zimo Z, Shujun W, Fanbin M. Novel method for microencapsulation of eutectic hydrated salt as a phase change material for thermal energy storage. 2022;(April):760–7.

[96]. Mahakul AJ, Ganguly S. Inorganic salt hydrate PCM microencapsulated in silica shell by electrohydrodynamic splitting of coaxial streams. 2024;97(February).

[97]. Dey A, Mahakul AJ, Ganguly S. Microencapsulation of a salt hydrate phase change material by resorcinol formaldehyde through electrohydrodynamic disintegration of coaxially layered filament. J Energy Storage [Internet]. 2023;73(PD):109298. Available from: https://doi.org/10.1016/j.est.2023.109298

[98]. Erlbeck L, Schreiner P, Fasel F, Methner F, Rädle M. Investigation of different materials for macroencapsulation of salt hydrate phase change materials for building purposes. Constr Build Mater [Internet]. 2018;180:512–8. Available from: https://doi.org/10.1016/j.conbuildmat.2018.05.204

[99]. Abdur O, Palomba V, Verez D, Borri E, Frazzica A, Brancato V, et al. Experimental evaluation of different macro-encapsulation designs for PCM storages for cooling applications. J Energy Storage [Internet]. 2023;74(PA):109359. Available from: https://doi.org/10.1016/j.est.2023.109359

[100]. Izadi M, Taghavi SF, Neshat Safavi SH, Afsharpanah F, Yaïci W. Thermal management of shelter building walls by PCM macro-encapsulation in commercial hollow bricks. Case Stud Therm Eng [Internet]. 2023;47(April):103081. Available from: https://doi.org/10.1016/j.csite.2023.103081

[101]. Kalidasan B, Pandey AK, Saidur R, Samykano M, Tyagi V V, Pandey AK, et al. Nano additive enhanced salt hydrate phase change materials for thermal energy storage. Int Mater Rev [Internet]. 2022;1–44. Available from:

https://doi.org/10.1080/09506608.2022.2053774

[102]. Zhao BC, Li TX, Gao JC, Wang RZ. Latent heat thermal storage using salt hydrates for distributed building heating: A multi-level scale-up research. Renew Sustain Energy Rev. 2020;121(January).

[103]. Shen Z, Kwon S, Lee HL, Toivakka M, Oh K. Enhanced thermal energy storage performance of salt hydrate phase change material: Effect of cellulose nanofibril and graphene nanoplatelet. Sol Energy Mater Sol Cells [Internet]. 2021;225(February):111028. Available from: https://doi.org/10.1016/j.solmat.2021.111028

[104]. Li W, Zhao J, Wang J, Li S, Zhang X, Zhao J. Review of sodium acetate trihydrate as phase change material : Mechanism analysis , modification scheme and application. J Energy Storage [Internet]. 2024;97(PB):112923. Available from: https://doi.org/10.1016/j.est.2024.112923

[105]. Zhou G, Li Y, Chen W. Experimental investigation on triggering solidification of supercooled sodium acetate trihydrate with extra water and different thickening agents by local cooling. J Energy Storage [Internet]. 2023;74(PB):109381. Available from: https://doi.org/10.1016/j.est.2023.109381

[106]. Xiao Q, Zhang M, Fan J, Li L, Xu T, Yuan W. Solar Energy Materials and Solar Cells Thermal conductivity enhancement of hydrated salt phase change materials employing copper foam as the supporting material. 2019;199(April):91–8.

[107]. Mansour MS, Abdel-megeed A, Al-oufy A. Swelling Properties of Superabsorbent Hydrogels Based on Carboxymethyl Cellulose With Silica , Kaolin , and Bentonite Particles for Agricultural Applications. 2025;1–19.

[108]. Nsengiyumva EM, Heitz MP. Salt and Temperature Effects on Xanthan Gum Polysaccharide in Aqueous Solutions. 2024;

[109]. Chakraborty A, Ahmed S, Shamberger P, Yu C. Achieving extraordinary thermal stability of salt hydrate eutectic composites by amending crystallization behaviour with thickener. Compos Part B [Internet]. 2023;264(June):110877. Available from: https://doi.org/10.1016/j.compositesb.2023.110877

[110]. Bonnassieux S, Pandya R, Skiba A, Seem P, Grimaud A. Revisiting the driving force inducing phase separation in PEG – phosphate aqueous biphasic systems †. 2024;181–92.

[111]. Kumar R, Vyas S, Kumar R, Dixit A. Development of sodium acetate trihydrate-ethylene glycol composite phase change materials with enhanced thermophysical properties for thermal comfort and therapeutic applications. 2017;(January):1–11.

[112]. Wang Y, Yu K, Peng H, Ling X. Preparation and thermal properties of sodium acetate trihydrate as a novel phase change material for energy storage. Energy [Internet]. 2019;167:269–74. Available from: https://doi.org/10.1016/j.energy.2018.10.164

[113]. Sun W, Xu X, Zhang T, Wu Z, Xu Y. Preparation and Thermal Performance Study of a Novel Organic – Inorganic Eutectic Phase Change Material Based on Sodium Acetate Trihydrate and Polyethylene Glycol for Heat Recovery. 2025;1–16.

[114]. Zhang S, Ma X, Min X, Zhang X, Li J. Expanded Vermiculite-Based Calcium

Chloride Hexahydrate Phase Change Materials: Preparation, Characterization, and Phase Change Kinetics. ChemistrySelect. 2025;10(9):1–10.

[115]. Aramesh M, Shabani B. Metal foams application to enhance the thermal performance of phase change materials : A review of experimental studies to understand the mechanisms. J Energy Storage [Internet]. 2022;50(November 2021):104650. Available from: https://doi.org/10.1016/j.est.2022.104650

[116]. Han J, Song M, Yoo JS, Qin S. Numerical Evaluation of Effective Thermal Conductivity of PCM with Metal Foam Incorporating Buoyancy Effects for Thermal Energy Storage. 2024;(June).

[117]. Amirkhani M, Roudini G, Barahuie F, Sheybani H, Ibrar M. Heliyon Evaluation of phase change material-graphene nanocomposite for thermal regulation enhancement in buildings. Heliyon [Internet]. 2023;9(11):e21699. Available from: https://doi.org/10.1016/j.heliyon.2023.e21699

[118]. Vigneshwaran P, Shaik S, Suresh S, Abbas M, Saleel CA, Cuce E. Solar Salt with Carbon Nanotubes as a Potential Phase Change Material for High-Temperature Applications : Investigations on Thermal Properties and Chemical Stability. 2023;

[119]. Xie C. Nano-enhanced phase change material using salt hydrate and cooper nanoparticles for battery thermal management system : Buoyancy-driven approach. J Energy Storage [Internet]. 2023;74(PA):108788. Available from: https://doi.org/10.1016/j.est.2023.108788

[120]. Saini P, Dhar A, Powar S, Doddamani M. Cesaro fins parametric optimization for enhancement in the solidification performance of a latent heat storage system with combined fins , foam , and nanoparticle. Energy Reports [Internet]. 2023;9:5670–87. Available from: https://doi.org/10.1016/j.egyr.2023.04.375

[121]. Ahmad M, Hamdan MO, Abu-nabah BA. Enhanced electronic cooling with optimized metal foam / PCM composite heat sinks : A numerical study. Int J Thermofluids [Internet]. 2025;30(November):101512. Available from: https://doi.org/10.1016/j.ijft.2025.101512

[122]. Yu J, Wang Y, Qi C, Zhang W. Colloids and Surfaces A : Physicochemical and Engineering Aspects Reverse latent heat power generation properties of PCM / nanoparticles / metal foam at night. Colloids Surfaces A Physicochem Eng Asp [Internet]. 2023;665(February):131240. Available from: https://doi.org/10.1016/j.colsurfa.2023.131240

[123]. Shkatulov A, Joosten R, Fischer H, Huinink H. Core − Shell Encapsulation of Salt Hydrates into Mesoporous Silica Shells for Thermochemical Energy Storage. 2020;

[124]. Wang F, Zhang J, Jia S, Chen X, Cheng Z. A review of modification strategies and applications for hydrated salts : Insights from energy storage materials encapsulation technology. Renew Sustain Energy Rev [Internet]. 2025;223(July):115998. Available from: https://doi.org/10.1016/j.rser.2025.115998

[125]. Toomey MD, Kanbargi N, Kearney LT, Hinton H, Gupta S, Sawafta R, et al. Manufacturing of Continuous Core – Shell Hydrated Salt Fibers for Room Temperature Thermal Energy Storage. 2024;2400012:1–8.

[126]. Li J, Yuan Y, Chen H, Jia L, Zhang N, He S, et al. Highly stable and nonflammable

hydrated salt nanocapsules with inorganic-organic composite shell for sustainable building technology. J Energy Storage [Internet]. 2024;79(May 2023):110173. Available from: https://doi.org/10.1016/j.est.2023.110173

[127]. Mu B, Li M. Fabrication and thermal properties of tetradecanol/graphene aerogel form-stable composite phase change materials. Sci Rep [Internet]. 2018;8(1):1–14. Available from: http://dx.doi.org/10.1038/s41598-018-27038-4

[128]. Bie Y, Li M, Malekian R, Chen F, Feng Z, Li Z. Effect of phase transition temperature and thermal conductivity on the performance of Latent Heat Storage System. Appl Therm Eng. 2018;135:218–27.

[129]. Xing D, Dong C, Li Z, Liu Y, Wang B, Hua Q, et al. Preparation and Characterization of Sodium Sulfate Decahydrate-Sodium Acetate Trihydrate Shape-Stabilized Phase Change Materials. Energy and Fuels. 2022;36(9):4947–56.

[130]. Dong X, Mao J, Geng S, Li Y, Hou P, Lian H. Study on performance optimization of sodium sulfate decahydrate phase change energy storage materials. J Therm Anal Calorim [Internet]. 2021;143(6):3923–34. Available from: https://doi.org/10.1007/s10973-020-09306-6

[131]. Liu X, Tie J, Wang Z, Xia Y, Wang CA, Tie S. Improved thermal conductivity and stability of Na2SO4·10H2O PCMs system by incorporation of Al/C hybrid nanoparticles. J Mater Res Technol [Internet]. 2021;12:982–8. Available from: https://doi.org/10.1016/j.jmrt.2021.02.096

[132]. Akamo DO, Cladek B, Goswami M, Gluesenkamp KR, Rios O, Keffer DJ. Nanoscale Stabilization Mechanism of Sodium Sulfate Decahydrate at Polyelectrolyte Interfaces. ACS Omega. 2024;9(16):18051–61.

[133]. Yan L, Charles J, Romero CE, Neti S, Balasubramanian G. Optimizing supercooling and phase stability by additives in calcium chloride hexahydrate for cyclical latent heat storage. Int Commun Heat Mass Transf [Internet]. 2023;149(October):107119. Available from: https://doi.org/10.1016/j.icheatmasstransfer.2023.107119

[134]. Gholami A, Gorji M. Experimental study for the use of Na2SO4.10H2O as a PCM with fixed blades for temperature and efficiency parameters of photovoltaic panel. Case Stud Therm Eng [Internet]. 2023;49:103219. Available from: https://doi.org/10.1016/j.csite.2023.103219

[135]. Zhang B, Zhu Y, Zhao H, Yuan Y, Wang G. Preparation and properties of sodium sulfate decahydrate shape-stabilized composite phase change material for solar greenhouse. Mater Today Commun [Internet]. 2025;42(26):111422. Available from: https://doi.org/10.1016/j.mtcomm.2024.111422

[136]. Li Y, Xie Y, Gao J, Yang X, Sundén B. Solidification characteristics in rotating gradient metal foam based on Taguchi and response surface analysis. Int J Heat Mass Transf. 2025;250(February).

[137]. Li Y, Huang X, Li Z, Xie Y, Yang X, Li MJ. Structural optimization of latent heat storage tank filled with nickel foam. Appl Therm Eng. 2025;267(January).

[138]. Sang G, Zeng H, Guo Z, Cui H, Zhang Y, Cui X, et al. Studies of eutectic hydrated salt/polymer hydrogel composite as form-stable phase change material for building thermal energy storage. J Build Eng [Internet]. 2022;59(July):105010. Available

from: https://doi.org/10.1016/j.jobe.2022.105010

[139]. Cui H, Zou Y, Yang H, Bao X. Thermal-mechanical behaviors of concrete with innovative salt hydrate PCM-based thermal energy storage aggregate. Energy Convers Manag [Internet]. 2023;293(July):117477. Available from: https://doi.org/10.1016/j.enconman.2023.117477

[140]. Mustafa M, Elmegaard B, Weinberger P, Arabkoohsar A. Salt hydrates in renewable energy systems : A thorough review. Energy [Internet]. 2024;313(October):133808. Available from: https://doi.org/10.1016/j.energy.2024.133808

[141]. Togun H, Basem A, Mohammed HI, Biswas N, Abed AM, Lafta F, et al. Harnessing solar energy with phase change materials : A review of melting point impacts. Int Commun Heat Mass Transf [Internet]. 2025;165(PB):109094. Available from: https://doi.org/10.1016/j.icheatmasstransfer.2025.109094

[142]. Singh B, Shankar R, Yadav P, Srivastava S. Solar Energy Materials and Solar Cells Application of phase change materials in solar water heating systems- A comprehensive review. Sol Energy Mater Sol Cells [Internet]. 2025;293(June):113888. Available from: https://doi.org/10.1016/j.solmat.2025.113888

[143]. Jagadeeswara Reddy V, Fairusham Ghazali M, Kumarasamy S. Innovations in phase change materials for diverse industrial applications: A comprehensive review. Results Chem [Internet]. 2024;8(May):101552. Available from: https://doi.org/10.1016/j.rechem.2024.101552

[144]. Kuznik F, Virgone J, Noel J. Optimization of a phase change material wallboard for building use. Appl Therm Eng. 2008;28(11–12):1291–8.

[145]. Zhang Y, Huang J, Fang X, Ling Z, Zhang Z. Optimal roof structure with multilayer cooling function materials for building energy saving. Int J Energy Res. 2020;44(3):1594–606.

[146]. Benkaddour A, Faraji M, Faraji H. Numerical study of the thermal energy storage behaviour of a novel composite PCM/Concrete wall integrated solar collector. Mater Today Proc [Internet]. 2019;30:905–8. Available from: https://doi.org/10.1016/j.matpr.2020.04.348

[147]. Xu Z, Sheng X, Chen J, Chen Y, He J, Luo X, et al. Industrial-grade hydrated salt-based PCM thermal energy storage device : Thermal and economic performances. Appl Therm Eng [Internet]. 2025;262(October 2024):125233. Available from: https://doi.org/10.1016/j.applthermaleng.2024.125233

[148]. Song J, Zhang H, Zhang Y, Ma Z, He M. Research progress on industrial waste heat recycling and seasonal energy storage. 2025;13(January):147–87.

[149]. Zare M, Mikkonen KS. Phase Change Materials for Life Science Applications. 2023;2213455.

[150]. Purohit BK, Sistla VS. LAPONITE® based hydrogel for cold thermal energy storage application. Bull Mater Sci [Internet]. 2021;44(2):1–7. Available from: https://doi.org/10.1007/s12034-021-02416-3

LIST OF RESEARCH PUBLICATIONS

Journals Papers related to thesis:

- **Amarendra Uttam,** Purohit BK, Le MT, Venkata Subbarayudu Sistla. Disodium Phosphate Dodecahydrate Salt Hydrate-Based Approach for Thermal Energy Storage Systems. Technical Education Science/Giáo dục Kỹ thuật. 2023 Jan 16;(74):1-7. https://doi.org/10.54644/jte.74.2023.1330

- **Amarendra Uttam**, Kumar B, Venkata Subbarayudu Sistla. Performance analysis of a multi-scale thermal energy storage system with varying volumes using polyurethane-encapsulated sodium sulphate decahydrate for building applications. Energy and Buildings. 2025 Sep 5;347:116390-0. **(IF= 7.1).** https://doi.org/10.1016/j.enbuild.2025.116390.

- **Uttam A,** Kumar B, Sistla VS. Development of $Na_2SO_4 \cdot 10H_2O$ Salt Hydrate PCMs for Thermal Energy Storage in Building Systems: A Scale-Up Approach. ChemistrySelect. 2025 Nov;10(43). **(IF= 2).** https://doi.org/10.1002/slct.202504616.

- Submitted manuscript on the title **"**Performance Evaluation and Integration of Salt Hydrate-Based PCMs with Wall Materials for Passive Cooling of Buildings" in Journal of Building Engineering **(IF=7.4). (Under Review).**

Journals Papers other than thesis work:

- Kumar B, **Uttam A**, Agrahari GK, Sistla VS. Effect of distinct carboxylic acid modulators on Ni-Zn MOF synthesis and their application in "hydroxy naphthol blue" dye removal from aqueous solutions. Materials Science and Engineering: B. 2026 Mar;325:119074. **(IF=4.6).** https://doi.org/10.1016/j.mseb.2025.119074.

- Manuscript under preparation on the title "Effect of a Thickening Agent on Eutectic Salt Hydrate-Based Phase Change Materials ($Na_2SO_4 \cdot 10H_2O$ and $MgSO_4 \cdot 7H_2O$) for Thermal Energy Storage"**.**

Conference attended

- Oral presented my work on "Disodium Phosphate Dodecahydrate Salt Hydrate-Based Approach for Thermal Energy Storage Systems" at the 6th International Conference on Green Technology and Sustainable Development held at **Vietnam** in online mode.